

MICHIGAN STATE UNIVERSITY LIBRARIES
3 1293 01405 1845

This is to certify that the

thesis entitled

MAGNIFICATION IN DIGITAL RADIOGRAPHY AND DETERMINATION OF VESSEL DIAMETER IN ANGIOGRAPHY OF THE EQUINE DISTAL LIMB

presented by

DIANA SUE ROSENSTEIN

has been accepted towards fulfillment
of the requirements for
MASTER OF SCIENCE
degree in

LARGE ANIMAL CLINICAL SCIENCES

Major professor

Date APRIL 26, 1996

**O**-7639

MSU is an Affirmative Action/Equal Opportunity Institution

# LIBRARY Michigan State University

PLACE IN RETURN BOX to remove this checkout from your record. TO AVOID FINES return on or before date due.

DATE DUE	DATE DUE	DATE DUE

MSU is An Affirmative Action/Equal Opportunity Institution

# MAGNIFICATION IN DIGITAL RADIOGRAPHY AND DETERMINATION OF VESSEL DIAMETER IN ANGIOGRAPHY OF THE EQUINE DISTAL LIMB

Ву

Diana Sue Rosenstein

#### A THESIS

Submitted to
Michigan State University
in partial fulfillment of the requirements
for the degree of

MASTER OF SCIENCE

Department of Large Animal Clinical Sciences

#### ABSTRACT

MAGNIFICATION IN DIGITAL RADIOGRAPHY AND DETERMINATION OF VESSEL DIAMETER IN ANGIOGRAPHY OF THE EQUINE DISTAL LIMB

By

#### Diana Sue Rosenstein

The size of an object may be determined from its radiographic image and the magnification factor of the imaging system. Magnification factors of a digital radiographic system were quantified by comparison of a metallic marker to its image and by calculation of geometric, electronic and photographic magnification factors from the equipment specifications. Angiography was performed in six invitro equine feet, in the standing and lateral recumbent positions, for identification and measurement of the digital arterial vessels. These measurements were corrected for magnification to determine actual vessel diameters. Focal-film distance, image intensifier mode of function and printer format were significant predictors of variability in magnification factors. Total magnification factors determined by the two methods differed due to widened penumbra with increased magnification. Digital arterial diameters ranged from 0.71 mm to 2.54 mm and were consistently larger in lateral recumbency, possibly due to vascular reactions and pressure changes between the two positions.

# **DEDICATION**

This manuscript is dedicated to my family who taught me to pursue my interests with devotion and to my teacher and friend, John "Doc" Walters, who encouraged my intrigue for physics.

#### **ACKNOWLEDGMENTS**

I want to express my gratitude to my graduate committee members for their guidance and patience in this endeavor: Drs. R. Bowker, N.E. Robinson, J. Stick and R. Stickle. I also appreciate the technical assistance and support that was generously given by V. Hoelzer-Maddox and P. Ocello.

# **TABLE OF CONTENTS**

LIST OF TABLES	vii
LIST OF FIGURES	ix
LIST OF ABBREVIATIONS	xiv
INTRODUCTION	
Radiography	
Characteristics of the radiographic image	
Angiography	22
LITERATURE REVIEW	29
Image magnification	29
Angiography	30
Statement of hypothesis	43
MATERIALS AND METHODS	45
Magnification factors	45
Limb perfusion and angiography	
RESULTS	59
Magnification factors	
Angiography of the equine distal limb	
DISCUSSION	73
Magnification	<b>7</b> 3
Angiography of the equine distal limb	

APPENDICESAppendix AAppendix B	.86 .86
Appendix AAppendix B	22
Appendix B	
	.87
••	100
	110

# LIST OF TABLES

Table 1	Following euthanasia, the right thoracic limb was removed on each of six horses.	51
Table 2	The palmar digital artery and its major branches to the foot were identified on digital angiograms.	56
Table 3	Total magnification factors (TMFm) were determined by measurement of a metallic marker and its radiographic image.	60
Table 4	Total magnification factors (TMFc) were calculated for the imaging system.	63
Table 5	Arterial vessels were identified on angiograms of six equine feet.	66
Table 6	Arterial vessels were measured on digital angiograms in the palmarodorsal (PD) and lateromedial (LM) views and vessel size was corrected for magnification.	71
Table 7	A metallic marker was radiographed at several focal-film distances (FFD), using three different image intensifier modes (II mode) and printed at four formats. Each image was measured three times with calipers.	87
Table 8	A linear function, defined by linear regression analysis, was used to calculate fitted values for TMFm at each focal-film distance (FFD), image intensifier tube mode (II mode) and printer format.	95
Table 9	Magnification factors were calculated for individual components of the digital radiographic imaging system, at each focal-film distance, image intensifier mode and printer format.	100
Table 10	There was some variation in the difference between measured and calculated total magnification factors (delta) between the radiographic technique variables.	101

Table 11 Arterial vessels of six in-vitro equine feet were measured on digital angiograms 110 (image size) in the palmarodorsal (PD) and corrected for magnification to determine the diameter of each vessel (vessel size).

# **LIST OF FIGURES**

Figure 1	Electrons strike the target causing the release of xrays from the xray tube.	3
Figure 2	The image intensifier tube converts xray energy to electrons and then light photons.	4
Figure 3	The video camera records the light signal from the image intensifier tube and transmits the image to the digital image processor. The image may then be viewed on a television monitor or printed by the laser imager.	5
Figure 4	The triangles formed by the focal spot, object (a) and film (A) by the xray beam (b, B, c, C) illustrate the geometrical relationship between the object and its image.	10
Figure 5	As focal-object distance decreases, image size increases (A) and as focal-film distance increases, image size increases (B).	11
Figure 6	Xrays may originate from any random point in the target and this range causes indistinct margins to the radiographic image called penumbra (P).	12
Figure 7	One light source casts a sharper image of a box (A) than the light from several sources (B).	12
Figure 8	Electrons released at the input screen are directed towards the output screen by electrostatic focusing lenses.	14
Figure 9	The image intensifier tube functions in the 9 inch mode (A), 6 inch mode (B) and 4.5 inch mode (C) to cause electronic magnification by changing the focal point of the electron stream.	16

Figure 10	Light from the laser source is directed to the film by a series of lenses and photographic magnification is determined by focal length of the collimator lens (A) and focal length of the camera lens (B).	18
Figure 11	In a magnified image (A) the individual dots are discernable, while a minified image (B) blends together these dots, creating a sharper appearance.	20
Figure 12	Edge absorption causes image unsharpness due to the gradual attenuation of xrays at the periphery of a structure. This effect is related to the shape of an object and is least apparent with a conical object (A), moderate with a cubic object (B) and most apparent with a spherical object (C).	22
Figure 13	Differences between the common radiopaque contrast media are illustrated by their structural formulas. The ionic compounds (A) dissociate in solution resulting in a higher osmolarity than the non-ionic compounds (B,C). The monoacid dimer (D) is ionic, but the anion has six iodine atoms.	28
Figure 14	Digital radiographic images of a metallic marker were produced with the marker on the patient table.	47
Figure 15	The vasculature was perfused with an oxygenated (95% $O_2/5\%$ $CO_2$ ), heated (37°C) Krebs Henseleit solution at 100 mm Hg arterial perfusion pressure.	53
Figure 16	The palmarodorsal study was performed with the limb in a standing position, FFD=87.5 cm, FOD=49.5 cm and object-film distance=38.0 cm.	54
Figure 17	The lateromedial study was performed with the limb in lateral recumbency, FFD=74.5 cm, FOD=49.5 cm and object-film distance=25.0 cm.	55
Figure 18	The palmar digital artery was measured at three locations: 1) 1.0 cm proximal to the origin of the bulbar a., 2) 1.0 cm proximal to the origin of the dorsal phalangeal a. and 3) at the entrance to the solar canal.	57
Figure 19	The total magnification factors (TMFm) increased as FFD increased.	61
Figure 20	As II mode increased, the total magnification factors (TMFm) decreased steadily.	61
Figure 21	The total magnification factors (TMFm) decreased as the number of images per sheet of film (format) increased.	61

Figure 22	As FFD increased, the difference between TMFm and TMFc (delta) remained unchanged.	64
Figure 23	As II mode increased, the difference between TMFm and TMFc (delta) decreased.	64
Figure 24	As printer format increased, the difference between TMFm and TMFc (delta) decreased.	64
Figure 25	The palmar digital artery and its major arterial branches to the equine foot were visible on digital angiograms in the palmarodorsal view (A) and diagrammed as an atlas of these vessels (B).	67
Figure 26	The palmar digital artery and its major arterial branches to the equine foot were visible on digital angiograms in the lateromedial view (A) and diagrammed as an atlas of these vessels (B).	68
Figure 27	Dorsal branches of the terminal arch and distal branches of the dorsal phalangeal artery supply a vascular bed at the dorsal aspect of the coronary region.	69
Figure 28	Minor variations were present in the pattern of the terminal arch and solar branches, as seen on the palmarodorsal view.	<b>7</b> 0
Figure 29	Arterial vessels of the equine foot were measured on digital angiograms of six feet and corrected for image magnification in the palmarodorsal (PD) and lateromedial (LM) views.	<b>7</b> 2
Figure 30	Penumbra contributed to image magnification, but due to the ill-defined, gradually fading margins, it was not completely included in the measurements.	74
Figure 31	The magnitude of penumbra depends on the relative size of the object and the focal spot. Penumbra (P) is small when the object is larger than the focal spot (A) and penumbra is larger than the umbra (U) when the object is smaller than the focal spot (B).	<i>7</i> 5
Figure 32	Fitted values for total magnification factors (TMFm), averaged over all II modes and formats, increased gradually with increasing FFD.	97

Figure 33	Fitted values for total magnification factors (TMFm), averaged over all formats, were higher for smaller II modes, but as FFD increased, the trend of increasing magnification factors was the same for each II mode.	97
Figure 34	Fitted values for total magnification factors (TMFm), averaged over all II modes, were higher for formats with fewer images per sheet of film, but as FFD increased, the trend of increasing magnification factors was the same for each format.	97
Figure 35	Fitted values for total magnification factors (TMFm), averaged over all FFD's and formats, decreased steadily with increasing II mode.	98
Figure 36	Fitted values for total magnification factors (TMFm), averaged over all FFD's, were higher for formats with fewer images per sheet of film. As II mode increased, fitted TMFm decreased at every format.	98
Figure 37	Fitted values for total magnification factors (TMFm), averaged over all formats, were higher for longer FFD's, but as II mode increased, the trend of decreasing magnification was the same for each FFD.	98
Figure 38	Fitted values for total magnification factors (TMFm), averaged over all FFD's and II modes, decreased as format increased.	99
Figure 39	Fitted values for total magnification factors (TMFm), averaged over all II modes, were higher for longer FFD's, but as format increased, the trend of decreasing magnification factors was the same for each FFD.	99
Figure 40	Fitted values for total magnification factors (TMFm), averaged over all FFD's, decreased as the number of images per sheet of film (format) increased.	99
Figure 41	Fitted delta (the difference between measured and calculated magnification factors), averaged over all II modes and formats, was the same at every FFD.	107
Figure 42	Fitted delta, averaged over all formats, was highest at the 4.5 inch II mode.	107
Figure 43	Fitted delta, averaged over all II modes, was highest at the 1:1 format.	107
Figure 44	Fitted delta, averaged over all formats and FFD's, was greatest at the 4.5 inch II mode.	108

Figure 45	Fitted delta, averaged over all FFD's, was highest at the 1:1 format.	108
Figure 46	Fitted delta, averaged over all formats, was the same at every FFD.	108
Figure 47	Fitted delta, averaged over all II modes and FFD's, was greatest at the 1:1 format.	109
Figure 48	Fitted delta, averaged over all II modes, was the same at every FFD.	109
Figure 49	Fitted delta, averaged over all FFD's, was highest at the 4.5 inch II mode.	109

# LIST OF ABBREVIATIONS

a. artery

DR digital radiography

FFD focal-film distance

FOD focal-object distance

format laser imager (printer) format

II mode image intensifier tube mode of function

kVp kilovolts peak

LM lateromedial

mA milliamperage

PD palmarodorsal

ECG electrocardiogram

TMFc calculated total magnification factor

TMFm measured total magnification factor

#### INTRODUCTION

#### RADIOGRAPHY

# Physics of radiography

Radiography is a commonly performed diagnostic procedure in veterinary medicine that provides visual images of structures within an animal's body, based on xray attenuation by the tissues. The atomic number of the tissue and energy of the xray determine the type of interaction that will occur between the patient and the xray beam. When an xray is attenuated, either by absorption in the patient, or by scatter to the environment, the corresponding region of the radiograph is radiopaque and it appears clear, or white when the film is viewed on a white lightbox. The area of a radiograph that is exposed to xrays and light from transmission of the xrays through the patient is radiolucent and it appears as shades of gray to black. Thus, a radiograph is a black and white image representing xray attenuation characteristics of the subject, such as a patient's body. Since the xray beam is composed of thousands of individual xrays which vary in energy over a range and an animal has a variety of internal structures, then the resulting radiographs contain a spectrum of gray shades between white and black.

A conventional radiographic system includes an xray tube that emits x-radiation, a cassette that contains two fluorescent screens and the radiographic film, housed between these screens. Xrays that are transmitted through the patient strike the cassette and interact with crystals in the screens, causing these crystals to emit visible light. It is this light that exposes the radiographic film to produce an image. Digital radiography (DR) is a new development in radiology that incorporates computer processing of data into image production to enhance the appearance of radiographic images.

# Digital radiography

#### Equipment

A basic explanation of xray production and digital radiographic equipment illustrates the advantages of this sophisticated system. A radiograph is the product of a series of complex events that uses energy from an electrical current to heat a wire filament, causing the wire to release electrons. These electrons are attracted, at an accelerating velocity across the tube, by the electrical potential difference between the anode and cathode. The electrons strike the target, causing rapid deceleration of the electrons and the release of xrays and heat from the tube (Figure 1). The heat generated in this reaction must be dissipated to avoid melting the target, while the xrays are filtered and collimated to form a useful beam. Xrays in this primary beam are absorbed by the patient, scattered to the environment or transmitted through the patient to create the latent xray image. In conventional radiography, this latent

image is a pattern of xrays that excites crystals in the screens within the cassette causing them to emit light to expose the adjacent film. At this point digital radiography differs from conventional radiography in its xray detection system and image production.

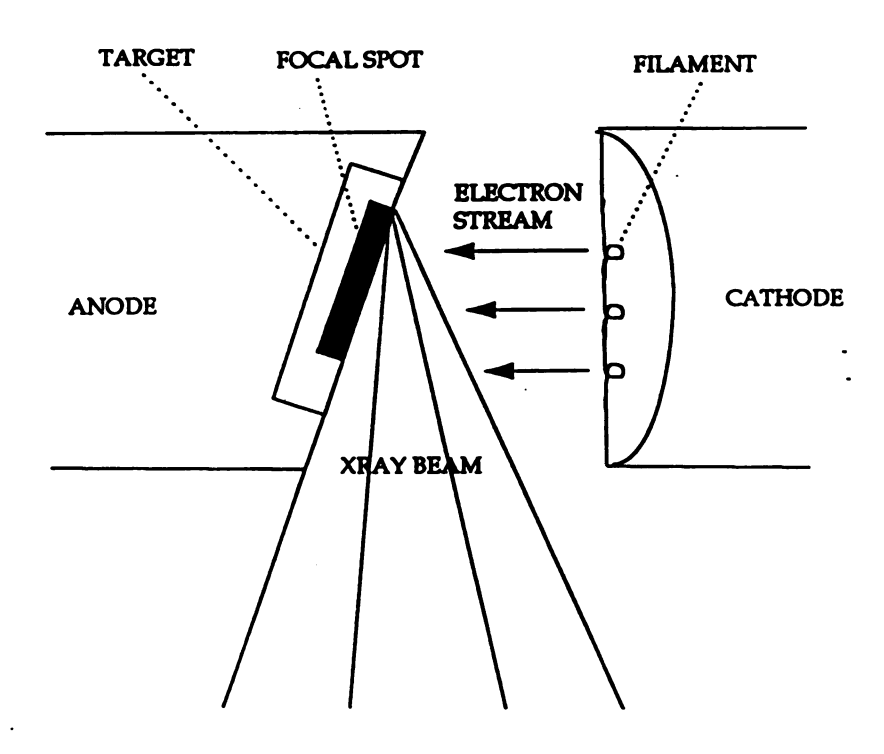


Figure 1 Electrons strike the target causing the release of xrays from the xray tube.

Transmitted xrays that form the latent image are detected by the image intensifier tube, which is positioned above the patient. At the input screen of the intensifier tube, xray energy is converted to electrons that are attracted across the tube and focused at the output screen, where the energy is converted to light

photons (Figure 2). The image intensifier tube is a sensitive xray detector that enhances the latent image signal by accelerating these electrons across a potential difference, to release more light energy at the output screen than was present in the initial latent image. The output image also appears brighter due to the relatively smaller size of the output screen as compared to the input screen, which concentrates the light photons over a smaller area.<sup>1</sup>

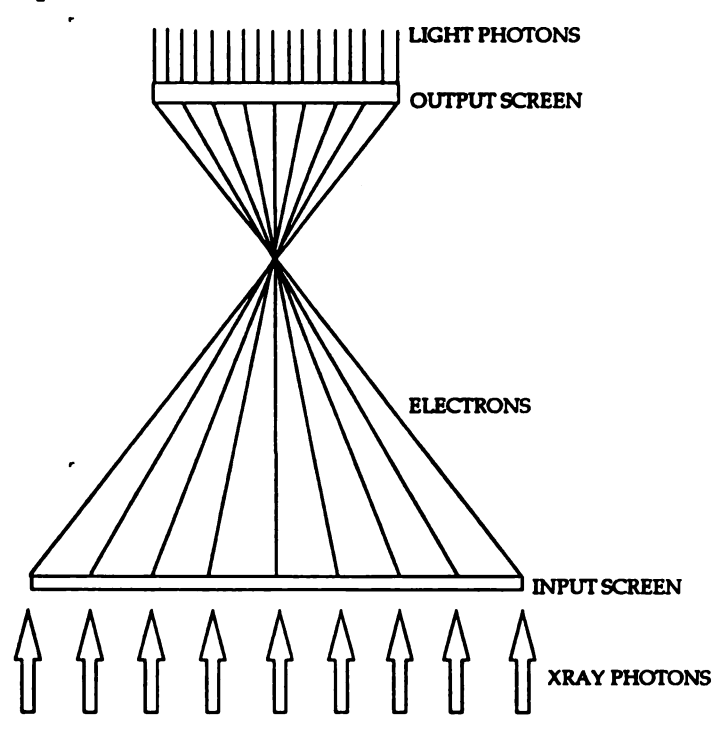


Figure 2 The image intensifier tube converts xray energy to electrons and then light photons.

The intensifier tube is optically linked to a television camera which records the output light signal to produce a video signal. This message is transmitted to the computer digital image processor for analog-to-digital conversion of the image data, processing of the data and memory storage of the images. Data are then converted

back to an analog signal for viewing on a television monitor or transmitted to the printer to produce a tangible radiograph. In the laser printer, this image signal controls the intensity of a laser beam that exposes radiographic film. The exposed film is chemically developed in a processor to make the final image visible and permanent.

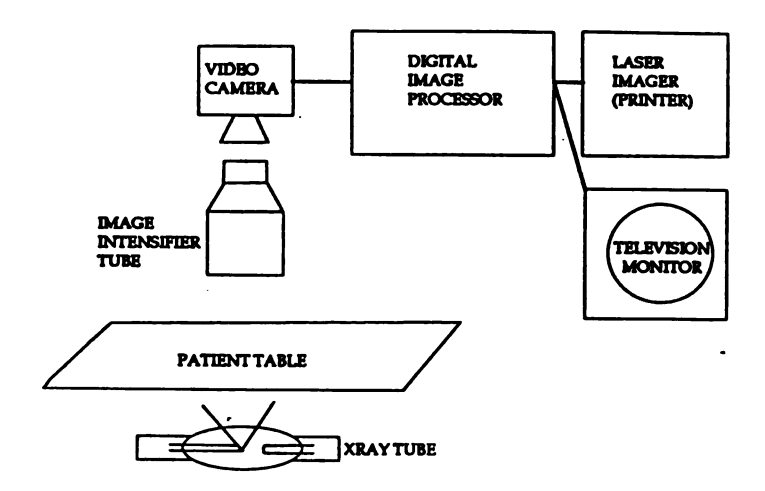


Figure 3 The video camera records the light signal from the image intensifier tube and transmits the image to the digital image processor. The image may then be viewed on a television monitor or printed by the laser imager.

# Advantages of the DR system

The principles of xray production and film exposure are similar in conventional and digital radiography, however the modifications present in the DR system increase the efficiency of xray detection, incorporate computer manipulation of the image data and allow for instantaneous viewing of the images on a monitor. Characteristics of each component in the DR system contribute to its enhanced image quality.

The xray tube used in digital radiography is designed to dissipate heat efficiently to avoid tube damage under a heavy work load, which increases the ability of the system to produce rapid interval exposures and to repeat series of exposures without prolonged waiting periods for tube cooling.<sup>2</sup> Turning of the target by a rotating anode spreads the heat and wear, due to electron bombardment, over a larger surface area to increase the heat loading capacity and extend the useful life of the tube.<sup>12</sup> The shaft and bearings which attach to the rotating anode readily conduct heat away from the target while an external blower cools the tube.<sup>2</sup> The target is constantly bombarded by electrons during an exposure which causes roughening or pitting of the target surface. The target material in the DR xray tube is an alloy of tungsten (90%) and rhenium (10%) to increase resistance of the surface to wear, over the conventional tungsten target.<sup>2</sup>

The intensifier input screen is more efficient at detecting transmitted xrays and converting this energy to electrons, than the calcium tungstate screens in conventional cassettes.<sup>1,3</sup> The crystals in the intensifier tube input screens are cesium iodide, which form long narrow crystals that pack together more densely than calcium tungstate, which increases the likelihood that a transmitted xray will interact with a crystal and improves image resolution by decreasing the dispersion of light that occurs with large crystals, to create an electron signal that more precisely represents the latent xray image.<sup>1,3</sup> The intensifier tube also amplifies the signal intensity by accelerating electrons across the tube. Faster electrons strike the output screen with more energy, which causes the release of more light, thereby enhancing

image brightness. This enhancement of image brightness due to electron acceleration between the input and output screens is called flux gain.<sup>1</sup> So the intensifier screens in DR are more efficient at detecting xrays than conventional screens and DR has the additional advantage of flux gain to brighten the image.

The television camera and monitor allow for immediate viewing of the image without chemical processing of film. This visual system also links to a video cassette recorder (VCR) to permit continuous recording of a dynamic study.<sup>1,2</sup> In conventional radiography, each exposed film must be chemically processed to create a visible image and VCR capabilities are not available. The television chain, composed of the camera and monitor, is the weakest link in the imaging system, since it limits overall resolution.<sup>1,3</sup> The standard system has 512 horizontal lines and 512 vertical lines and is called a 512x512 matrix; however, a newer television system is now available with a 1024x1024 matrix to improve image resolution. The television monitor enables the radiographer to visualize images during the procedure for immediate interpretation and to make adjustments in technique or patient positioning as needed for a diagnostic study.

The digital image processor converts the electrical signal to a digital form, in binary code, to process the image data. The computer may store 130 images in its memory and recall these images for viewing and printing. The contrast and brightness settings of each image may be changed by the windowing function, which serves a similar purpose as fast, slow and par speed screens with high and low contrast film in conventional radiography.<sup>1,2</sup> Since the windowing selections may be

altered after an exposure is complete, a single image may be viewed and printed at several windows, to enhance various structures without repeating the radiation exposure to the patient. The digital image processor has an image inversion function which reverses the gray scale, such that radiolucent regions appear white and radiopaque tissues appear black. An inverted image may enhance visualization of subtle radiographic findings, especially small structures in a thick body part.

The laser imager prints images on single-sided emulsion film which has a higher resolution than conventional double-sided emulsion radiographic film.<sup>1,4</sup> This improvement is due to the direct exposure of the film to light from the laser beam, instead of exposure to dispersed light from screens on two sides of the film.<sup>1</sup> These advantages of digital radiography, over conventional film-screen radiography, make this newer imaging system well adapted for studies of small structures that require multiple, rapid interval exposures and high detail, high contrast images.

#### CHARACTERISTICS OF THE RADIOGRAPHIC IMAGE

The product of radiography is a two dimensional image that represents a three dimensional object, therefore some discrepancy always exists between the radiographic image and the object's true physical qualities. The image characteristics that represent these differences are magnification, distortion and edge unsharpness and each must be considered by the radiologist during image interpretation. Some of the factors which contribute to these characteristics are controlled by the radiologist and others are inherent in the imaging modality. The

effects of these characteristics may enhance or detract from image quality, so a knowledge of these factors enables the radiologist to manipulate the equipment for maximum image quality.

#### Magnification

# Geometric magnification

Magnification is defined as the apparent enlargement of an object<sup>5</sup> and three types of magnification have been described: 1) geometric, 2) electronic and 3) photographic.<sup>16,7,8</sup> In regards to radiography, geometric magnification is the most commonly recognized form of image magnification. 1,6,7,8 Xrays emitted from the xray tube travel in straight lines from their point of origin at the target, diverging outward towards the patient. Geometric magnification is the enlarged appearance of an image due to this diverging pattern of xray dispersion. 16 The focal spot is the area of the target that is bombarded by electrons to produce xrays. The distances between this focal spot and the object and between the focal spot and the film determine the magnitude of geometric magnification. The triangles formed by the focal spot, an object and the film illustrate the geometric relationship between the object and its image (Figure 4).18 Two triangles of the same shape but different size are called similar triangles and the sides of these triangles are proportional in the ratio:

$$a/A = b/B = c/C = h/H.$$

The altitudes of these triangles represent the distances from the focal spot to the object (h) and focal spot to the film (H). The object (a), produces an image (A) on the film and the sides of each triangle (b, c, B and C) represent the diverging xray beam.

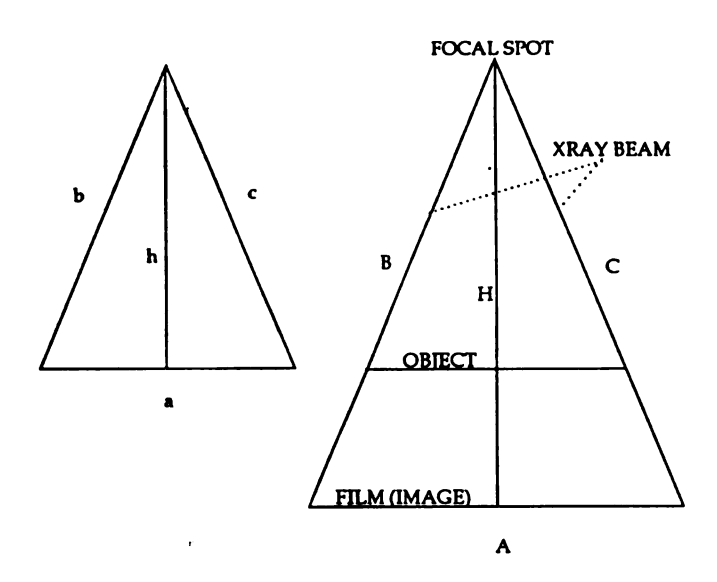


Figure 4 The triangles formed by the focal spot, object (a) and film (A) by the xray beam (b, B, c, C) illustrate the geometrical relationship between the object and its image.

The proportional relationship of the sides of similar triangles may be used to calculate the size of an object from its image, or, vice versa, to predict the image size of a known object. This geometric principle is used to explain how the focal spot to object distance (FOD) and the focal spot to film distance (FFD) affect image size (Figure 5). As FOD decreases, the size of the image increases due to the divergence of the xray beam (Figure 5A). As FFD increases, image size increases, also due to the diverging pattern of the xray beam (Figure 5B). The term focal-film distance comes

from conventional radiography, in which the film is housed in the cassette. However, in digital radiography, the image intensifier input screen detects the transmitted xrays, but the film is not exposed until the signal is processed by the computer and sent to the laser imager. In order to maintain consistency in the terminology between the two imaging systems, the distance from the focal spot to the input screen of the intensifier tube is still called the focal-film distance.

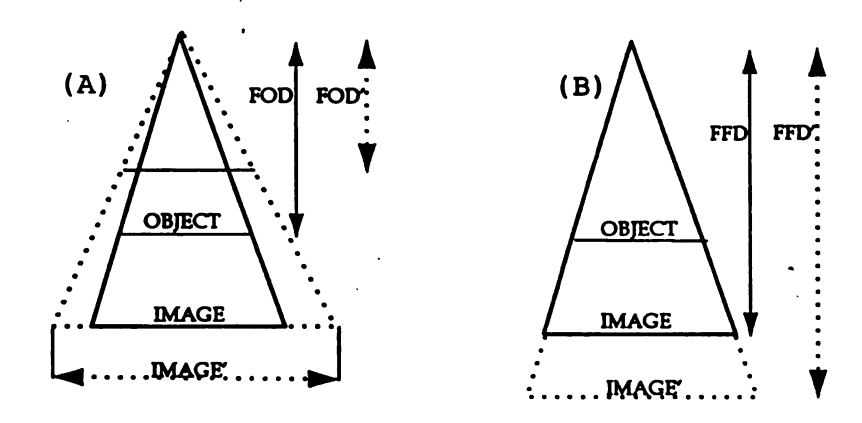


Figure 5 As focal-object distance decreases, image size increases (A) and as focal-film distance increases, image size increases (B).

#### Penumbra

In addition to FOD and FFD, the focal spot size contributes a small amount to image enlargement.<sup>1</sup> The specific area of the target struck by electrons to release xrays is the focal spot and each individual xray may be emitted from any random point in the focal spot. This range of origins of the xrays causes an indistinct appearance to the margins of an image, called the penumbra effect (Figure 6).<sup>17</sup> Penumbra, also called edge gradient, is defined as the region of partial illumination that surrounds the complete shadow, or umbra.<sup>1</sup> The penumbra appears as a region

of gradually dimming shades of gray at the margin of a structure's image. To illustrate this phenomenon, one may imagine the light beam from one flashlight, casting a shadow of a box on a wall, resulting in a square with sharp edges (Figure 7A). By comparison, a box's shadow, cast by the light from four flashlights, would have less distinct edges due to the variety of angles from which the lights strike the box (Figure 7B).

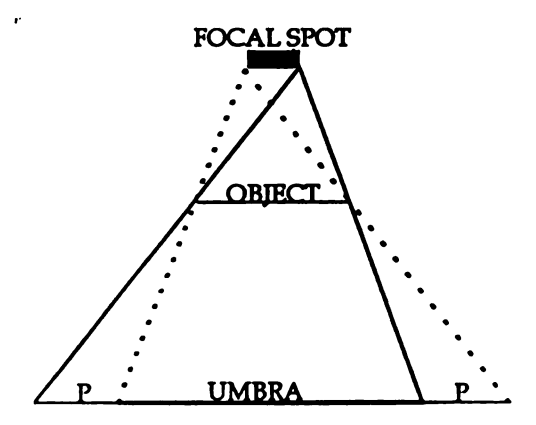


Figure 6 Xrays may originate from any random point in the target and this range causes indistinct margins to the radiographic image called penumbra (P).

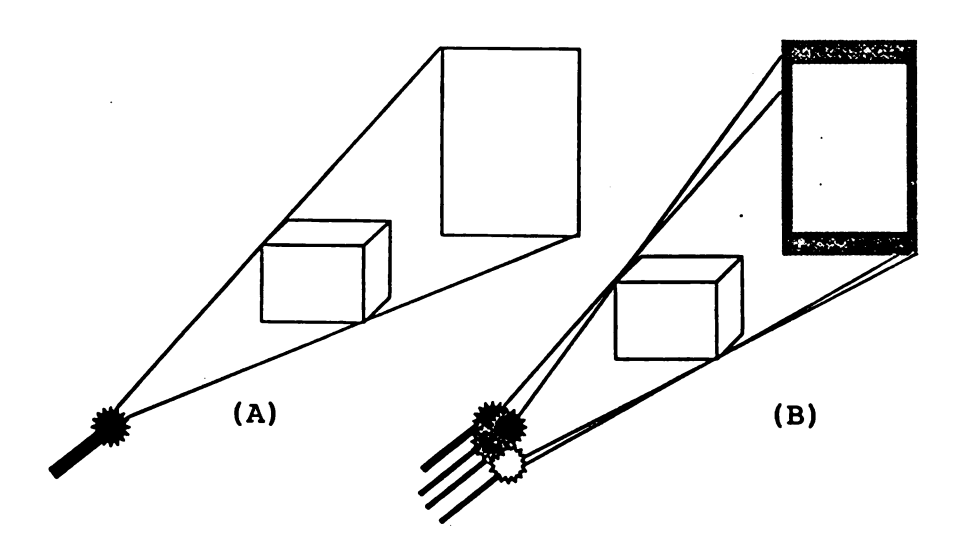


Figure 7 One light source casts a sharper image of a box (A) than the light from several sources (B).

A larger focal spot will produce a wider penumbra, increase overall size of the image and increase edge unsharpness, while a smaller focal spot will produce a more narrow penumbra, resulting in a sharper image with less effect on magnification.<sup>1,9</sup> In most xray tubes used in conventional radiography, the focal spot is 1-2 mm, but the digital radiography unit has an xray tube with two focal spot sizes, 1.0 mm and 0.3 mm.<sup>2</sup> The smaller focal spot (0.3 mm) is used in studies of small structures to produce the sharpest possible images. The larger focal spot is used to image larger structures, when fine detail is less critical.<sup>1,8</sup>

Geometric magnification is created intentionally, in some studies, by using a short FOD and long FFD, which is called the air gap technique.<sup>6,10</sup> The advantage of this method is enlargement of the image and absorption of scattered radiation in the air gap, but penumbra degrades image quality, thereby limiting the applications of this technique.<sup>10</sup> These three factors, FOD, FFD and focal spot size, affect every radiograph and in conventional radiography their impact is the predominant factor that determines image size. While geometric magnification does occur in digital radiography, there are other factors to consider, which affect image size during transmission of the image signal through the image intensifier tube, computer and laser printer that must be recognized by the radiologist for proper image interpretation.

#### Electronic magnification

There are two additional forms of image magnification that occur in digital radiography, namely electronic and photographic magnification. Electronic magnification is the alteration of image size by electronic manipulation of the image signal, which occurs within the image intensifier tube between the input and output screens. The electrons from a large input screen are focused to a smaller output screen by electrostatic focusing lenses that line the intensifier tube (Figure 8).

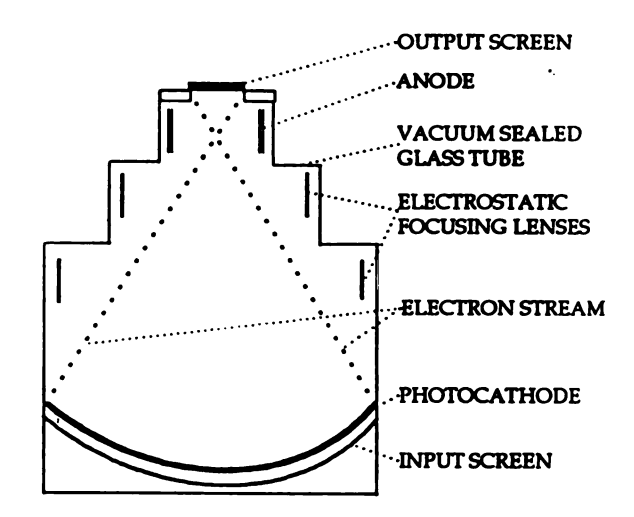


Figure 8 Electrons released at the input screen are directed towards the output screen by electrostatic focusing lenses.

The image is concentrated by projecting the signal on a smaller area, which increases the density of electrons striking the output screen and releases light in a more concentrated pattern, resulting in a smaller, brighter image with greater detail.<sup>1,3</sup>

The intensifier tube also functions in three modes to produce additional electronic magnification.<sup>1,7</sup> The input screen is approximately 9 inches in diameter

(22 cm) so these modes are called, by convention, 9 inch, 6 inch and 4.5 inch (Figure 9). In the 9 inch mode, all of the xrays detected at the input screen contribute to the final image (Figure 9A) and this all-inclusive relationship from the input to output screens, in the 9 in. mode, does not cause a change in image size.¹ In the 6 inch mode, the electrons are focused at a point farther from the output screen by the electrostatic focusing lenses, causing greater dispersion of the electrons, so that information from only the central 6 in. (66%) of the input screen contributes to the image at the output side of the intensifier tube (Figure 9B). The overall size of the final radiograph is the same, but contents within the image have been magnified 1.5 times (9 inch/6 inch=1.5).¹ Finally, the 4.5 inch mode functions on this same principle, utilizing the central 50% of the input screen information to produce the same size radiograph, so the signal is electronically magnified by a factor of 2 (Figure 9C).

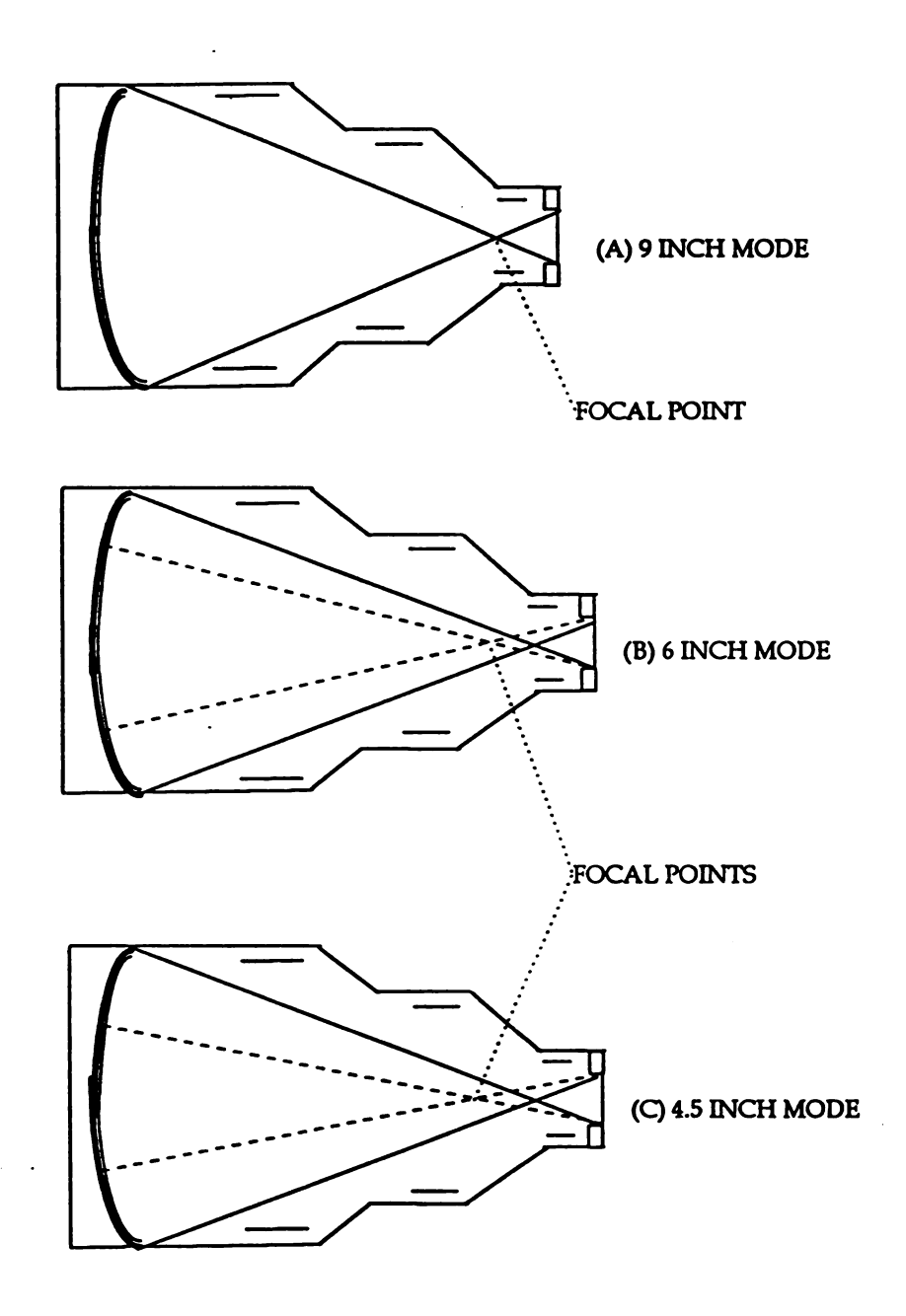


Figure 9 The image intensifier tube functions in the 9 inch mode (A), 6 inch mode (B) and 4.5 inch mode (C) to cause electronic magnification by changing the focal point of the electron stream.

The intensifier tube mode of magnification may be easily interchanged during a study, making it convenient for the radiologist to observe electronically magnified images on the television monitor. This flexibility allows the radiologist the opportunity to survey a large area, center on a selected region of interest, then magnify the image by 1.5X or 2X. This technique is only available with an intensifier tube, which is a distinct advantage of digital radiography over conventional radiography. The disadvantage of electronic magnification is decreased image detail, since the same amount of image data is displayed over a larger area. To maintain image brightness, in this electronic magnification mode, the computer automatically increases the exposure technique, which increases radiation exposure to the patient and adjacent personnel. In the 6 in. and 4.5 in. modes, the entire area of the patient that is being exposed to the primary xray beam is not completely visualized on the television monitor or on the final radiograph. Therefore, personnel restraining the patient may not realize their close proximity to the primary beam, resulting in excessive radiation exposure. In these magnified modes, the field of view within the patient is small, so only a limited area may be examined on each image.

# Photographic magnification

The third type of image enlargement is photographic magnification, which uses optical equipment, such as a camera lens, magnifying lens or microscope to alter the size of an image.<sup>6</sup> This type of magnification is well recognized in photog-

raphy with the use of macro and zoom lenses to project light from subjects of various sizes onto film and to produce photographs of various sizes from a single negative. A technique has been described for magnification radiography in which ultra fine detailed radiographs were produced of thin tissue specimens with a specialized xray tube, using low kVp, low mA and long exposure time settings. The resulting radiographs were then photographed with a zoom lens or viewed with a magnifying lens.<sup>6,11</sup>In digital radiography, photographic magnification occurs in the laser imager by altering the position of two lenses which control the laser beam.<sup>4,12,13</sup> Light from the laser beam is aligned in parallel by the collimator lens, then dispersed by the camera lens to expose the film (Figure 10).<sup>4,13</sup>

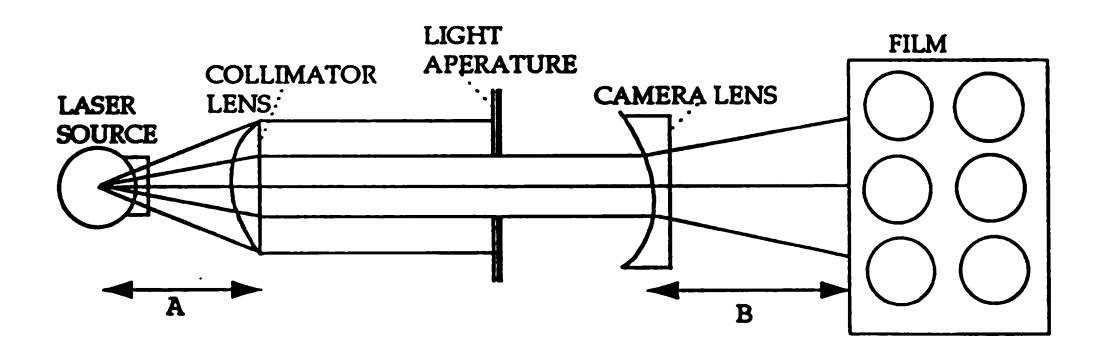


Figure 10 Light from the laser source is directed to the film by a series of lenses and photographic magnification is determined by focal length of the collimator lens (A) and focal length of the camera lens (B).

Photographic magnification is controlled by the focal length of the camera lens and the focal length of the collimator lens. Moving the camera lens closer to the film creates a smaller image, while moving the camera lens further away from the film produces a larger image.<sup>13</sup> The laser imaging printer is programmed to

produce images of various sizes, to fit 1, 4, 6 or 12 circular images on one 14x17" sheet of film and these formats are named 1:1, 4:1, 6:1 and 12:1, respectively.<sup>12</sup> The printer format is selected by the operator to suit the specific needs of an examination. This option is cost effective, since less film is required to print multiple images and a smaller volume of developing chemicals is used to process the film.

These three types of magnification, geometric, electronic and photographic, occur in digital radiography to create circular images on film that may be smaller or larger than the actual area of the patient within the xray field. If the circular image is smaller than the field of view in the patient, then the image is minified, or magnified by a factor less than one. Of these three types of magnification, only electronic and photographic magnification may have factors less than one, so minification within the radiographic system can only occur in digital radiography and not in conventional radiography.

Minification of an image is beneficial to image quality because the visual information is condensed into a smaller area, increasing the density of information per unit area. For example, if a newspaper photograph is enlarged, the individual dots that create the picture are discernible as separate spots of gray ink on white paper and the subject appears less distinct (Figure 11A). But when the picture is small, the dots blend together and the subject appears well defined (Figure 11B).¹ This logic applies to digital images where minified images appear sharper because a discrete quantity of data is printed in a smaller area on the film. In minified images, the penumbra is smaller so the edges of structures appear sharper.



Figure 11 In a magnified image (A) the individual dots are discernible, while a minified image (B) blends together these dots, creating a sharper appearance.

#### Distortion

Distortion is the second characteristic of a radiograph that represents the disparity between an object and its image. Distortion is the unequal magnification of different parts of an object due to varying distances from the film.<sup>18</sup> This detracts from image quality due to the awkward, asymmetrical representation of the object. To avoid distortion, an object should be aligned parallel to the patient table and intensifier tube such that every part of the object is equidistant to the film.<sup>1</sup> However, positioning of irregularly shaped, three dimensional patients usually means that internal organs cannot all be equidistant to the film. Interpretation of distorted images requires comprehension of the anatomy and experience by the radiologist.

### Image unsharpness

Image unsharpness is the third characteristic of radiographs that changes the appearance of an object. Unsharpness refers to the indistinct margins of an object and it is caused by three factors, including, penumbra, patient or tube motion and edge absorption. Use of a small focal spot will decrease penumbra, thus improving image sharpness (Figure 7, p. 12). Patient restraint by physical or chemical means, or use of a short exposure time, will decrease blurring from patient motion. Xray tube motion may occur with a portable xray unit that is not properly stabilized, but this is not a problem in digital radiography, since the xray tube is fixed in position.

Edge absorption is the gradual change in xray attenuation at the margins of an object, associated with the shape of a structure (Figure 12).<sup>1,8</sup> A spherical object causes the greatest edge absorption because there is always a gradual transition in object thickness at the periphery.<sup>1</sup> A cone shaped object causes the least edge absorption since there is an abrupt transition between the thick portion of the object and the surrounding air and a cube causes a moderate amount of edge absorption, between the sphere and cone. The shape of an organ cannot be altered to avoid edge absorption, so the radiologist must learn to interpret images with this characteristic. These causes of magnification, distortion and unsharpness contribute to the quality of a radiograph and are important to consider in image interpretation.

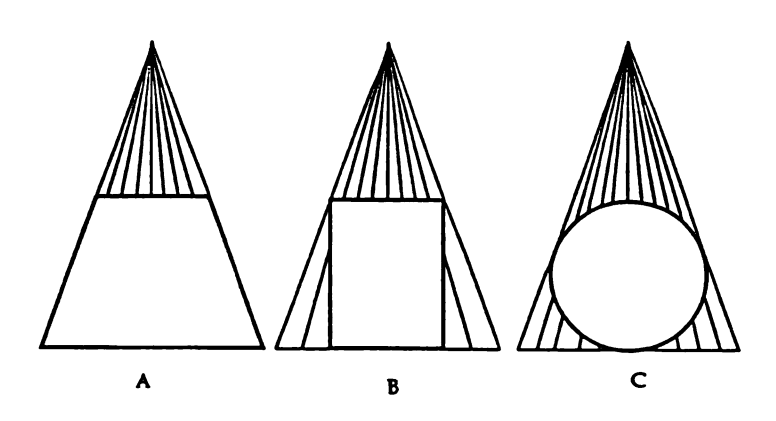


Figure 12 Edge absorption causes image unsharpness due to the gradual attenuation of xrays at the periphery of a structure. This affect is related to the shape of an object and is least apparent with a conical object (A), moderate with a cubic object (B) and most severe with a spherical object (C).

### **ANGIOGRAPHY**

## Purpose and technique

Since blood vessels and blood are soft tissues, composed mainly of water, they have the same xray attenuation characteristics as the surrounding muscles, ligaments and tendons. To enhance visualization of the blood vessels, a radiopaque solution may be injected into the vasculature immediately prior to radiography and this procedure is called angiography.<sup>5</sup> Vessels are evaluated on angiograms for their size, number and distribution within an organ, integrity of their walls and uniformity of luminal diameter.<sup>6</sup>

Angiography of the heart may be performed following injection of a contrast solution in a peripheral vein (non-selective cardiography) or following catheterization of specific cardiac chambers (selective cardiography). For the

examination of other blood vessels, a peripheral artery or vein is selected based on the region of interest.

#### Contrast media

Systemic reactions to contrast media

Ideally, the only action of the contrast material is to attenuate radiation so as to enhance visualization of the vessel lumen on the radiograph, without having any biological effects. However, when these radiopaque compounds are administered into the vascular system, a number of local and systemic reactions may occur, which in turn, may affect the radiographic appearance of the vessels. These effects must be considered in interpretation of angiographic findings, but are rarely mentioned in the veterinary angiography literature.

Several body systems are commonly involved in contrast media induced reactions including the neurological, respiratory, cardiovascular, gastrointestinal, urinary and cutaneous systems.<sup>7,10,14</sup> Neurological reactions vary in severity from mild ataxia, weakness and muscle twitching, to syncope, seizures, paralysis and coma.<sup>14,15</sup> Reactions of the respiratory system include sneezing, coughing, dyspnea, tachypnea, laryngospasm, cyanosis, pneumothorax, pulmonary edema, pleural effusion and respiratory arrest.<sup>10,14</sup> Cardiovascular responses may be observed in the electrocardiogram, such as, depression of the S-T segment, lowering or inversion of the T wave, premature ventricular beats and sinus arrhythmias.<sup>10,14,16</sup> Vasodilation is reported with decreased vascular resistance, decreased blood pressure and

increased blood flow, followed by a gradual return to normal pressures. 10,14,15 Gastrointestinal reactions commonly include vomiting, nausea and a metallic taste sensation.<sup>10,17</sup> These symptoms reported in human medicine may be displayed in the veterinary patients as retching and licking of the lips. Other gastrointestinal complications, associated with abdominal aortic angiography are paralytic ileus, mesenteric thrombosis and intestinal perforation.<sup>14,15</sup> Reactions of the renal system vary from transient oliguria and albuminuria to hemorrhagic nephrosis, anuria and acute renal failure.14.17 Cutaneous reactions in humans are often mild hyperemia and warmth sensation near the injection site, while urticaria, edema and gangrene have also been reported. 10,14 The exact mechanisms of these systemic reactions are unknown, but several physical properties of the contrast media have been implicated as the causal factors. Osmolality, iodine concentration, viscosity, pH and iodine content of the various contrast solutions have been proposed as significant characteristics of the compounds which relate to contrast-induced reactions.<sup>14-17</sup> These chemical properties were modified during the development of less toxic contrast media in order to decrease the incidence and severity of contrast-induced reactions.18

# Evolution of contrast media

### Inorganic and organic compounds

In 1896, only two months after Wilhelm Roentgen announced the discovery of xrays, the first angiogram was performed on an amputated human hand that

demonstrated the potential use of radiography for visualization of the arterial vasculature. The original contrast media used on post-mortem specimens contained lead or mercury to provide excellent radiographic contrast to illustrate the anatomical structures, but these compounds were not safe for use in live patients.<sup>14</sup> In 1923, Sicard and Forestier used a bismuth and oil suspension, Lipidol®<sup>a</sup>, for intravascular studies, which produced adequate radiographic contrast, but formed globules in the vessels, causing pulmonary emboli and death in experimental dogs. 14 In 1927, an inorganic, sodium iodide compound was used for contrast radiography of the kidney that provided good image contrast, but it was too toxic for use in live patients.<sup>14</sup> By the end of this decade, an organic iodide compound, called Selectan®, was discovered, that opacified the blood vessels and the collecting system of the kidneys following an intravascular injection and was well tolerated by the body.14 Several variations of organic contrast agents were developed over the following twenty years with the purpose of increasing radiographic contrast while decreasing the incidence and severity of systemic reactions.

# Triiodinated benzoic acid derivatives: ionic and non-ionic compounds

There was little improvement in contrast media during this time, until the 1950's, when the organic, triiodinated benzoic acid derivatives were simultaneously

Savage Laboratories, Inc., Houston, TX

<sup>&</sup>lt;sup>b</sup> Schering AG, West Germany

discovered in the United States and Germany.14 The diatrizoates (Hypaque®c, Renografin®d) and iothalamate (Conray®e) are relatively safe organic contrast agents that are still used in modern angiography (Figure 13A). These compounds dissociate in solution to an anion containing three iodine atoms, and a cation, which is usually sodium or methylglucamine (meglumine). These ionized particles create a high osmolar compound that is hypertonic to plasma, which may account for many of the adverse effects of intravascular contrast media.<sup>14-17</sup> The most significant advancement in contrast media evolution was Torsten Almén's discovery of the nonionic compounds.18 Metrizamide (Amipaque®f) was the first generation of nonionic contrast media that did not dissociate in solution, however, metrizamide was expensive to produce and unstable during autoclave sterilization (Figure 13B).<sup>19</sup> Iopamidol (Isovue®<sup>9</sup>, Niopam®<sup>h</sup>) and iohexol (Omnipaque®<sup>i</sup>) contain three iodine atoms per molecule, do not dissociate in solution and retain their stability through steam sterilization (Figure 13C).18-20 Ioxaglate (Hexabrix®<sup>1</sup>) achieves the same ratio

<sup>&</sup>lt;sup>c</sup> Winthrop Pharmaceuticals, Sterling Drug Inc., New York, NY

d E.R. Squibb & Sons, Inc., Princeton, NJ

Mallinckrodt, Inc., St. Louis, MO

<sup>&</sup>lt;sup>f</sup> Nyegard & Co., Oslo, Norway

<sup>8</sup> Squibb Diagnostics, Princeton, NJ

h Bracco Industria Chimca Spa, Milan, Italy

<sup>&</sup>lt;sup>1</sup> Nyegard & Co., Oslo, Norway (now available through Nycomed, Inc., New York, NY)

May and Baker, LTD., Essex, England

of iodine atoms to particles in solution (3:1) by linking together two triiodinated benzene rings to form a monoacid dimer (Figure 13D). Only one cation is released in solution and the anion contains six iodine atoms, so the ratio of iodine atoms to particles in solution is 6:2, which is equivalent to 3:1.18,20 Therefore, the second generation of non-ionic compounds has a 50% lower osmolality than the ionic compounds and produces the same radiopacity since it contains the same number of iodine atoms per molecule. The non-ionic, low osmolar, contrast media have a lower incidence rate of reactions, following angiographic procedures.18,20,21 Such advances in contrast materials have improved the quality and safety of angiographic studies.22

In human radiography, the benefits of non-ionic, low osmolar contrast agents have been recognized for years and clinically applied in high-risk patients.<sup>23</sup> The disadvantage of this new generation of contrast media is their high cost, which often limits their use in veterinary radiography to studies involving the brain and spinal cord, in which the high osmolar, ionic agents are highly toxic to neural tissues.<sup>20</sup> Since digital radiography is capable of producing and recording rapid interval exposures, repeat injections are rarely necessary and the volume of contrast material needed for a study is decreased, thereby reducing the cost and the likelihood of contrast-induced reactions.<sup>15</sup>

**IOHEXOL** 

носнустонсну

Figure 13 Differences between the common radiopaque contrast media are illustrated by their structural formulas. The ionic compounds (A) dissociate in solution resulting in a higher osmolarity than the non-ionic compounds (B, C). The monoacid dimer (D) is ionic, but the anion has six iodine atoms.

IOPAMIDOL

### LITERATURE REVIEW

#### **IMAGE MAGNIFICATION**

Several reference textbooks provide an explanation of the geometry and physical characteristics of radiography.<sup>1,8,13</sup> Based on these principles, formulas have been written that account for geometric and electronic image magnification. A mathematical formula has also been written that incorporates the contribution of penumbra to the size of a radiographic image. Unfortunately, since penumbra is literally a 'gray zone', each observer may determine the edge of an image to be at a slightly different location. Spears, et al, recorded angiographic studies of phantommodel vessels on 35 mm film then digitized these images for computer analysis. The computer program determined the vessel margins based on an algorithm that located points of increased radiopacity at specific spatial densities. A comparison of the computer-derived vessel diameters to the known diameters showed that the only variable which affected accuracy of the computed data was the concentration of contrast material within the vessel. The computer program was unable to locate the luminal edges of vessels less than 1 mm in diameter.<sup>24</sup>

Mensuration of structures, based on their radiographic appearance has been described by two methods in the veterinary literature. Linford, et al, reported on the normal length of the epiglottis in the Thoroughbred horse.25 To account for image magnification, two radiopaque markers were positioned, one on each side of the horses head. The magnification factor at each side of the head was determined by division of the actual marker size by the radiographic marker size. The epiglottis is a midsagittal structure, so the magnification factor at this level was determined by the average of the magnification factors at each side. The second approach to magnification is comparison of structures within the patient, included on the same radiograph, as a ratio, such as pulmonary vessel size to rib width<sup>26</sup> or heart diameter to thoracic cavity width. These relationships are not uniformly accepted within the No reports were found in the radiology literature that compared magnification factors based on the geometry of the imaging system to magnification factors determined by measurement of the radiographic image. No quantitative accounts have been made for electronic or photographic magnification, which are inherent in digital radiography.

### ANGIOGRAPHY

# Angiocardiography

Soon after the discovery of xrays by W. Roentgen in 1895, the science of radiography was used for anatomical studies and medical diagnostic procedures.

The original angiographic studies were performed on post mortem human and non-

human specimens, with a variety of radiopaque substances.<sup>14</sup> In 1896, Morton and Hammer published a book on radiography, entitled, *The xray, or, photography of the invisible and its value in surgery,* in which they wrote:

In teaching the anatomy of the blood vessels, the xray opens out a new and feasible method. The arteries and veins of dead bodies may be injected with a substance opaque to the xray and thus, their distribution may be more accurately followed than by any possible dissection.<sup>29</sup>

Angiography has been used in veterinary medicine for identification of normal vascular anatomy and pathology in many species. Non-selective angiocardiography is a radiographic study of the heart, following a peripheral venous injection of a contrast solution. Techniques for this procedure have been described in the normal dog, cat<sup>28,30</sup> and horse<sup>31</sup> with an iodine based contrast solution followed by serial radiographs. Wise, et al, used an ionic contrast media and reported electrocardiographic arrhythmias and two fatalities following repeated high dose injections in dogs.30 Carlsten also reported mild transient alterations in the ECG with occasional ventricular premature contractions, following a peripheral venous ionic contrast media injection, in horses undergoing non-selective angiocardiography.<sup>31</sup> No severe reactions were observed in Carlsten's study; however, the advantages of the non-ionic compounds for lowering the likelihood of adverse reactions were discussed, indicating the awareness of veterinary radiologists to the concern of direct and systemic effects of these ionic contrast media.31 Non-selective angiocardiography has been reported for diagnosis of congenital anomalies in dogs.<sup>32</sup> The technique described in this paper suggested

that any organic iodine contrast media may be used, at a dose of 0.5-1.0 ml/kg. A peripheral venous injection was made as a rapid bolus, followed by 4-6 radiographs at 1-2 second intervals. A simple design for a radiographic cassette changer was described so that the procedure may be completed without sophisticated equipment. Radiographs taken 4-5 seconds after the injection demonstrated contrast enhancement of the right heart and pulmonary circulation and later films showed contrast material in the left heart. The authors acknowledged that a slow bolus injection caused dilution of the contrast and late enhancement of the right heart. Superimposition of the left and right side structures made interpretation and diagnosis of some anomalies more difficult. Some ionic contrast media are more viscous therefore more difficult to inject rapidly, than the non-ionic media.<sup>15</sup> Use of a low viscosity, non-ionic compound would improve image quality by increasing the concentration of contrast material in a rapid bolus and decreasing the problems associated with delayed right heart filling from the slow bolus.

Selective angiocardiography involves the placement of a catheter into specific cardiac chambers, permitting the contrast agents to be delivered at the target site of interest, followed rapidly by serial radiography.<sup>28</sup> Fluoroscopy, a form of radiography that produces a dynamic visual image, is recommended for catheter guidance to the target location. Most modern cardiac catheterization imaging equipment is a form of digital radiography with specialized programs for cardiac studies.<sup>3</sup> The rapid interval images require use of an xray tube that can withstand the heat production and be cooled rapidly to avoid tube damage. Digital

subtraction angiography, a specific function of digital radiography for cardiac catheterization studies, uses a mask image to subdue the images of background structures so that successive images will only show the injected contrast material.<sup>1,3</sup>

# Peripheral angiography

Peripheral angiography has been used to demonstrate the arterial anatomy of the abdominal aorta in the goat, dog, pig and rabbit.33 This study noted excellent radiographic contrast with a lead suspension contrast media for illustration of the anatomy of the abdominal aorta, however, this technique cannot be used in live patients to be recovered from the procedure, since the lead suspension obstructs capillary beds.<sup>33</sup> Singh, et al, performed angiography using iothalamate and lead suspension on bovine tissue specimens to assess intestinal healing following three anastomotic procedures.<sup>34</sup> Two images of tissues injected with iothalamate, on the first day following surgery, demonstrated hypervascularity of the intestinal tissues and vessel dilation, but later studies, performed on post-mortem tissues with the lead suspension, did not show this dilated appearance to the vessels. The tissue hypervascularity seen on the earlier images may have been associated with the surgical procedure and early tissue healing; however, the vascular response to the infusion of the ionic contrast material, iothalamate, may have caused this vasodilation.<sup>21</sup> Singh, et al, also examined the vascular response to fracture healing in the ox by serial angiography following various methods of fracture repair.<sup>35</sup> A pattern of increased soft tissue vascularity and vasodilation was demonstrated with iothalamate, at the fracture site for four weeks following stabilization of the traumatized bone. Angiographic studies of the post-mortem specimens in this study, using lead suspension, did not demonstrate this hypervascular pattern, which was interpreted as regression of the vascular proliferation with the healing process. However, the lead suspension angiograms also failed to enhance major arteries to the long bone. The disparity between the hypervascular pattern on the iothalamate angiograms and the hypovascular pattern on the lead suspension angiograms may have been associated with the healing process, as suggested by the authors, but the affect of the contrast media should also have been considered.

Rendano, et al, performed repeated arteriographic studies in foals, to assess the changes in the cranial mesenteric artery with *Strongylus vulgaris* parasitism.<sup>36</sup> A catheter was passed, using fluoroscopic guidance with an image intensifier tube, from the common carotid artery to the abdominal aorta, ending just cranial to the celiac artery. Thirty to forty milliliters of an ionic contrast media was used for the angiogram and a single radiograph was taken one second after the injection. A second dose of contrast media was administered, in order to take a second radiograph, two seconds post-injection. The use of a digital radiography system with rapid interval exposures would have eliminated the need for a repeat injection, which would decrease the risks and expenses associated with additional contrast material administration. Vascular dilation, corrugation and thrombosis of the cranial mesenteric, ileocolic and right colic arteries were observed in infected foals, as well as dilations and irregularities in the hepatic, left gastric, caudal mesenteric,

jejunal and cecal arteries. With treatment, the vascular lesions regressed but there was some persistence of mildly dilated arteries on subsequent angiograms. The authors attributed the persistently abnormal vascular patterns observed in this study, including vascular occlusion and delayed blood flow, to the parasitic infection, because it was contrary to the vasodilation and increased blood flow associated with contrast media. However, the ionic contrast agents have been shown to cause alterations in red blood cell morphology that may lead to vascular thrombosis<sup>14,21</sup> and direct myocardial toxicity of the contrast media may cause bradycardia, secondary to increased vagal tone. Therefore, the results described in the study by Rendano, et al, may still have been due to contrast-induced hemodynamic reactions.

# Other imaging modalities: ultrasonography, MRI, nuclear scintigraphy

Several less invasive imaging modalities have been applied to the examination of the cardiovascular system, including ultrasonography<sup>37-41</sup>, Doppler ultrasonography<sup>42-45</sup>, magnetic resonance imaging<sup>46, 47</sup> and nuclear scintigraphy.<sup>48, 49</sup> While each of these modalities offers certain advantages, they are limited in their examinations of the smaller peripheral vessels. In ultrasonography, an image is created by the attenuation and reflection of sound waves at tissue interfaces.<sup>37</sup> This modality is effective for identification of large vessels; however, the resolution of small structures is limited by the probe size for axial resolution and length of a sound wave packet for depth resolution.<sup>1</sup> Contrast sonography has been described

for examination of the equine heart and identification of cardiac shunting anomalies, using saline, blood, 5% dextrose, CO<sub>2</sub>, and indocyanine green for contrast agents.<sup>31</sup> A mixture of CO<sub>2</sub> and blood provided the most sonographic contrast in the heart, but this technique has not been applied to peripheral vessels.<sup>31</sup> Transrectal sonography has been used to evaluate the cranial mesenteric and ileocolic arteries in normal horses and horses infected with *S. vulgaris.*<sup>38, 39</sup> Ultrasonography has been reported as an effective, relatively non-invasive method for diagnosis of aorto-iliac thrombosis in the horse for evaluation of large vessels, accessible via the transabdominal or transrectal approach.<sup>40,41</sup>

The Doppler effect is an apparent change in the frequency of sound waves reflected from the interface of a tissue that is moving relative to the sound wave receiver.<sup>42</sup> Doppler ultrasonography is used for evaluation of laminar and turbulent blood flow through the heart and peripheral vessels.<sup>43</sup> Continuous and pulsed Doppler produce a graphic image of flow velocities and direction, while color flow Doppler adds the visual aid of color to various velocities and directions of flow on a real time, two dimensional image.<sup>1</sup> A subcutaneous arteriovenous fistula on the thoracic body wall of a horse, was diagnosed with Doppler sonography.<sup>44</sup> Contrast angiography was not performed in that case because the originating vascular supply to the lesion could not be identified. The applications of ultrasonography are limited by the inability of sound waves to effectively penetrate air, bone and the keratinized hoof wall, so a soft tissue window of access is necessary to image deep structures. Adair, et al, used laser Doppler flowmetry to measure blood flow at the

coronary band and dorsal hoof laminae in normal horses. This technique is similar to Doppler ultrasound, but it uses a beam of light in place of the sound wave. An 8 mm hole was cut in the dorsal hoof wall, to the junction of epidermal and dermal laminae, to measure flow in the underlying laminar vessels. This method had limited utility, as the window of access was limited to a small area and limited in duration of access due to drying of the laminae with exposure to air. The effect of mechanically drilling the hole may have altered local hemodynamics by traumatizing the underlying tissues. This technique appears to be useful for quantifying blood flow at a restricted but specific location, while angiography allows for visualization of vessels over a larger field of view.

Magnetic resonance imaging (MRI) uses magnetic forces to cause vibration of the atomic particles within the body tissues. Leach particle vibrates at a specific frequency, characteristic of the atom and the magnetic field. The contrast between tissues is altered by varying the sequence of pulsation of one magnetic field or by the addition of gadolinium as an intravenous contrast material. In MRI angiography, the movement of blood helps to differentiate the vessels from the surrounding tissues. Many artifacts are caused by turbulent or slow flowing blood that interfere with image interpretation and MRI angiography produces images of lesser resolution than radiographic angiography so this newer modality is not considered as specific as contrast radiography for delineation of vascular lesions.

Nuclear scintigraphy is also a non-invasive modality for imaging vascular flow patterns, that records gamma radiation emitted from the patient, following

administration of a radioactive pharmaceutical.<sup>48</sup> Nuclear angiocardiography follows the vascular distribution of a radioactive material, 99mTechnetium, after a peripheral venous injection. The energy emitted from the patient is detected by a large crystal in the camera, creating a signal that is transmitted to a dedicated computer for image production. First pass nuclear angiocardiography (FPNA) monitors activity during the initial phase of radioactivity through the heart. Specialized computer programs are then used to calculate several cardiac function indices, such as left ventricular ejection fraction, cardiac output, valvular regurgitant fraction and pulmonary/systemic perfusion ratios.48,49 This technique is effective for identification of cardiac abnormalities, such as, valvular insufficiencies, intracardiac shunts and myocardial failure.<sup>49</sup> Gaited equilibrium nuclear angiocardiography (GENA) uses an ECG signal to trigger data acquisition at a selected phase of the cardiac cycle, after the radiopharmaceutical has distributed throughout the vascular pool. This method accumulates information over many cardiac cycles, increasing the activity counts for each image. Patient motion is the limiting factor in this procedure, since data are summated over a prolonged period of time.<sup>49</sup> Nuclear angiography provides visual and quantitative information about the physiological distribution of a radiopharmaceutical in the body by a relatively non-invasive procedure as compared to cardiac catheterization for selective radiographic angiography. However, the anatomical detail produced in scintigraphic images is not as well defined as those produced by digital radiography. Regions of tissue may be evaluated for blood perfusion by scintigraphy, but individual vessels are not distinctly delineated by this technique.<sup>50</sup> In summary, there are advantages to each of these alternative imaging modalities, but not one of them provides images of small peripheral vessels that are equal or superior in detail to contrast enhanced digital angiography.

### Angiography of the distal limb

The vascular supply of the distal limb has been investigated in several species, using contrast radiography.<sup>51-56</sup> The normal angiographic appearances of the bovine<sup>51</sup> and caprine<sup>52</sup> digits have been reported. Gogoi, et al, examined the blood supply to normal and abnormal bovine feet, in anesthetized patients.<sup>51</sup> The median artery (thoracic limb) or dorsal metatarsal artery (pelvic limb) were catheterized, followed by intraarterial injection of 15-20 ml sodium iothalamate, an ionic contrast agent. Significant alterations in the vascular pattern were observed in various pathological conditions.

Angiography has been performed in normal and laminitic horses, to assess distal limb perfusion. 53-56 In all of these studies, the patients were anesthetized for catheterization of a distal limb artery and injection of a radiopaque solution. Radiographs of the distal limb were produced at various time intervals following contrast media injection, with the limb in various positions. Coffman, et al, performed angiovenography on four horses, before and after production of alimentary-induced acute laminitis. 53 Sodium and meglumine diatrizoate (Hypaque®), 20-30 ml, was injected via the common digital artery for each sequence

of radiographs. Angiograms were performed in the dorsopalmar and mediolateral views, using high speed film and high speed intensifying screens. While this filmscreen combination was useful to minimize patient motion artifact and to decrease radiation exposure, this technique was done at the expense of image detail.<sup>1</sup> In an anesthetized patient, when motion is not a significant concern, sharper images would have been produced with slower speed, detail screens. In the normal feet, each study demonstrated contrast enhancement of the medial and lateral digital arteries, terminal arch, several branches through the distal phalanx, circumflex artery and arteriovenous plexuses at the digital cushion and coronary corium. Images of the laminitic feet demonstrated dilation of the arteries to the proximal and middle phalanges and dilation of the digital arteries proximal to the terminal arch. There was a marked decrease in size of the terminal arteries and poor filling of the arteriovenous plexuses of the hoof. It was concluded that the digital arteries constrict at the entrance of the volar foramina during acute laminitis, that blood pools in capillary beds and that blood is shunted through other vessels of the distal limb.<sup>53</sup> Angiographic images from the same horses, before and after induction of laminitis, provided useful information for comparative purposes.

Clinically normal and chronically laminitic feet have been examined by angiography, using sodium and meglumine diatrizoate (Hypaque®) for vascular contrast.<sup>54</sup> Radiographs were taken at a consistent technique using par speed film and high speed screens. The arterial vessels visualized in the clinically normal horses included the digital arteries, the terminal arch and its branches to the distal

margin of the third phalanx and fine vessels in the corium of the coronary band. In this paper, Ackerman, et al, reported the diameter of the digital arteries to be 0.4 cm, tapering to 0.2-0.3 cm at the terminal arch and there were 8-10 branches from the terminal arch that were 0.1-0.2 cm in diameter. In the laminitic subjects, filling of the terminal arch and its branches was variable, with some studies showing increased size and decreased number of arterial branches while other studies had poor filling of the terminal arch and normal branches along with focal avascular regions. A pattern of alternating vascular widening and narrowing was observed in one laminitic study, however histopathological examination of this artery did not reveal any abnormalities. Arterial catheterization and vessel irritation from the contrast material may cause vascular spasms, which may have accounted for this pattern.<sup>57</sup> Ackerman, et al, concluded that chronically laminitic feet were characterized by an irregular vascular pattern in the corium and by poor filling of the terminal arch, in comparison to the symmetrical pattern observed in normal feet.<sup>54</sup> While this information is the only study that describes the diameter of arteries in the equine foot based on their angiographic appearances, no information was provided regarding the method of measurement or the contributing factors of radiographic magnification on vessel size. This information on measurement and radiographic technique is important in order to compare and assess the results of this studies to other research or clinical data.

In a study designed to examine the collateral blood flow to the equine foot, Scott, et al, ligated the medial palmar arteries and medial palmar digital arteries of seven ponies, then performed angiographic studies under general anesthesia.<sup>55</sup> Meglumine iothalamate was the contrast agent used to identify changes in the vascular pattern and filling time associated with arterial ligation. Collateral vessels were identified on the angiograms that maintained blood flow to the distal limb following ligation of the arteries. Immediately after ligation of the medial palmar artery, the second and third dorsal and palmar metacarpal arteries were found to be the main alternate channels of collateral blood flow and the lateral palmar artery continued to supply blood to the terminal arch. This study demonstrated the ability of the equine digit to compensate for vascular occlusion by using collateral vessels to maintain perfusion to the foot.<sup>55</sup>

In a clinical case report, Scott, et al, used angiography to assess vascular perfusion of the distal limb in three horses. These angiograms demonstrated the presence of vascular lesions, including partial to complete obstruction of the medial and lateral palmar digital arteries and retained contrast media within the corium. Several possible causes were proposed for these observations, including decreased arterial pressure, increased venous pressure, vasoactive factors, reduced frog and digital pressures and alterations in blood flow due to heparinization.<sup>56</sup>

Van Kraayenburg, et al, performed peripheral angiographic studies in conscious, standing horses and distal limb specimens to assess the effect of vertical force on blood flow in the palmar digital arteries. This report demonstrated interruption of blood flow at the level of the distal sesamoid bone and in the solar canal under conditions of high vertical force. Cessation of blood flow was absent in

limb specimens that were not under stressed conditions. The intraarterial catheter was advanced beyond the bifurcation of the medial palmar artery to enter one branch of the palmar digital artery, so that injected contrast medium entered the terminal arch from only one direction. Histologic sections of the palmar digital artery were taken at the level of the constriction and wall thickness was measured to determine percentage wall thickening and circumferencial luminal reduction. The angiographic images were useful for subjective assessment of luminal patency, but quantitative measurements were acquired only from the histologic sections and not from the radiographic images of intact vessels in the live horses or limb specimens.<sup>58</sup>

All of these reports were attempts to document the angiographic appearance of normal and laminitic feet. 53-56.58 They were performed using conventional fluorescent screens with thick phosphor layers that decreased image sharpness. In contrast, the fluorescent screens in digital radiography, within the image intensifier tube, have a thinner phosphor layer with more crystals, designed to improve image sharpness. The xray tube is constructed to provide a high amperage so the exposure time may be kept short. Both of these factors contribute to improved image detail and resolution of small vessels within and around the distal phalanx of the horse.

### STATEMENT OF HYPOTHESIS

Development of a technique for visualization of the intricate vessels of the equine foot and measurement of their diameters would be useful for evaluation of

vascular perfusion to the distal limb. There are two hypotheses established for this thesis. First, the total magnification factor for a digital radiographic imaging system may be quantified by two methods, 1) comparison of a radiopaque object to measurements of its radiographic image, and 2) calculation of individual magnification factors for each component of the DR system based on physics of radiography, then multiplication of these factors to determine the total magnification factor. The results of these two methods for determining the total magnification factor should be equal. The second hypothesis states that arterial vessels of an invitro model of the equine foot may be identified and vessel luminal diameter may be measured on angiographic images of the limb in two positions. Correction of these measurements for image magnification in each view should result in equal values for luminal diameter of each vessel between the two positions.

#### **METHODS AND MATERIALS**

### **MAGNIFICATION FACTORS**

Two methods were employed to calculate the total magnification factor of the imaging system, used in the present study. The first method used a radiopaque metallic object of known size and the radiographic images of this marker to determine total magnification (M) from the formula:

M = image size + object size.

The second method calculated each component of total magnification independently, then combined these factors to determine total magnification (M) from the formula:

$$M = M_e \times M_e \times M_p$$

M = total magnification

M<sub>g</sub>= geometric magnification

Me= electronic magnification

M<sub>p</sub>= photographic magnification

The total magnification factors determined by these two procedures were compared to identify instrument settings under which they produce similar results.

#### Method 1

The width of a rectangular metallic marker was measured with digital calipers<sup>a</sup> and this value was called the object width. The marker was placed on the patient table of a General Electric ADVANTX<sup>®</sup> radiography unit<sup>b</sup> and imaged with the digital radiography system, at 65 kVp, 100 mA, phototimer controlled exposure time and 0.3 mm focal spot. The intensifier tube was positioned at 25, 30, 35, 38, 40 and 45 cm above the table and the intensifier tube was in the 9 inch, 6 inch and 4.5 inch modes of function (Figure 14). These images were printed at 1:1, 4:1, 6:1 and 12:1 formats by the laser imager<sup>c</sup> to fit 1, 4, 6 or 12 images, respectively, on each sheet of 14x17" sheet of film,<sup>d</sup> then the film was developed in an automatic processor.<sup>c</sup> The width of the marker was measured on each radiograph three times with digital calipers and these values were called the image widths.

<sup>&</sup>lt;sup>a</sup> Digomatic calipers, Model M500=351, Mitutoyo, Japan

<sup>&</sup>lt;sup>b</sup>General Electric SFX II ADVANTX®, GE Medical Systems, Milwaukee, WI

<sup>&</sup>lt;sup>c</sup> Laser Imager XLD, 3M Medical Imaging Systems Division, St. Paul, MN

<sup>&</sup>lt;sup>d</sup> Infrascan® MC Laser Imaging film, DuPont Medical Systems, Wilmington, DE

<sup>\*</sup> Kodak RP X-OMAT\*, Model M6B, Eastman Kodak Company, Rochester, NY

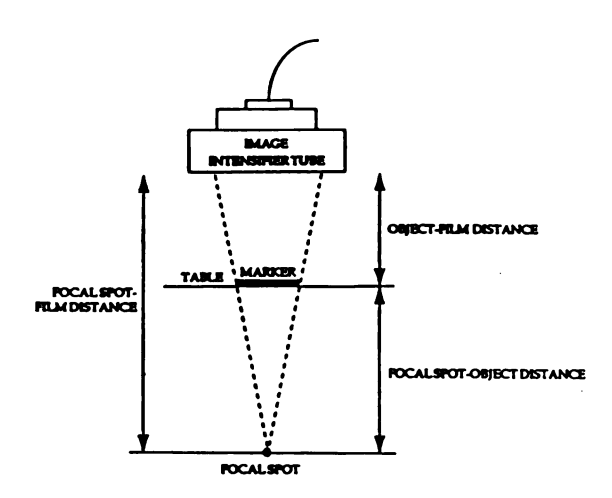


Figure 14 Digital radiographic images of a metallic marker were produced with the marker on the patient table.

The total magnification factor (M) for each focal-film distance, intensifier tube mode and printer format were calculated, using the object width and the image widths in the formula:

# M=image width + object width

Since these marker images incorporated all of the magnification effects of digital radiography, these values for magnification factors represented total magnification of the system.

### Method 2

The three components to image magnification in digital radiography include geometric, electronic and photographic magnification. The magnification factor from each component was calculated individually, based on the theories of image

magnification in radiography and photography, using dimensions of the imaging system obtained from the specifications manual for the General Electric ADVANTX® imaging system², GE service engineers¹² or measured directly from the equipment.

### Geometric magnification

The xray tube was positioned at a fixed distance below the table, so focal-object distance (FOD) was 49.5 cm for every image. Focal-film distance was the sum of FOD and the distance from the table to the intensifier tube (25, 30, 35, 38, 40 and 45 cm). Using these values for FOD (49.5 cm) and FFD (74.5, 79.5, 84.5, 87.5, 89.5, 94.5 cm), geometric magnification (Mg) was calculated for each position of the intensifier tube from the formula:

M<sub>g</sub>=focal-film distance + focal-object distance.<sup>1</sup>

## Electronic magnification

Electronic magnification occurred within the image intensifier tube, when the electronic signal was focused on the output screen by the electrostatic focusing lenses. The intensifier tube input screen was 22.0 cm in diameter and the output screen was 2.20 cm in diameter, so all images were magnified by a factor of 0.10, or minified by 10X, across the tube. The electrostatic focusing lenses altered the focal point of the electronic signal to cause additional magnification of the image which varied with the intensifier tube mode of function. In the 9 inch mode, all of the electrons from the input screen were focused onto the output screen, so the

magnification factor was 1.0. In the 6 inch mode, only the central 66% of the input screen electrons were included on the output screen, so the image was magnified by a factor of 1.5 and in the 4.5 inch mode, the central 50% of the electron signal was magnified by 2.0X to fill the output screen. Thus, electronic magnification ( $M_e$ ) in the 9 inch mode was 0.10 (0.10 x 1). In the 6 inch mode  $M_e$  was 0.15 (0.10 x 1.5) and in the 4.5 inch mode  $M_e$  was 0.20 (0.10 x 2).

### Photographic magnification

Photographic magnification occurred from the output screen of the intensifier tube to the laser imager, where the laser beam was directed to expose the film. The output screen was 2.20 cm in diameter and the radiographic image diameter was 28.0 cm in the 1:1 format, 14.0 cm in the 4:1 format, 12.2 cm in the 6:1 format and 9.0 cm in the 12:1 format. Magnification is equal to image size divided by object size, so photographic magnification (M<sub>p</sub>) was determined by the formula:

M<sub>p</sub>=radiographic image diameter + output screen diameter.

# Total magnification

Total magnification factors were calculated by the product of geometric, electronic and photographic magnification factors:

$$M=M_g \times M_e \times M_p$$

### Statistical analysis

In Method 1, the average of three repeated measurements of each image was used for image size, to determine the total magnification factors. These values for the measured total magnification factors (TMFm) were analyzed by the linear models procedure, multiple regression analysis. Univariate and multivariate analyses were performed on the independent variables, including focal-film distance (FFD), image intensifier tube mode of function (II mode) and laser printer format (format).

The calculated total magnification factors (TMFc) from Method 2 were compared to the TMFm values from Method 1 by the paired T-test. A variable, delta, was defined as the difference between the magnification factors from these two methods (delta=TMFm-TMFc) for further analysis. A linear models procedure, multiple regression analysis of delta was performed to identify relationships between these independent variables and delta.

The statistical models built by these regression analyses were used to determine fitted values for TMFm and delta and their residuals were tested by the Wilk-Shapiro test for normal distribution.

f STATISTIX 3.1, Analytical software, St. Paul, MN

### LIMB PERFUSION AND ANGIOGRAPHY

### In-vitro perfusion model

The right thoracic limb was removed, on each of six horses, at the mid-diaphyseal region of the third metacarpus, immediately following euthanasia with a barbiturate overdose (Table 1). The medial palmar artery was catheterized from the severed end of the vessel, by advancing a piece of polyethylene tubing 5.0 cm distad. The catheter was 10 cm long, with an internal diameter 1.67 mm and an external diameter 2.42 mm (PE 240), connected to a 16 g intravenous needle. The vessels were flushed with 120 ml heparinized saline (2000 units/100 ml saline) and the external surfaces of the limb were cleansed of debris.

Table 1 Following euthanasia, the right thoracic limb was removed on each of six horses.

HORSE	BREED	AGE (yr)	BODY WEIGHT (kg)	GENDER
1	Grade	3	420	gelding
2	Thoroughbred	3	340	gelding
3	Arabian	4	370	mare
4	Standardbred	4	400	gelding
5	Grade	unknown	365	gelding
6	Grade	4	320	gelding

Within ten minutes of euthanasia, the limb was placed in a standing position on the digital radiography patient table, supported by a three prong clamp and ring stand. The support prongs contacted the limb over its dorsolateral and dorsomedial cutaneous surfaces, to avoid interference with the palmar vessels. The metacarpophalangeal joint was in slight extension (approximately 10° from

perpendicular to the table) to allow collection of venous effluent, draining from the metacarpal veins. The collection bin was placed palmar to the foot to be excluded from the imaging field. The arterial catheter was connected to a pump<sup>g</sup> by polyethylene tubing (internal diameter 2.0 mm) and a short segment of an intravenous fluid line, including an injection port. The foot vasculature was perfused with a Krebs Henseleit solution (Appendix A), that was maintained at 37°C and aerated with 95% O<sub>2</sub> and 5% CO<sub>2</sub> (Figure 15). This isolated limb perfusion technique was adapted from the method reported by Elmes and Eyre for investigation of vascular reactivity in the bovine foot.<sup>59</sup> The pump flow rate was initially set to perfuse the limb at a flow rate of 150 ml/min. This rate was calibrated at position 8 on the pump setting dial and measured by the volume of solution pumped into a graduated cylinder in one minute. A pressure monitorh was connected between the pump and foot to register arterial perfusion pressure. The pump flow setting was adjusted between 150-175 ml/min. to maintain a perfusion pressure of 100 mm Hg.60 The limb was perfused for five minutes at this flow rate to demonstrate a steady state of vessel diameter as determined by a consistent arterial perfusion pressure of 100 mm Hg.

<sup>&</sup>lt;sup>9</sup> Masterflex<sup>®</sup>, Model 7014, Cole Palmar

<sup>&</sup>lt;sup>h</sup> Simultrace Recorder, VR 12/16, Honeywell, Pleasantville, NY

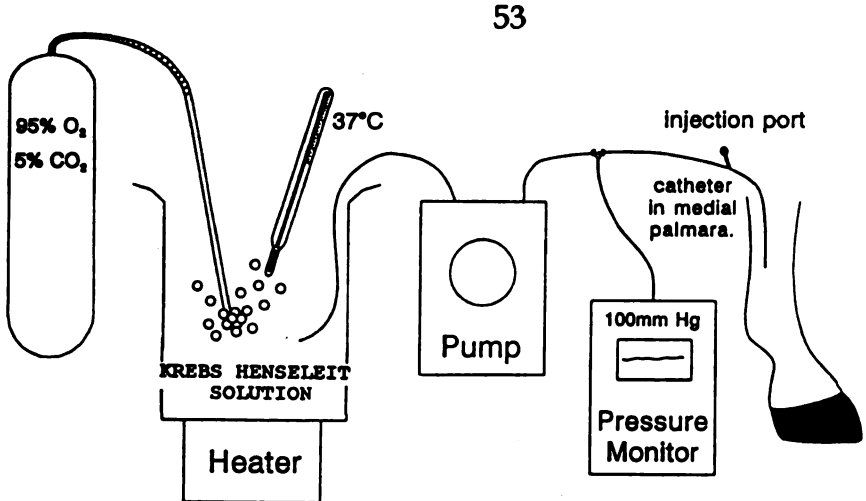


Figure 15 The vasculature was perfused with an oxygenated (95% O2/5% CO2), heated (37oC) Krebs Henseleit solution at 100 mm Hg arterial perfusion pressure.

# **Angiography**

Angiographic studies were performed on each limb, in the standing and lateral recumbent positions. In both studies, the radiographic technique was 65 kVp, 100 mA, phototimer controlled exposure time and 0.3 mm focal spot. The contrast medium was 10 ml of iopamidol 61% (37°C), injected as a rapid bolus, via the injection port in the tubing. Images were acquired at one frame per second for 25 seconds, beginning at the initiation of the contrast medium injection. Changes in arterial perfusion pressure following injection of the contrast medium were noted. All of the palmarodorsal studies and five (5/6) of the lateromedial studies were recorded in the 9 inch mode of the image intensifier tube. One lateromedial study (horse 1) was recorded in the 6 inch mode. All of the images were printed at a

<sup>&</sup>lt;sup>1</sup> Isovue-300°, 300 mg I/ml, Squibb Diagnostics, Princeton, NJ

consistent window width (255) for image contrast and window level (110-125) for image brightness in the 6:1 format and developed in an automatic processor.

#### Palmarodorsal view

The first angiogram was performed with the limb in a standing position, on the table. This was called the palmarodorsal (PD) view due to the direction of xray transmission through the foot, from the xray tube below the table, to the image intensifier tube above the foot (Figure 16). The image intensifier tube was positioned 38.0 cm above the table, with the foot centered in the field of view. This table to intensifier tube distance was selected to avoid interference of the limb preparation by the intensifier tube. The xray tube was located in a fixed position, 49.5 cm below the table, so focal-film distance for the PD study was 87.5 cm.

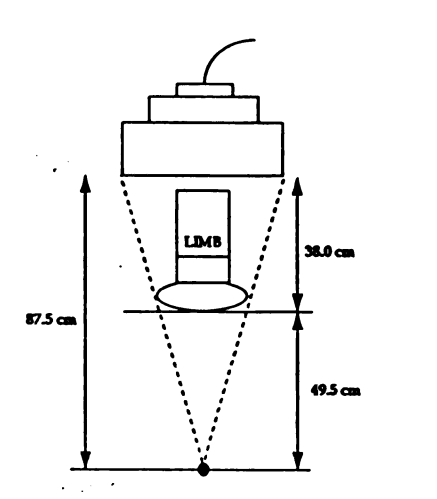


Figure 16 The palmarodorsal study was performed with the limb in a standing position, FFD=87.5 cm, FOD=49.5 cm and object-film distance=38.0 cm.

#### Lateromedial view

Following the palmarodorsal study, each limb was repositioned in lateral recumbency for the lateromedial (LM) study. The arterial perfusion pressure decreased during repositioning so the perfusion rate was increased to approximately 175 ml/min to maintain arterial perfusion pressure at 100 mm Hg. The image intensifier tube was positioned 25.0 cm above the table and the xray tube remained at 49.5 cm below the table, resulting in the new FFD of 74.5 cm (Figure 17).

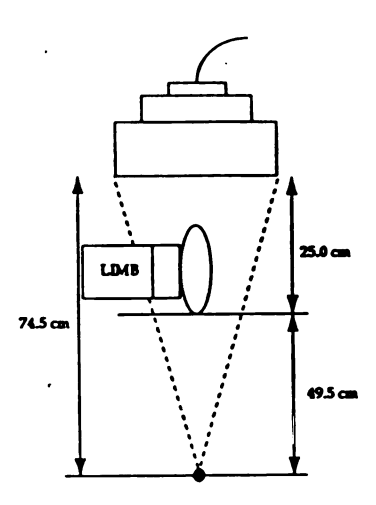


Figure 17 The lateromedial study was performed with the limb in lateral recumbency, FFD= 74.5 cm, FOD=49.5 cm and object-film distance=25.0 cm.

### Vessel identification and measurement

### Vessel identification

Anatomy of the normal blood vessels of the equine foot was examined, using several published references.<sup>61-64</sup> Four equine thoracic distal limb specimens were

perfused with Batson's solution followed by soft tissue digestion by a colony of Dermestes lardius and Dermestes vulpinus beetles to create corrosion casts of the digital arteries. Two additional limbs were perfused with red colored latex and permitted to solidify for three days prior to dissection to visualize the arteries. These limb preparations were from the same horses as those used in the perfusion studies and served only to familiarize the author with the vascular anatomy. No attempt was made to measure and correlate the size of the plastic column within the dissected vessels with the vessels observed radiographically. Table 2 is a list of the arterial vessels identified on angiograms in the palmarodorsal and lateromedial studies.

Table 2. The palmar digital artery and its major branches to the foot were identified on digital angiograms.

Common name <sup>61</sup>	Nomina Anatomica Veterinaria Terminology <sup>62</sup>
palmar digital a.	A. digitalis palmaris communis II
bulbar a.	Ramus tori digitalis
coronary a.	A. coronalis
dorsal phalangeal a.	Ramus dorsalis phalangis proximalis
palmar phalangeal a.	Ramus palmaris phalangis proximalis
distal dorsal phalangeal a.	Ramus dorsalis phalangis distalis
distal palmar phalangeal a.	Ramus palmaris phalangis distalis
dorsal branch of distal dorsal phalangeal a.	Ramus dorsalis of ramus dorsalis phalangis distalis
palmar branch of distal dorsal phalangeal a.	Ramus palmaris of ramus dorsalis phalangis distalis
terminal arch	Arcus terminalis
dorsal branches of terminal arch	Ramus dorsalis arcus terminalis
solar branches of terminal arch	Ramus palmaris arcus terminals
solar margin a.	Ramus marginis solearis

<sup>&</sup>lt;sup>1</sup> Batson's No. 17 Plastic Replica and Corrosion Kit, Polysciences, Inc., Warrington, PA

#### Vessel measurement

The total magnification factors determined by comparison of a metallic marker width to its radiographic image width (method 1) were used to calculate vessel diameters, since both the marker images and the vessel images were measured with the digital calipers. The formula:

Magnification factor = image size + object size

was rewritten to solve the equation for object size:

Object size = image size + magnification factor

Using this formula, the sizes of the vessels within the body were determined by their radiographic images. Vessel size measurements from the radiographs were divided by the total magnification factor, for the appropriate FFD, intensifier tube mode and printer format to determine the actual vessel widths.

#### Statistical analysis

The repeatability of this angiographic technique was described by the frequency of vessel identification as a percentage of the six feet examined. Descriptive statistics of the vessels included mean values for each vessel diameter, in each position, averaged for the six feet and reported with the standard deviation of the mean. Measurements of vessels that were only identified on one view, were discarded for further statistical analysis. The vessel diameters, as determined from the digital angiographic images in the palmarodorsal and lateromedial views were compared by the paired T-test (P<.05).

The diameter of the contrast enhanced lumen of these vessels were measured with digital calipers on one image of each foot in the palmarodorsal and lateromedial angiograms. The images were selected from the late arterial perfusion phase prior to contrast enhancement of the small capillaries and venules of the foot. All the measurements were performed within a 24 hour period to maintain consistency in the technique. In both views, the palmar digital artery was measured at three locations: 1) 1.0 cm proximal to the bulbar artery, 2) 1.0 cm proximal to the dorsal phalangeal artery and 3) at the entrance of the solar canal of the third phalanx (Figure 18). The terminal arch and solar margin arteries were measured at the sagittal midline and the remaining vessels were measured 1.0 cm distal to their origin from the palmar digital artery.

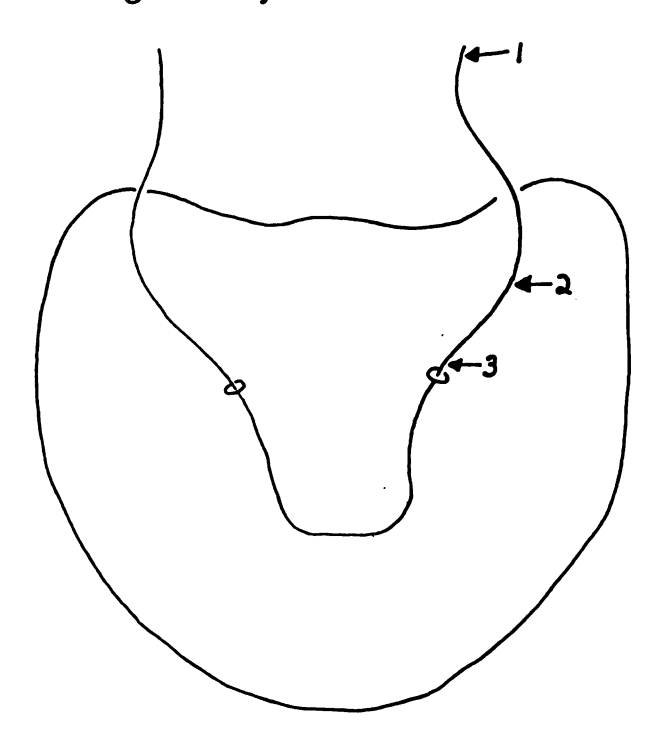


Figure 18 The palmar digital artery was measured at three locations: 1) 1.0 cm proximal to the origin of the bulbar a., 2) 1.0 cm proximal to the origin of the dorsal phalangeal a. and 3) at the entrance to the solar canal.

#### **RESULTS**

#### **MAGNIFICATION FACTORS**

Total magnification factors (TMFm) determined by comparison of the size of a metallic object to measurements of its radiographic image, are presented in Table 3, for each combination of focal-film distance (FFD), image intensifier tube mode (II mode) and printer format (format). The image widths from the three repeated measurements of each radiographic image with the mean and standard deviation of the mean values are listed in Appendix B. Image magnification factors ranged from 0.70 (at the shortest FFD, largest II mode and highest format) to 5.41 (at the longest FFD, smallest II mode and lowest format).

Several trends were identified in these magnification factors, which related to the independent variables, FFD, II mode and printer format. As FFD increased, the magnification factors increased slightly (Figure 19). As the II mode increased, the total magnification factors decreased markedly (Figure 20) and as the number of images printed per sheet of film (format) increased, the total magnification factor decreased (Figure 21).

Table 3 Total magnification factors (TMFm) were determined by measurement of a metallic marker and its radiographic image.

II MODE 9 inch	PRINTER FORMAT				
FFD (cm)	1:1	4:1	6:1	12:1	
74.5	2.15	1.07	0.93	0.70	
79.5	2.27	1.13	0.97	0.73	
84.5	2.39	1.18	1.03	0.77	
87.5	2.47	1.22	1.05	0.79	
89.5	2.54	1.25	1.09	0.81	
94.5	2.65	1.31	1.14	0.86	

II MODE 6 inch	PRINTER FORMAT				
FFD (cm)	1:1	4:1	6:1	12:1	
74.5	3.10	1.54	1.33	1.01	
<i>7</i> 9.5	3.28	1.62	1.39	1.08	
84.5	3.47	1.72	1.50	1.12	
87.5	3.61	1.77	1.54	1.15	
89.5	3.69	1.82	1.59	1.18	
94.5	3.88	1.90	1.65	1.24	

II MODE 4.5 inch	PRINTER FORMAT				
FFD (cm)	1:1	4:1	6:1	12:1	
74.5	4.35	2.14	1.85	1.40	
79.5	4.57	2.27	1.93	1.50	
84.5	4.88	2.40	2.09	1.55	
87.5	5.04	2.47	2.16	1.61	
89.5	5.17	2.53	2.20	1.66	
94.5	5.41	2.64	2.29	1.71	

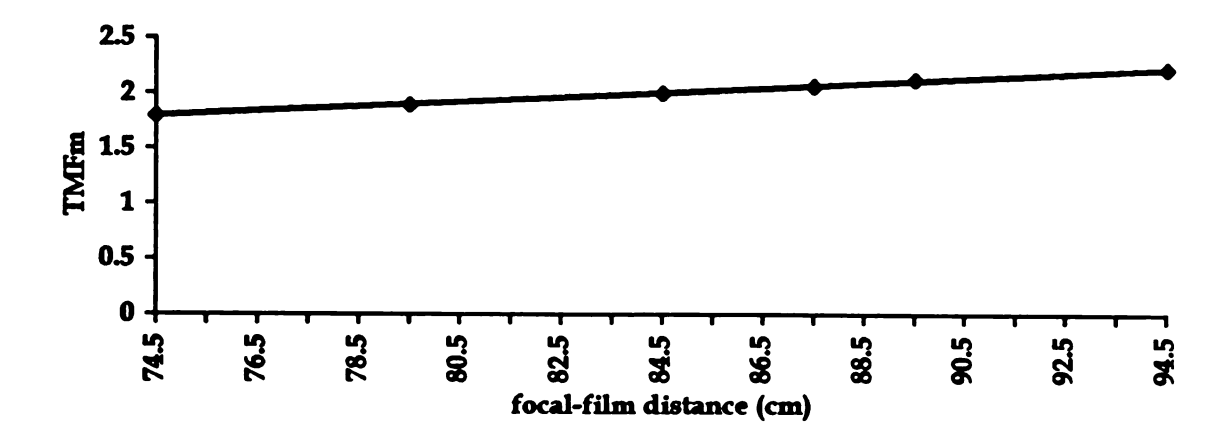


Figure 19 The total magnification factors (TMFm) increased slightly as FFD increased.

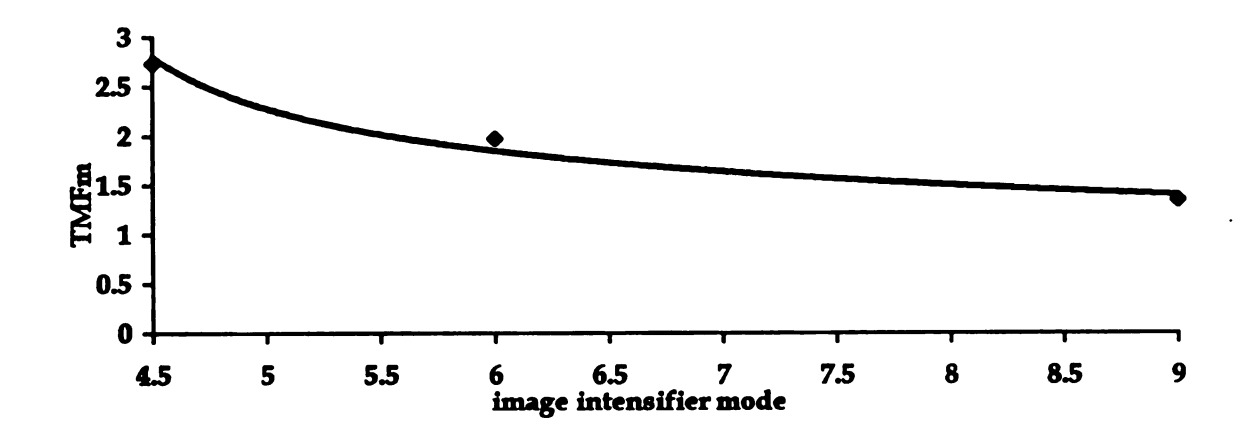


Figure 20 As II mode increased, the total magnification factors (TMFm) decreased steadily.

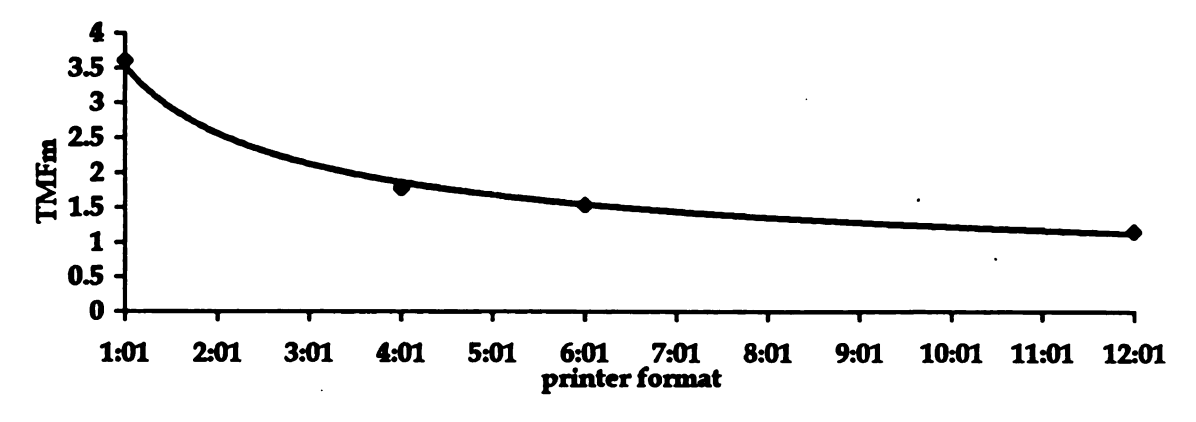


Figure 21 The total magnification factors (TMFm) decreased as the number of images per sheet of film (format) increased.

Statistical analysis determined that the total magnification factors (TMFm) were significantly different at each FFD, II mode and format at P<.0001. Other significant predictor variables included the interaction of FFD and format, (format)<sup>2</sup>, (II mode)<sup>2</sup> and (format)<sup>3</sup>. The formula for the linear function of TMFm, as defined by the linear models procedure, was:

Fitted TMFm = 8.968 + 0.021663(FFD) - 1.5701(FORMAT) - 1.4139(II MODE) + 2.8479(FFD x II MODE) + 0.18996(FORMAT)<sup>2</sup> + 0.069753(II MODE)<sup>2</sup> - 0.0083247(FORMAT)<sup>3</sup>

The R<sup>2</sup> value for this model was 97.5% and the residuals were normally distributed, as determined by the Wilk-Shapiro test (P=0.9472). The output of each univariate and multivariate analysis is presented in Appendix B. The values for FFD, II mode and format, used in this study, were entered into this formula to calculate fitted values for TMFm, based on the linear function. Graphs of the fitted TMFm values for each FFD, II mode and format are presented in Appendix B. These graphs are almost identical to the experimental data because the statistical model accounted for 97.5% of the variability in TMFm.

Total magnification factors (TMFc) calculated for each FFD, II mode and printer format, using formulas derived from the physics of radiography and photography, are listed in Table 4. The contributing magnification factors for each component, geometric, electronic and photographic magnification, are listed in Appendix C. TMFc was significantly smaller than TMFm for every combination of FFD, II mode and format.

Table 4 Total magnification factors (TMFc) were calculated for the imaging system.

II MODE 9 inch	PRINTER FORMAT			
FFD (cm)	1:1	4:1	6:1	12:1
74.5	1.92	0.96	0.83	0.62
79.5	2.05	1.02	0.88	0.66
84.5	2.18	1.09	0.94	0.70
87.5	2.27	1.13	0.97	0.73
89.5	2.30	1.15	0.99	0.74
94.5	2.43	1.22	1.05	0.78

II MODE 6 inch	PRINTER FORMAT			
FFD (cm)	1:1	4:1	6:1	12:1
74.5	2.88	1.44	1.24	0.92
79.5	3.07	1.54	1.32	0.98
84.5	3.26	1.63	1.40	1.05
87.5	3.40	1.70	1.46	1.09
89.5	3.46	1.73	1.49	1.11
94.5	3.65	1.82	1.57	1.17

II MODE 4.5 inch	PRINTER FORMAT				
FFD (cm)	1:1	4:1	6:1	12:1	
74.5	3.84	1.92	1.65	1.23	
79.5	4.10	2.05	1.76	1.31	
84.5	4.35	2.18	1.87	1.39	
87.5	4.53	2.27	1.95	1.45	
89.5	4.61	2.30	1.98	1.48	
94.5	4.86	2.43	2.10	1.56	

There was no significant difference in delta (TMFm-TMFc) over the six focal-film distances (Figure 22). As the II mode increased, delta decreased (Figure 23) and as printer format increased, delta decreased (Figure 24).

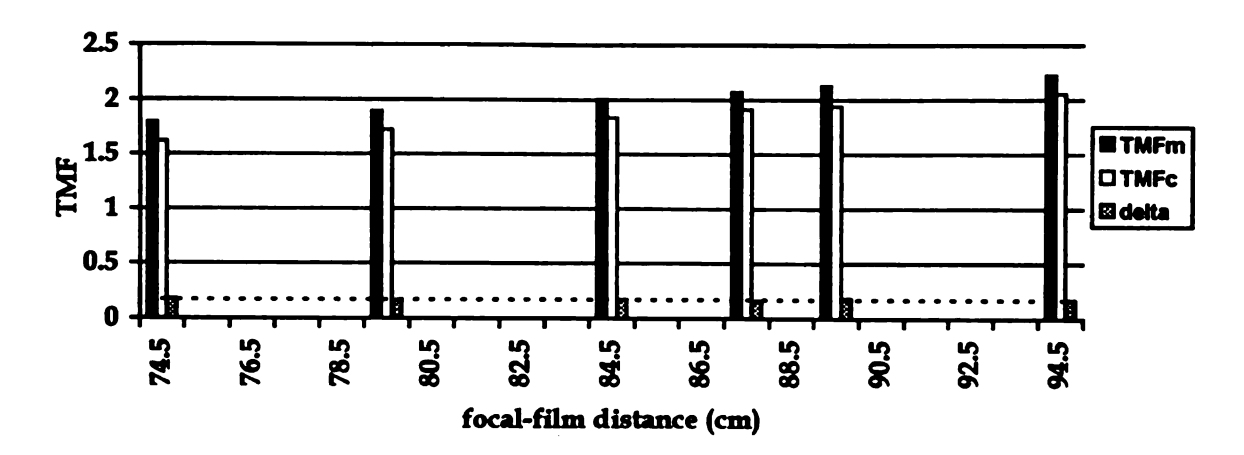


Figure 22 As FFD increased, the difference between TMFm and TMFc (delta) remained unchangd.

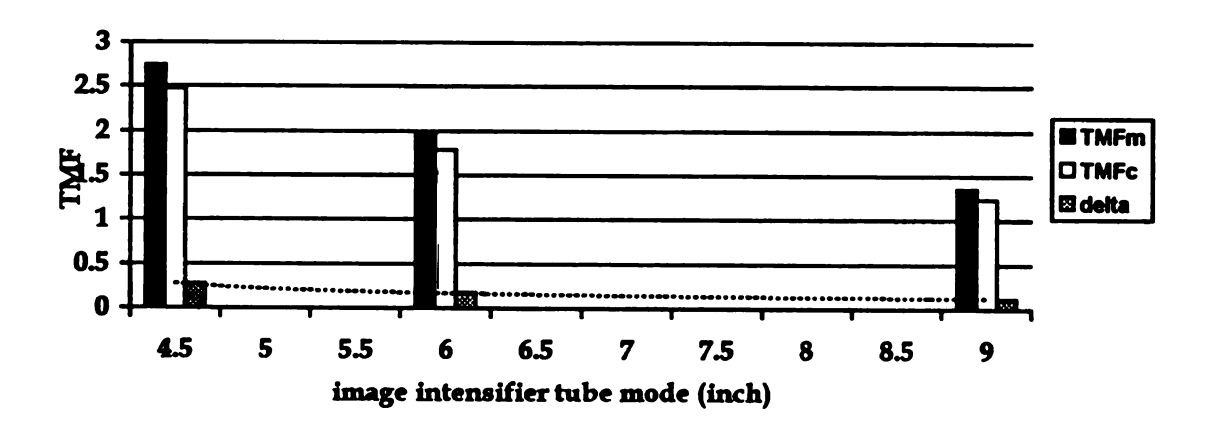


Figure 23 As II mode increased, the difference between TMFm and TMFc (delta) decreased.

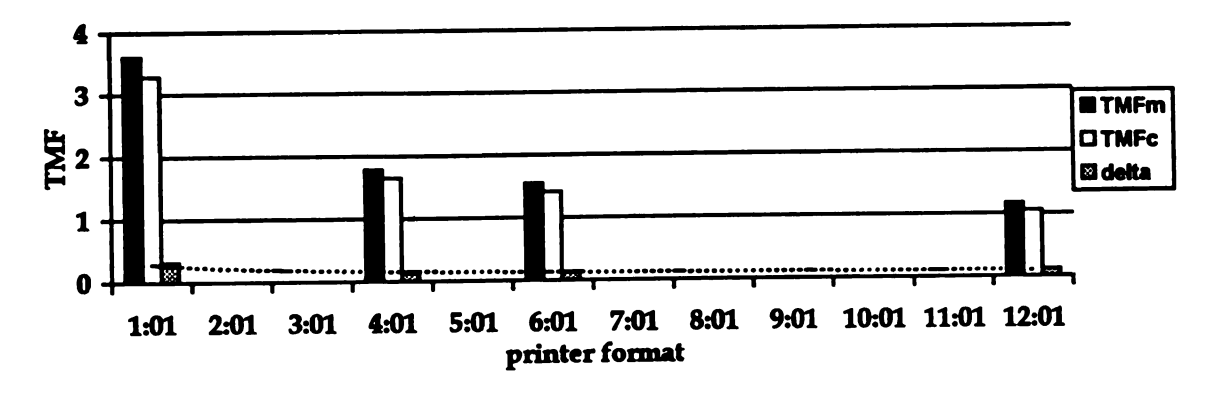


Figure 24 As printer format increased, the difference between TMFm and TMFc (delta) decreased.

Delta was significantly different for magnification factors at various II modes and printer formats. Other predictor variables included the interaction of II mode and format, (II mode)<sup>2</sup>, (format)<sup>2</sup> and (format)<sup>3</sup>. The formula for the linear function of delta, as defined by the linear models procedure, was:

Fitted delta = 1.8004 - 0.37619(II MODE) - 0.17657(FORMAT) + 0.0029212(II MODE x FORMAT) + 0.024043(II MODE)<sup>2</sup> + 0.023579(FORMAT)<sup>2</sup>- 0.0010728(FORMAT)<sup>3</sup>

The R<sup>2</sup> value for this model was 91.4% and the residuals were normally distributed, according to the Wilk-Shapiro test (P=0.9720). The output of each univariate and multivariate analysis is presented in Appendix C. The values for FFD, II mode and format used in this study were entered into this formula to calculate fitted values for delta, based on this linear function. Graphs of the fitted delta values for each FFD, II mode and format are presented in Appendix C. These graphs are quite similar to the experimental data because the statistical model accounted for 91.4% of the variability of delta.

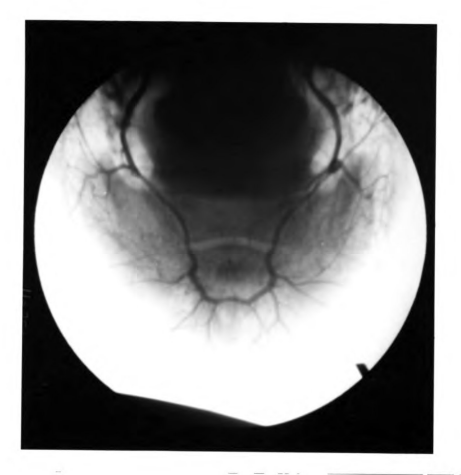
### ANGIOGRAPHY OF EQUINE DISTAL LIMB

The digital radiographic technique produced adequate quality images for consistent identification of the palmar digital artery and its major branches to the foot in the palmarodorsal and lateromedial views (Figures 25A and 26A). The bulbar and coronary arteries were not included in the field of view on most of the PD images and the palmar digital artery at the entrance of the solar canal was not identified on the LM view in two feet, due to the poor image contrast and overall image darkness. Otherwise, the percentage of identification was 83-100% for the remaining arterial vessels (Table 5). Atlases of these vessels were drawn from the angiographic images (Figures 25B and 26B).

Table 5 Arterial vessels were identified on angiograms of six equine feet.

VESSEL		PD*	LM*
palmar digital a.	proximal to bulbar a. proximal to dorsal phalangeal a.	100% 100%	100% 100%
	entering solar canal	100%	67% (4/6)
bulbar a.		0% (0/6)	100%
coronary a.		17% (1/6)	100%
dorsal phalangeal	la.	100%	100%
palmar phalange	al a.	83% (5/6)	100%
distal dorsal phal	angeal a.	100%	100%
distal palmar pha	langeal a.	100%	100%
dorsal branch of distal dorsal phalangeal a.		100%	100%
palmar branch of distal dorsal phalangeal a.		100%	100%
terminal arch		100%	83% (5/6)
dorsal branches o	f terminal arch	100%	100%
solar branches of	terminal arch	100%	100%
solar margin a.		100%	83% (5/6)

Units are % of feet in which these vessels were identified.



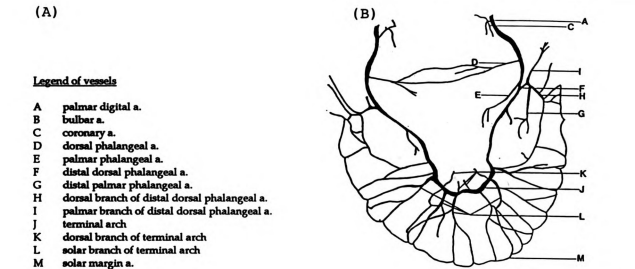
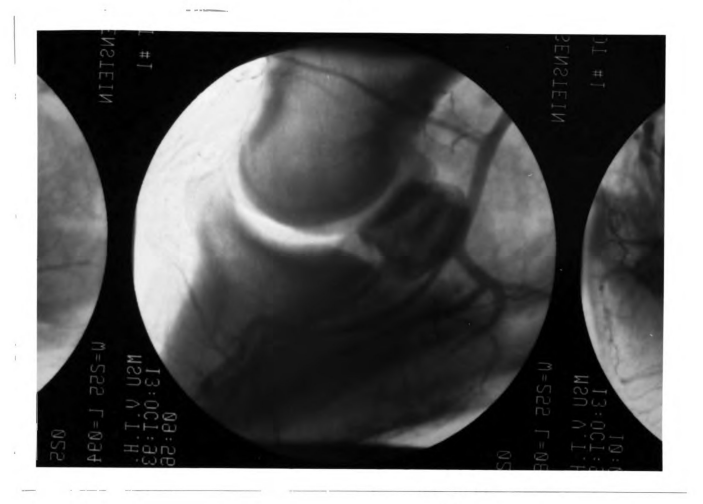


Figure 25 The palmar digital artery and its major arterial branches to the equine foot were visible on digital angiograms in the palmarodorsal view (A) and diagrammed as an atlas of these vessels (B).



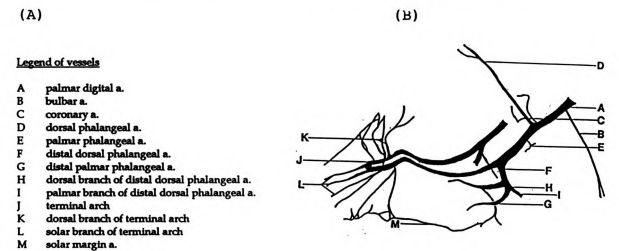


Figure 26 The palmar digital artery and its major arterial branches to the equine foot were visible on digital angiograms in the lateromedial view (A) and diagrammed as an atlas of these vessels (B).

A vascular bed was visualized at the dorsal aspect of the coronary region, supplied by vessels from two directions. Dorsal branches of the terminal arch filled with contrast material in the distal to proximal direction and distal branches of the dorsal phalangeal artery enhanced from the proximal to distal direction (Figure 27). This finding suggests an alternative route of vascular supply to the dorsal aspect of the hoof via the dorsal phalangeal artery in case of a decrease in perfusion from the terminal arch.

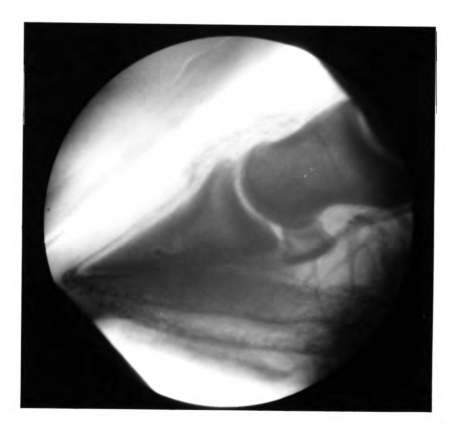


Figure 27 Dorsal branches of the terminal arch and distal branches of the dorsal phalangeal artery supply a vascular bed at the dorsal aspect of the coronary region.

Some minor variations were observed in the pattern of the terminal arch and solar branches, but the overall distribution of vessels was the same among the six feet in this study (Figure 28).

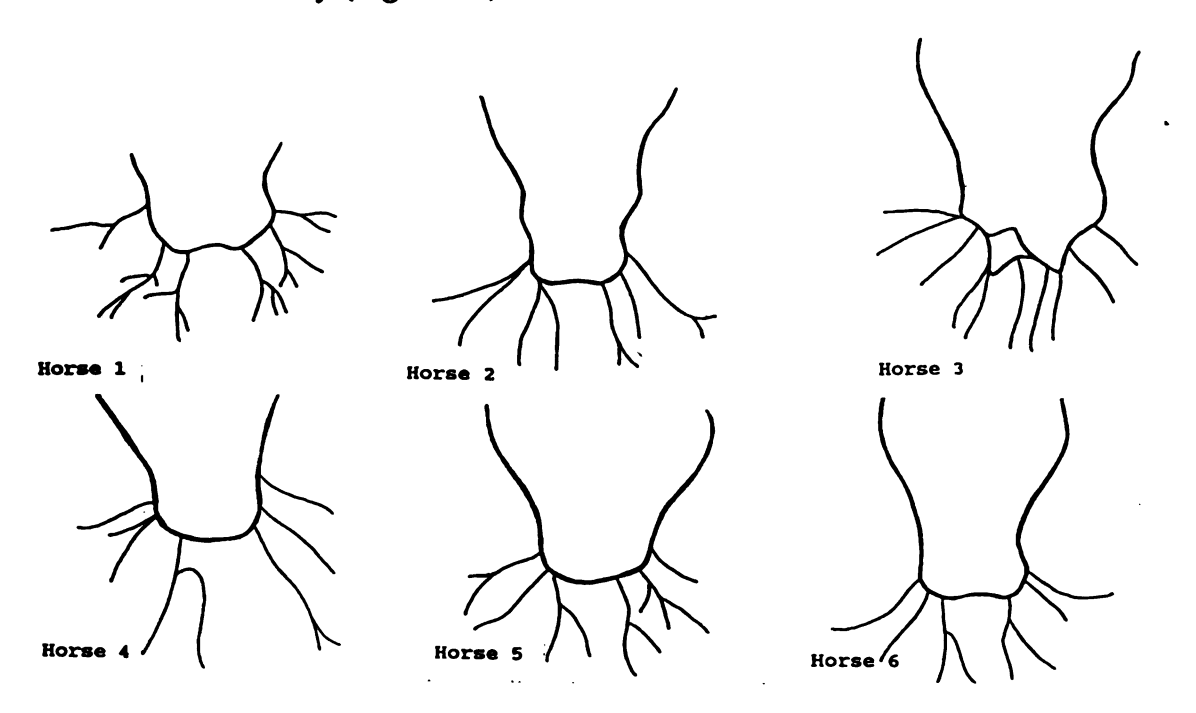


Figure 28 Minor variations were present in the pattern of the terminal arch and solar branches, as seen on the palmarodorsal view.

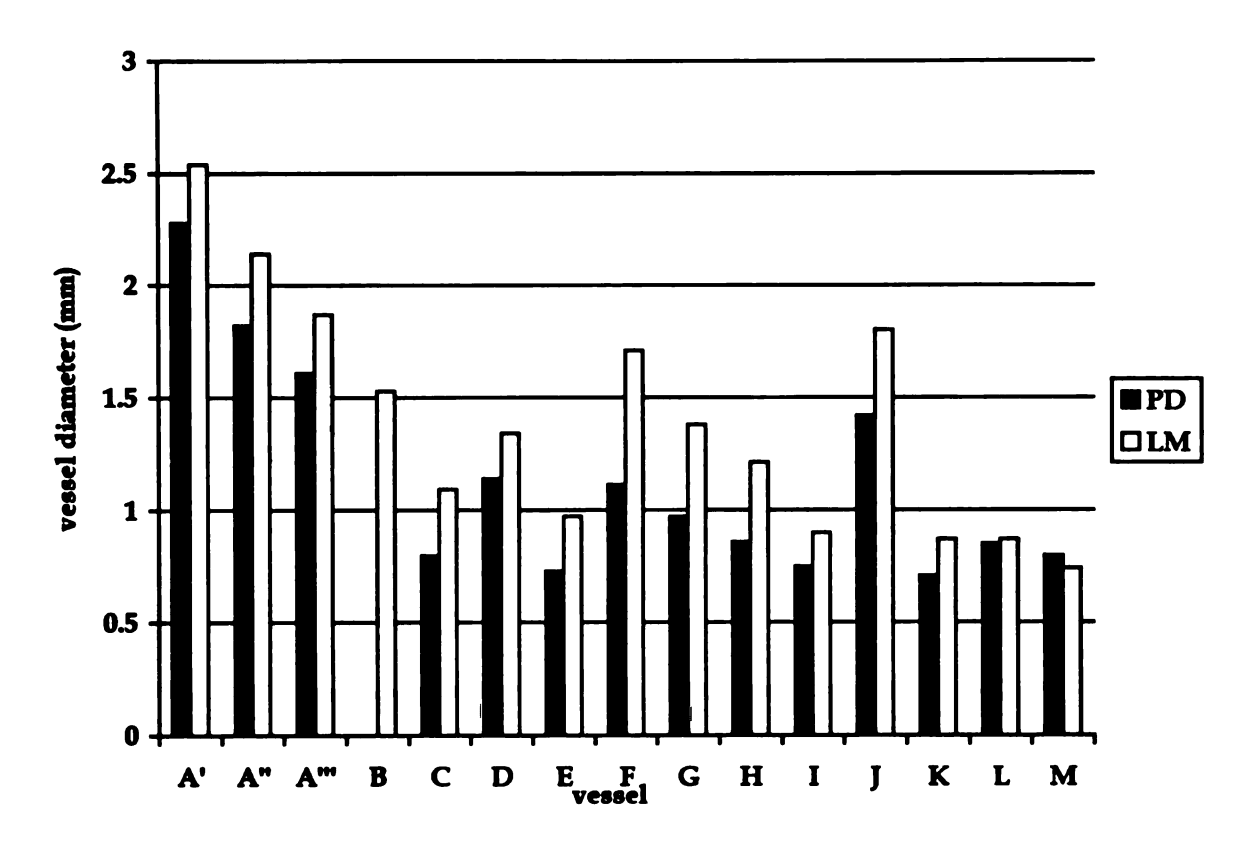
Alterations in arterial perfusion pressure, following injection of the contrast medium, occured in two feet. In one foot, the presure rose rapidly from 100 to 350 mm Hg then gradually returned to its original pressure within three minutes. In a different foot, the opposite response occured with a rapid decline in pressure from 100 to 70 mm Hg, followed by a gradual return to the initial pressure over 3-5 minutes. In both feet, the same vascular reactions reoccurred following the second contrast medium injection in lateral recumbency.

#### Vessel measurement

The mean size and standard deviation of the mean for each arterial vessel, averaged over the six feet, are listed in Table 6. These values were corrected for image magnification using the factors determined by method 1. For all of the PD studies, the magnification factor was 1.05. In the LM studies that were imaged in the 9 inch II mode (horses 2-6), the magnification factor was 0.93 and in horse 1, images were acquired in the 6 inch II mode, so the magnification factor was 1.33. Image measurements and vessel sizes for each foot are listed in Appendix D. All of the vessels were significantly larger on the lateromedial views, as determined by the paired T-test (P<.05) except for the terminal arch, in which the lateromedial view vessel sizes were significantly smaller (Figure 29).

Table 6 Arterial vessels were measured on digital angiograms in the palmarodorsal (PD) and lateromedial (LM) views and vessel size was corrected for magnification.

	VESSEL	PD VESSEL SIZE (mm)	LM VESSEL SIZE (mm)
		X ± SD	X ± SD
palmar digital a.	proximal to bulbar a.	$2.28 \pm 0.55$	$2.54 \pm 0.48$
	proximal to dorsal phalangeal a.	$1.82 \pm 0.43$	2.14 ± 0.22
	entering solar canal	$1.61 \pm 0.53$	$1.87 \pm 0.23$
bulbar a.		not available	$1.53 \pm 0.62$
coronary a.		0.80	$1.09 \pm 0.35$
dorsal phalangeal	a.	$1.14 \pm 0.20$	$1.34 \pm 0.42$
palmar phalangeal a.		$0.73 \pm 0.14$	$0.97 \pm 0.20$
distal dorsal phalangeal a.		$1.11 \pm 0.30$	1.71 ± 0.70
distal palmar phalangeal a.		$0.97 \pm 0.23$	$1.38 \pm 0.82$
dorsal branch of distal dorsal phalangeal a.		$0.86 \pm 0.17$	$1.21 \pm 0.48$
palmar branch of distal dorsal phalangeal a.		0.75 ± 0.15	$0.90 \pm 0.31$
terminal arch		1.42 ± 0.24	$1.80 \pm 0.51$
dorsal branch of terminal arch		0.71 ± 0.17	$0.87 \pm 0.35$
solar branch of terminal arch		$0.85 \pm 0.23$	$0.87 \pm 0.33$
solar margin a.		$0.80 \pm 0.15$	$0.74 \pm 0.09$



### Legend of vessels

- A palmar digital a.
   A' proximal to bulbar a.
   A" proximal to dorsal phalangeal a.
   A" entering solar canal
- B bulbar a.
- C coronary a.
- D dorsal phalangeal a.

- E palmar phalangeal a.
- F distal dorsal phalangeal a.
- G distal palmar phalangeal a.
- H dorsal branch of distal dorsal phalangeal a.
- I palmar branch of distal dorsal phalangeal a.
- J terminal arch
- K dorsal branch of terminal arch
- L solar branch of terminal arch
- M solar margin a.

Figure 29 Arterial vessels of the equine foot were measured on digital angiograms of six feet and corrected for image magnification in the palmarodorsal (PD) and lateromedial (LM) views.

#### DISCUSSION

#### **MAGNIFICATION**

Magnification is inherent in radiography, yet there is not one standard method for quantifying the magnification factor of an imaging system. Comparison of a radiopaque marker to its image has been used as a crude assessment of image magnification. However, critical examination of a radiograph reveals an indistinct margin to the image that may cause an error in measurement. This ill-defined margin is called penumbra and it is due to the various origins of xrays at the focal spot. Use of the smallest available focal spot produces the highest quality image by minimizing the penumbra.<sup>1</sup>

A second method for quantifying the magnification of a radiographic system was described in this thesis, for comparison to the previous method. Geometric magnification is commonly acknowledged in radiology and quantified by the distances between the focal spot, object and film. Penumbra also contributes to geometric magnification and its magnitude may be calculated from the formula:

Penumbra = focal spot size x object-film distance ÷ focal spot-object distance<sup>1</sup>

Due to the indistinct appearance of the margins of this penumbra zone, it is difficult to consistently include the entire penumbra in the measurement of an image (Figure 30). Therefore, this formula overestimates the magnitude of penumbra that is included in a measurement.

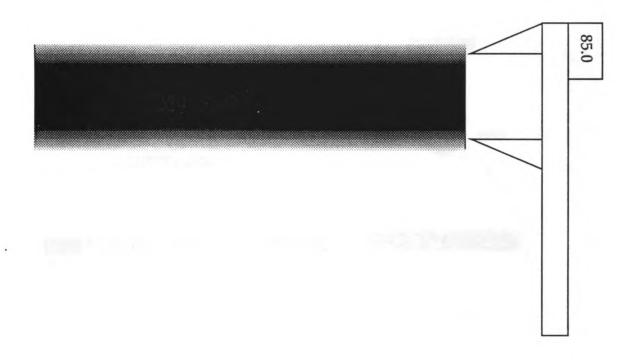


Figure 30 Penumbra contributed to image magnification, but due to the ill-defined, gradually fading margins, it was not completely included in the measurements.

The size of a focal spot is reported in the specifications manual of radiographic equipment. The actual size of a focal spot will vary from its reported size, depending on the radiographic technique. The National Electric Manufacturers Association has established standards for techniques for measurement of focal spot size and tolerance limits for deviation from the stated

size.<sup>1</sup> The magnitude of penumbra also depends on the relative size of the object and the focal spot. When an object is much larger than the focal spot, penumbra is small (Figure 31A). When the object is smaller than the focal spot, penumbra is larger than the umbra, rendering the image non-representative of the original object (Figure 31B).

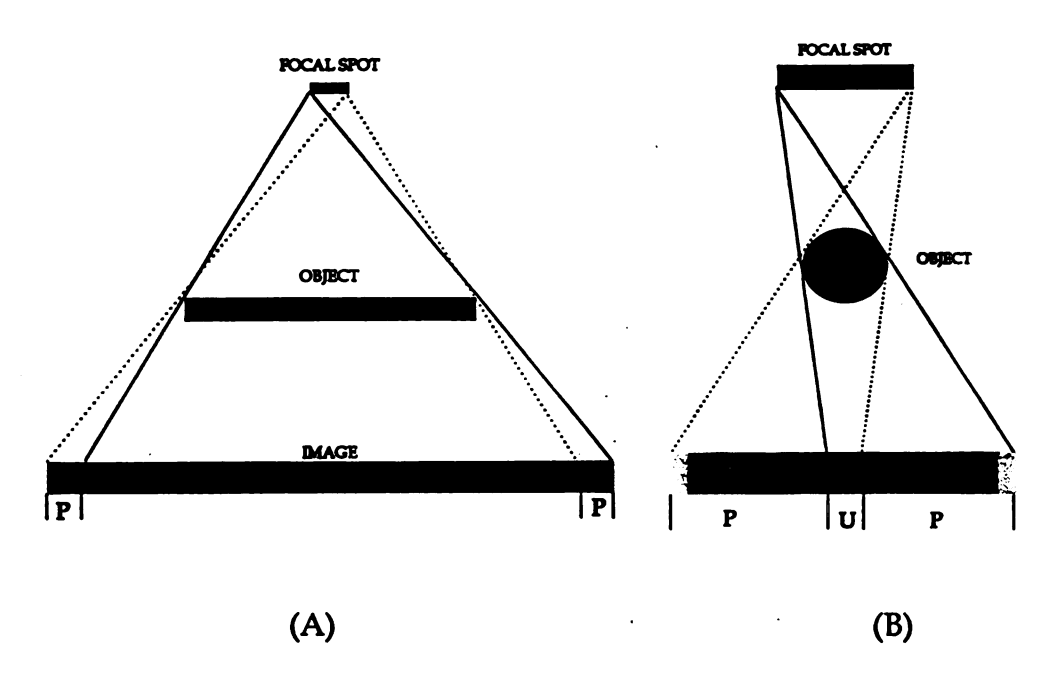


Figure 31 The magnitude of penumbra depends on the relative size of the object and the focal spot. Penumbra (P) is small when the object is larger than the focal spot (A) and penumbra is larger than the umbra (U) when the object is smaller than the focal spot (B).

The quantitative contribution of penumbra to total image magnification was not included in the formula for the calculated total magnification factor (TMFc) in method 2, due to these anticipated complications. By intentionally excluding penumbra from the equation, TMFc values were consistently smaller than the measured total magnification factors (TMFm). Had the theoretical

value for penumbra been included in the TMFc procedure, the TMFc values would have been consistently larger than the TMFm values.

Penumbra had a deleterious effect on image quality that was observed during measurement of the radiographic images of the metallic marker. The radiographic measurements of the metallic marker, from the three repetitions in method 1, indicated a slightly greater standard deviation of the mean at the 4.5 inch II mode, as compared to the lesser magnified images (Appendix B).

Electronic and photographic magnification significantly effected the final image size and their contributions were included in the calculation of TMFc. These components are not involved in conventional radiography where the film is directly exposed in the cassette. However, in digital radiography, the latent xray image is converted to an electrical signal and manipulated by the system to expose film in a remote printer. Linear regression analysis defined the relationship between TMFm and geometric magnification (FFD), electronic magnification (II mode) and photographic magnification (format). The statistically significant predictor variables included, FFD, II mode, format, the interaction of II mode and format, (II mode)2, (format)2 and (format)3. This analysis demonstrated the importance of considering electronic and photographic magnification in quantifying image magnification in digital radiography. Penumbra was part of the image at the input screen of the image Therefore, alterations in image size, by electronic or intensifier tube.

photographic magnification, also effected the size of penumbra on the final image.

There were distinctive trends in the disparity between TMFm and TMFc values (delta) that related to FFD, II mode and format. While FFD was significant in predicting variability in TMFm, it was not was not significant in predicting variability in delta. The magnification factors only increased slightly over a wide range of focal-film distances, so FFD had only a minute effect on penumbra. II mode, format, their interaction (II mode x format), (II mode)<sup>2</sup>, (format)<sup>2</sup> and (format)<sup>3</sup> were significant predictors of variability for both TMFm and delta. The similarity between these analyses suggests that a close relationship existed between the magnitudes of image magnification and delta. Penumbra was the link between these factors. As the images were increasingly magnified, the penumbra was enlarged and the underestimation of TMFc relative to TMFm increased.

Thus, if it is the intention to measure a radiographic image for determination of object size, then a radiographic technique should be used that minimizes penumbra in order to produce an image with sharp margins. Penumbra is smallest when image magnification is at its least. In digital radiography, this may be accomplished by using a short focal-film distance (assuming a fixed focal-object distance), using the largest image intensifier mode and printing the greatest number of images on each sheet of film. It must also be recognized that magnification may enhance one's ability to visualize small

structures, therefore, some compromise in technique is necessary depending on the specific application.

### ANGIOGRAPHY OF THE EQUINE DISTAL LIMB

The pattern of the arterial vessels observed in this study was consistent with the described anatomy in the literature. 54,61,62,64 Some minor variations were present in the shape of the terminal arch and number of solar branches, but the overall distribution of the vessels was the same among the six feet in this study.

It was possible to identify most of the arterial vessels in the palmarodorsal and lateromedial views. In the PD view, the bulbar and coronary arteries were usually outside the field of view, while these vessels were included in the LM images. The longer FFD used in the PD studies caused image magnification that eliminated the peripheral vessels from the images. A decrease in the field of view is a disadvantage of magnification that must be considered when geometric or electronic magnification techniques are used. However, photographic magnification allows for the enlargement of the entire image by printing the same information at larger dimensions. This technique is a unique feature of digital radiography.

The palmar phalangeal artery was not identified in one foot, due to its parallel orientation relative to the xray beam. Imaging of the foot from multiple projections was helpful for visualization of this small vessel and necessary for

localization of structures in a three-dimensional perspective. Repositioning the limb preparation, from the standing to the lateral recumbent position, caused alterations in arterial perfusion pressure that may have had a significant effect on the vessel diameter measurements. A radiographic technique for imaging of an object from multiple projections, without repositioning the object would be helpful to avoid this source of error. A C-arm unit is a flexible version of digital radiographic equipment that may be used to image an object from several angles by rotating the xray tube and the image intensifier tube without repositioning the subject. Use of a C-arm unit with this in-vitro foot model would eliminate the changes in perfusion pressure that occurred during repositioning of the limb.

The terminal arch and solar branches were easily identified on every PD image but the detail was less distinctive at the dorsal branches of terminal arch. These dorsal branches were the smallest vessels measured in this study (mean diameter =  $0.71 \pm 0.17$  mm) which was near the limit of resolution for a 0.3 mm focal spot. Thus, despite the use of the smallest available focal spot, its size was still a limiting factor in image quality for angiographic examination of the arterial vessels in the equine foot.

The LM view images were very dark within the region of the distal phalanx, so the palmar digital artery at the entrance to the solar canal was only identified in four of the six feet. This dark shading was due to underexposure of the thickest region, as seen in the inverted gray scale images. This problem was

<sup>&</sup>lt;sup>a</sup> General Electric Stenoscop LE, Milwaukee, WI

partially overcome by surrounding the limb with lead gloves on the table to absorb some of the background radiation. This caused a decrease in exposure of the phototimer cells in the table, resulting in an increased duration of exposure time and improved detail in the distal phalanx on the final images.

On the lateromedial view images, a vascular bed was observed at the coronary region which was supplied by dorsal branches of the terminal arch and distal branches of the dorsal phalangeal artery. This finding suggests an alternative route of vascular supply to the dorsal aspect of the hoof via the dorsal phalangeal artery in case of a decrease in perfusion from the terminal arch.

The diameter of the palmar digital artery and its major branches to the foot were determined from measurements of the contrast enhanced lumen on angiographic images, and corrected for magnification using the total magnification factors determined in method 1. The same technique of image measurement, using digital calipers, was used to measure the marker images and the angiographic images, so the source of error due to penumbra was consistent. Had the calculated total magnification factors (method 2) been used instead, then the vessel diameter results would have been larger. In the human medical literature on cardiac catheterization and contrast angiography, reference is made to a computer program that determines a precise location of the edge of a vessel for quantitative angiography.<sup>24,65</sup> Use of this program would enhance repeatability of measurements of the same vessel, but the accuracy of these

			!

measurements would still be uncertain since the actual size of the vessels is unknown.

The digital vessel diameters were consistently larger in the lateral recumbent position (LM images) than in the standing position (PD images). Repositioning of the limb from standing to lateral recumbency would have caused a decrease in hydrostatic pressure which was evident as a decrease in arterial perfusion pressure. The pump flow rate was increased from 150 ml/min to approximately 175 ml/min to return arterial perfusion pressure to 100 mm Hg. In so doing, this increase in flow rate may have caused vasodilation. Other causes for the larger vessel diameter results in the LM images may have been vascular reactions to the previous injection of contrast material from the PD study or progressive failure of the in-vitro limb with increased time since euthanasia of the horse. Further investigation is necessary to determine the impact of each of these factors on vessel size.

The results of this study determined that the diameters of the arterial vessels were significantly smaller than those reported by Ackerman, et al.<sup>54</sup> The disparity between the results of this current model and the previously published report may be due to several factors. This research project used in-vitro, perfused limbs that were removed from the horses immediately following euthanasia. The arterial perfusion pressure was maintained at 100 mm Hg by a pump and the perfusate was a heated, oxygenated Krebs-Henseleit solution (Appendix A). While these parameters were designed to mimic physiologic

conditions, there were vast differences between this in-vitro model and the live foot. Ackerman, et al, performed their angiographic study on live horses and ponies under general anesthesia, so systemic cardiovascular and neurological responses contributed to their results. The primary focus of this project was to quantify the total magnification factors of the digital radiographic imaging system then to use these factors to correct image measurements for magnification to determine actual vessel diameters. Ackerman, et al, did not discuss the effect of image magnification, so the reported vessel sizes may have been direct measurements from the radiographs resulting in larger diameter values than the results reported in this thesis. Without knowledge of the radiographic technique used in the previous study, the magnitude of magnification cannot be determined.

The advantages of the model described in this thesis include the ability to control the contents and temperature of the perfusate, the concentration of each component, and the perfusion pressure. This model may be useful for research in the role of vascular reactivity in equine laminitis. Several modifications to this model should be considered to approximate more closely the conditions of an invivo foot including, catheterization of the palmar digital veins to monitor or control venous pressure and weighing the limb before and after each angiographic study to determine tissue perfusion rates and to investigate the effect of interstitial edema formation.

#### **CONCLUSION**

This study investigated three major contributing factors to image magnification in digital radiography, including geometric, electronic and photographic magnification. Variables of the radiographic imaging design that influenced each of these components were focal-film distance, image intensifier mode of function and laser printer format, respectively.

Two methods for quantification of the total magnification factors were performed to determine the relationship between each of these variables and image magnification. The first method compared the size of a metallic marker to the size of its radiographic image. It was demonstrated by the results of this procedure that the total magnification factors increased with increasing focal-film distance, decreasing image intensifier mode and decreasing printer format (fewer images per sheet of film). This technique was simple to perform and would be convenient to repeat in a variety of clinical applications. The limitation of this method is the inaccuracy of defining the edge of an image due to the penumbra effect.

The second method calculated total magnification factors from the product of geometric, electronic and photographic magnification. This

procedure was designed to provide comparable values to results of method 1 and to quantify the contributions of the individual components to total magnification. The results of this second method produced smaller values for total image magnification than the first method. This underestimation of the magnification factor was likely due to the intentional exclusion of the contribution of penumbra to image magnification.

If it is the intention to measure an image and correct for magnification, in order to determine an object's size, then a radiographic technique should be selected to minimize image magnification. In so doing, the penumbra will be minimized and definition of the image margin will be more distinct. This may be accomplished in digital radiography by using a short focal-film distance, assuming a fixed focal-object distance. The largest image intensifier mode should be used and the greatest number of images possible should be printed on each sheet of film. However, if purpose of the radiographic study is for subjective evaluation of small structures, then image magnification may enhance visualization of the objects of interest, therefore a compromise between these techniques may be most useful. In either situation, the smallest available focal spot should be used to produce the best image detail by minimizing the penumbra.

Digital angiography of the equine distal limb provided detailed images with adequate resolution to consistently identify the palmar digital artery and its major branches to the foot. The terminal arch and its solar branches were

more easily seen on the palmarodorsal view while the lateromedial view was more useful for examination of the bulbar and coronary arteries and the dorsal branches of the terminal arch.

Diameters of the arterial vessels in these feet were determined, based on measurements of their radiographic images and correction for image magnification. The palmar digital artery tapered from 2.28 mm, proximal to the bulbar artery, to 1.61 mm at the entrance to the solar canal of the distal phalanx and 1.42 mm at the midsagittal point of the terminal arch. The values reported for vessel diameters in this thesis were based on in-vitro perfused equine limbs. This information may be applied to further research in normal and pathological vascular reactivity.

### APPENDIX A

### APPENDIX A

# Directions for preparation of Krebs Henseleit solution

# To prepare 4.0 L Krebs Henseleit solution:

# Prepare 4 stock solutions:

1)	KCL	28.034 g/L
2)	CaCl <sub>2</sub> -2H2O	30.58  g/L
3)	KH <sub>2</sub> PO <sub>4</sub>	12.63 g/L
4)	MgSO <sub>4</sub> ·7H <sub>2</sub> O	23.464 g/L

## <u>Step 1:</u>

Mix	1) 50 ml KCl solution	4.70	mM
	2) 50 ml KH <sub>2</sub> PO <sub>4</sub> solution	1.16	mM
	3) 50 ml MgSO <sub>4</sub> ·7H <sub>2</sub> O solution	1.19	mM
In	4) 3000 ml H <sub>2</sub> O		

## <u>Step 2:</u>

Add	1) NaCl	27.68 g
	2) Dextrose	8.43 g
	3) NaHCO <sub>3</sub>	8.40 g

## <u>Step 3</u>:

Add	1)	50 ml CaCl <sub>2</sub> ·2H <sub>2</sub> O	2.0	6	$\mathbf{m}\mathbf{M}$
	2)	780 ml H <sub>2</sub> O			

### APPENDIX B

:

.

### **APPENDIX B**

Table 7 A metallic marker was radiographed at several focal-film distances (FFD), using three different image intensifier tube modes (II mode) and printed at four formats. Each image was measured three times with calipers.

FFD cm	II mode	format	repl mm	rep2 mm	rep3 num	avg mm	St Dev X		
74.5	9	12	8.44	8.45	8.41	8.83	0.36083		
79.5	9	12	8.74	8.78	8.74	9.18	0.31969		
84.5	9	12	9.31	9.05	9.56	9.54	0.21119		
87.5	9	12	9.49	9.46	9.66	9.9	0.37175		
89.5	9	12	9.82	9.71	9.75	10.79	0.99629		
94.5	9	12	10.39	10.26	10.21	11.79	1.02596		
74.5	6	12	12.16	12.04	12.19	12.7467	0.45206		
79.5	6	12	12.82	12.77	13.39	13.2767	0.37985		
84.5	6	12	13.26	13.28	13.83	13.7133	0.35612		
87.5	6	12	13.75	13.8	13.98	14.21	0.41215		
89.5	6	12	14.13	14.22	14.14	15.28	1.21461		
94.5	6	12	14.75	14.95	14.98	16.4767	1.25974		
74.5	4.5	12	16.96	16.82	16.7	17.7267	0.62872		
79.5	4.5	12	17.72	17.58	18.67	18.47	0.6005		
84.5	4.5	12	18.5	18.4	19.17	19.1067	0.46507		
87.5	4.5	12	19.19	19.35	19.62	19.72	0.47378		
89.5	4.5	12	19.63	19.76	20.61	17.0067	4.22196		
94.5	4.5	12	20.34	20.58	20.79	14.3567	4.23867		
74.5	9	6	11.05	11.18	11.12	11.7	0.53907		
<i>7</i> 9.5	9	6	11.68	11.71	11.73	12.2733	0.45021		
84.5	9	6	12.37	12.41	12.44	12.7667	0.32252		
87.5	9	6	12.77	12.91	12.86	13.21	0.38131		
89.5	9	6	13.16	13.23	13.04	14.2533	1.18506		
94.5	9	6	13.7	13.75	13.53	15.4067	1.24208		
74.5	6	6	15.9	16.29	15.7	16.8533	0.88909		
<i>7</i> 9.5	6	6	16.62	16.62	16.78	17.66	0.74422		
84.5	6	6	18.04	18.21	17.74	18.47	0.42575		
87.5	6	6	18.32	18.64	18.62	19.09	0.64565		
89.5	6	6	19.05	19.04	19.09	20.3767	1.32152		
94.5	6	6	19.9	19.77	19.85	21.7567	1.37609		
74.5	4.5	6	22.18	22.21	22.24	23.53	1.26415		
79.5	4.5	6	23.19	23.31	23.17	24.82	1.20136		
84.5	4.5	6	25.22	25.07	25.03	25.8567	0.46162		
87.5	4.5	6	26.05	26.1	25.75	26.6567	0.68878		
89.5	4.5	6	26.3	26.59	26.3	22.2533	6.67801		
94.5	4.5	6	27.62	27.38	27.49	17.9567	6.83697		

Table 7 continued

FFD cm	II mode	format	repl mm	rep2 mm	rep3 mm	avg mm	St Dev X		
74.5	9	4	12.84	12.85	12.83	13.4467	0.51097		
79.5	9	4	13.41	13.46	13.71	14.09	0.55522		
84.5	9	4	14.09	14.28	14.29	14.56	0.33297		
87.5	9	4	14.77	14.6	14.67	15.0533	0.36591		
89.5	9	4	14.82	15.04	15.2	16.3133	1.61093		
94.5	9	4	15.57	15.94	15.68	17.8367	1.63905		
74.5	6	4	18.55	18.68	18.49	19.5267	0.85869		
79.5	6	4	19.39	19.67	19.36	20.4667	0.81757		
84.5	6	4	20.64	20.77	20.53	21.3033	0.51655		
87.5	6	4	21.37	21.28	21.17	22.0733	0.65657		
89.5	6	4	21.9	21.74	22.02	23.5	1.57956		
94.5	6	4	22.95	22.79	22.9	25.3533	1.85311		
74.5	4.5	4	25.65	25.73	25.75	27.2633	1.24478		
79.5	4.5	4	27.46	27.17	27.18	28.6067	0.90779		
84.5	4.5	4	28.68	28.85	28.93	29.4967	0.60599		
87.5	4.5	4	29.68	29.66	29.8	30.56	0.94435		
89.5	4.5	4	30.13	30.55	30.58	29.3	2.50691		
94.5	4.5	4	31.87	31.57	31.68	28.35	2.55198		
74.5	9	1	25.9	25.8	25.86	27.2867	1.13494		
79.5	9	1	27.28	27.19	27.26	28.5567	0.99587		
84.5	9	1	28.68	28.83	28.7	29.6467	0.76474		
87.5	9	1	29.71	29.67	29.64	30.74	0.92833		
89.5	9	1	30.55	30.64	30.48	33.22	2.83792		
94.5	9	1	31.96	31.9	31.88	36.0633	3.00657		
74.5	6	1	37.15	37.24	37.28	39.3067	1.86036		
79.5	6	1	39.08	39.66	39.45	41.3767	1.76129		
84.5	6	1	41.69	41.68	41.8	43.17	1.1388		
87.5	6	1	43.36	43.52	43.14	44.72	1.23039		
89.5	6	1	44.46	44.11	44.53	47.6333	3.25033		
94.5	6	1	46.34	46.74	46.68	51.1233	3.57421		
74.5	4.5	1	52.1	52.29	52.3	55.18	2.62284		
79.5	4.5	1	54.93	54.85	55.06	58.0333	2.36342		
84.5	4.5	1	58.51	58.78	58.62	60.5067	1.57142		
87.5	4.5	1	60.66	60.45	60.54	62.6833	1.8036		
89.5	4.5	1	62.35	62.32	61.89	63.695	26.0659		
94.5	4.5	1	65.04	64.79	65.22	65.04	26.5993		
					·				

# Statistical analysis of measured Total Magnification Factors (TMFm)

# General Linear models procedure, multiple regression analysis

## Output of Statistix 3.1 Analytical Software

PREDICTOR	•			
VARIABLES	COEFFICIENT	STD ERROR	STUDENT'S T	P
		4 22650 03	9.06	
CONSTANT	3.9290	4.3365E-U1	9.06	0.0000
				0.0000
CASES INCLUDE	D 72	MISSING P VALUE	CASES 0	
DEGREES OF FR	EEDOM 70			
OVERALL F	20.97	P VALUE	0.0000	
ADJUSTED R SQ	UARED 0.2195			
R SOUARED	0.2305			
RESID. MEAN S	0.2305 QUARE 1.036			
UNWEIGHTED LE	AST SQUARES L	INEAR REGRESSI	ON OF TMFM	
VARIABLES	COEFFICIENT	STD ERROR	STUDENT'S T	
	3.1406	1.7378F-01	18.07	0 0000
FORMAT	-1.9474E-01	2.4763E-02	-7.86	0.0000
CASES INCLUDE	D 72	MISSING	CASES 0 0.0000	
DEGREES OF FR	EEDOM 70			•
OVERALL F	61.84	P VALUE	0.0000	
ADJUSTED R SQ	UARED 0.4615		55555	
K SCUARED	0.4691			
RESID. MEAN S	QUARE 7.147	E-01		
PREDICTOR VARIABLES	-	INEAR REGRESSI	ON OF TMFM STUDENT'S T	P
				0.9193
CONSTANT FFD	2.1663E-02	2.0711R-02	0.10 1.05	0.2992
	2.10032 02	2.07222 05	2.00	0.2332
CASES INCLUDE DEGREES OF FR OVERALL F	D 72	MISSING	CASES 0	•
DEGREES OF FR	EEDOM 70	• *		
OVERALL F	1.094	P VALUE	0.2992	
ADJUSTED R SQ	UARED 0.0013			
K SQUAKED	0.0154			
RESID. MEAN S	0.0154 QUARE 1.325			

PREDICTOR				•	
VARIABLES	COEFFI	CIENT	STD ERROR	STUDENT'S T	P
CONSTANT	2.087	7	1.6109	1.30 .	0.1993
PPD	2.007	, 3F_02	1.6109 1.8256E-02 6.3927E-02	1 10	0.1333
FFD IIMODE	-2.100	3E-02	6 20278-02	1.19 -4.59	0.2394
TIMODE	-2.935	7E-01	6.392/6-02	-4.59	0.0000
CASES INCLU DEGREES OF	DED	72	MISSING	G CASES 0	
degrees of	FREEDOM	69			
OVERALL F		11.25	P VALUI	0.0001	
ADJUSTED R	SQUARED	0.2240	P VALUI		
R SQUARED		0.2459			
RESID. MEAN					
	040.20	2.000			
INWPICHTED	T.PACT CO	HIADRS T.T	NEAR REGRESS	TON OF THEM	
ONWEIGHTED	TENDI 3	MAKES III	MEAR REGRESS.	ION OF IMPM	
DDDDT.080D					
PREDICTOR					_
	COEFFI	CIENT		STUDENT'S T	P
CONSTANT	1.299	2	1.2946	1.00	0.3191
FFD	2.166	3E-02	1.5094E-02	1.44	0.1558
FORMAT				-7.92	
rolumi	1.74,	40 01	2.43/02 02	-,.,2	0.0000
OLCRO THOTH	DBD	70	WICCIN	C CACEC A	
CASES INCLU	DED	/2	WISSIM	CASES U	
DEGREES OF	PREEDOM	69	MISSING P VALU		
OVERALL F		32.42	P VALU	E 0.0000	
ADJUSTED R	SQUARED	0.4695			
R SQUARED		0.4845			
RESID. MEAN	SQUARE	7.040E	-01		
INWEIGHTED	LEAST SO	TIAPES I.T	NEAR REGRESS	ON OF THEM	
OMMDIGHTED .	DENIET OF	onedo di	MEAN MEGNESS.	ion of Imim	
DDBDTAROD					
PREDICTOR					_
VARIABLES	COEFFI	CIENT	STD ERROR	STUDENT'S T	P
CONSTANT	5.048			17.20	
FORMAT	-1.947	4E-01	1.8763E-02	-10.38 -7.28	0.0000
IIMODE	-2.935	7E-01	4.0350E-02	-7.28	0.0000
				*****	0.000
CASES THOUSE	DED	72	MICCIN	CASES 0	
CASES INCLUI	<u> </u>		MISSING	Cases U	
	FREEDUM	69			
OVERALL F		80.33	P VALUE	5 0.0000	
ADJUSTED R					
R SQUARED		0.6996			
RESID. MEAN	SOUARE	4.103E	-01		

PREDICTOR				
VARIABLES	COEFFICIENT	STD ERROR	STUDENT'S T	P
CONSTANT	3.2074 -	1.0032	3.20	0.0021
PFD	2.1663E-02	1.1306E-02	1.92	0.059 <i>6</i>
FORMAT	-1.9474E-01	1.8410E-02	-10.58	0.0000
IIMODE	-2.9357E-01	3.9591E-02	-7.42	0.0000
CASES INCLU	IDED 72	MISSING	CASES 0	
DEGREES OF				
OVERALL F	56.85		0.0000	
ADJUSTED R				
R SQUARED	0.7149			
RESID. MEAN				
			N OF THEM	
UNWEIGHTED	LEAST SQUARES I	INEAR REGRESSIC	ON OF THEM	
PREDICTOR				_
VARIABLES	COEFFICIENT	STD ERROR	STUDENT'S T	P
CONSTANT	1.3387	3.5777	0.37	0.7095
FFD	5.6170E-02	4.1766E-02	1.34	0.1833
FORMAT	-1.8977E-01	2.3561E-01	-0.81	0.4235
IIMODE	-1.7423E-01	4.9250E-01	-0.35	0.7247
<b>I</b> 1	-3.3306E-03	5.7425E-03	-0.58	0.5639
I2	-2.2362E-03	2.6702E-03	-0.84	0.4054
13	2.8479E-02	9.3502E-03	3.05	0.0033
•				
CASES INCL	UDED 7	MISSING	CASES 0	
CASES INCL			CASES 0	
DEGREES OF	FREEDOM 65	5		
DEGREES OF OVERALL F	FREEDOM 65	P VALUE		
DEGREES OF OVERALL F ADJUSTED R	FREEDOM 69 33.20 SQUARED 0.731	p VALUE		
DEGREES OF OVERALL F ADJUSTED R R SQUARED	FREEDOM 65 33.20 SQUARED 0.731 0.754	P VALUE		
DEGREES OF OVERALL F ADJUSTED R R SQUARED RESID. MEAN	FREEDOM 6: 33.20 SQUARED 0.731: 0.754 N SQUARE 3.560	5 ) P VALUE 3 ) 5E-01	0.0000	
DEGREES OF OVERALL F ADJUSTED R R SQUARED RESID. MEAN	FREEDOM 6: 33.20 SQUARED 0.731: 0.754 N SQUARE 3.560	5 ) P VALUE 3 ) 5E-01	0.0000	
DEGREES OF OVERALL F ADJUSTED R R SQUARED RESID. MEAN UNWEIGHTED	FREEDOM 65 33.20 SQUARED 0.731 0.754	5 ) P VALUE 3 ) 5E-01	0.0000	
DEGREES OF OVERALL F ADJUSTED R R SQUARED RESID. MEAJ UNWEIGHTED PREDICTOR	FREEDOM 6: 33.20 SQUARED 0.731: 0.754 N SQUARE 3.560	5 ) P VALUE 3 ) 5E-01	0.0000	
DEGREES OF OVERALL F ADJUSTED R R SQUARED RESID. MEAJ UNWEIGHTED PREDICTOR VARIABLES	FREEDOM 6: 33.20 SQUARED 0.731: 0.754 N SQUARE 3.560	D P VALUE  B D P VALUE  B D P VALUE  C D P V	0.0000 ON OF TMFM	B
DEGREES OF OVERALL F ADJUSTED R R SQUARED RESID. MEAN UNWEIGHTED PREDICTOR VARIABLES	FREEDOM 6: 33.20 SQUARED 0.731: 0.754 N SQUARE 3.560 LEAST SQUARES	5 ) P VALUE 3 ) 5E-01	0.0000	P
DEGREES OF OVERALL F ADJUSTED R R SQUARED RESID. MEAJ UNWEIGHTED PREDICTOR VARIABLES	FREEDOM 6: 33.20 SQUARED 0.731: 0.7540 N SQUARE 3.560 LEAST SQUARES COEFFICIENT	STD ERROR	0.0000 ON OF TMFM STUDENT'S T	
DEGREES OF OVERALL F ADJUSTED R R SQUARED RESID. MEAI UNWEIGHTED PREDICTOR VARIABLES CONSTANT FFD	FREEDOM 69 33.26 SQUARED 0.731 0.754 N SQUARE 3.566 LEAST SQUARES 1  COEFFICIENT 3.1789	STD ERROR 1.6452	0.0000 ON OF TMFM STUDENT'S T	0.0576
DEGREES OF OVERALL F ADJUSTED R R SQUARED RESID. MEAI UNWEIGHTED PREDICTOR VARIABLES CONSTANT	FREEDOM 69 33.26 SQUARED 0.731 0.7540 N SQUARE 3.560 LEAST SQUARES 1	STD ERROR 1.6452 1.8645E-02	O.0000 ON OF TMFM STUDENT'S T	0.0576 0.0686
DEGREES OF OVERALL F ADJUSTED R R SQUARED RESID. MEAI UNWEIGHTED PREDICTOR VARIABLES CONSTANT FFD	FREEDOM 69 33.26 33.26 SQUARED 0.731: 0.754 N SQUARE 3.566 LEAST SQUARES  COEFFICIENT 3.1789 3.4522E-02 -1.8977E-01	STD ERROR 1.6452 2.3443E-01	0.0000 ON OF TMFM  STUDENT'S T 1.93 1.85 -0.81	0.0576 0.0686 0.4211
DEGREES OF OVERALL F ADJUSTED R R SQUARED RESID. MEAI UNWEIGHTED PREDICTOR VARIABLES CONSTANT FFD FORMAT	FREEDOM 69 33.26 33.26 SQUARED 0.731: 0.754 N SQUARE 3.566 LEAST SQUARES  COEFFICIENT 3.1789 3.4522E-02 -1.8977E-01 -4.5733E-01	STD ERROR 1.6452 1.8645E-02 2.3443E-01 6.5288E-02	0.0000  ON OF TMFM  STUDENT'S T  1.93 1.85 -0.81 -7.00	0.0576 0.0686 0.4211 0.0000
DEGREES OF OVERALL F ADJUSTED R R SQUARED RESID. MEAJ UNWEIGHTED PREDICTOR VARIABLES	FREEDOM 69 33.26 33.26 SQUARED 0.731 0.754 N SQUARE 3.56 LEAST SQUARES  COEFFICIENT 3.1789 3.4522E-02 -1.8977E-01 -4.5733E-01 -2.2362E-03	STD ERROR 1.6452 1.8645E-02 2.3443E-01 6.5288E-02 2.6567E-03	0.0000  ON OF TMFM  STUDENT'S T  1.93 1.85 -0.81 -7.00 -0.84	0.0576 0.0686 0.4211 0.0000 0.4030
DEGREES OF OVERALL F ADJUSTED R R SQUARED RESID. MEAI UNWEIGHTED PREDICTOR VARIABLES CONSTANT FPD FORMAT IIMODE I2	FREEDOM 69 33.26 33.26 SQUARED 0.731: 0.754 N SQUARE 3.566 LEAST SQUARES  COEFFICIENT 3.1789 3.4522E-02 -1.8977E-01 -4.5733E-01	STD ERROR 1.6452 1.8645E-02 2.3443E-01 6.5288E-02	0.0000  ON OF TMFM  STUDENT'S T  1.93 1.85 -0.81 -7.00	0.0576 0.0686 0.4211 0.0000
DEGREES OF OVERALL F ADJUSTED R R SQUARED RESID. MEAI UNWEIGHTED PREDICTOR VARIABLES 	FREEDOM 33.26 33.26 SQUARED 0.731. 0.7546 N SQUARE 3.566 LEAST SQUARES  COEFFICIENT 3.1789 3.4522E-02 -1.8977E-01 -4.5733E-01 -2.2362E-03 2.8479E-02	STD ERROR 1.6452 1.8645E-02 2.3443E-01 6.5288E-02 2.6567E-03 9.3031E-03	0.0000 ON OF TMFM  STUDENT'S T 1.93 1.85 -0.81 -7.00 -0.84 3.06	0.0576 0.0686 0.4211 0.0000 0.4030
DEGREES OF OVERALL F ADJUSTED R R SQUARED RESID. MEAI UNWEIGHTED PREDICTOR VARIABLES CONSTANT FFD FORMAT IIMODE I2 I3 CASES INCLI	FREEDOM 33.26 33.26 SQUARED 0.731: 0.7544 N SQUARE 3.566 LEAST SQUARES 1  COEFFICIENT 3.1789 3.4522E-02 -1.8977E-01 -4.5733E-01 -2.2362E-03 2.8479E-02	STD ERROR 1.6452 1.8645E-02 2.3443E-01 6.5288E-02 2.6567E-03 9.3031E-03 MISSING	0.0000 ON OF TMFM  STUDENT'S T 1.93 1.85 -0.81 -7.00 -0.84 3.06	0.0576 0.0686 0.4211 0.0000 0.4030
DEGREES OF OVERALL F ADJUSTED R R SQUARED RESID. MEAN UNMEIGHTED PREDICTOR VARIABLES	FREEDOM 69 33.26 33.26 SQUARED 0.731: 0.7546 N SQUARE 3.566 LEAST SQUARES 1  COEFFICIENT 3.1789 3.4522E-02 -1.8977E-01 -4.5733E-01 -2.2362E-03 2.8479E-02  JDED 72 FREEDOM 66	STD ERROR 1.6452 1.8645E-02 2.3443E-01 6.5288E-02 2.6567E-03 9.3031E-03 MISSING	0.0000 ON OF TMFM  STUDENT'S T  1.93 1.85 -0.81 -7.00 -0.84 3.06  CASES 0	0.0576 0.0686 0.4211 0.0000 0.4030
DEGREES OF OVERALL F ADJUSTED R R SQUARED RESID. MEAI UNWEIGHTED PREDICTOR VARIABLES	FREEDOM 65 33.26 33.26 SQUARED 0.731: 0.7546 N SQUARE 3.566 LEAST SQUARES 1  COEFFICIENT 3.1789 3.4522E-02 -1.8977E-01 -4.5733E-01 -2.2362E-03 2.8479E-02  JDED 72 FREEDOM 66	STD ERROR 1.6452 1.8645E-02 2.3443E-01 6.5288E-02 2.6567E-03 9.3031E-03 MISSING P VALUE	0.0000 ON OF TMFM  STUDENT'S T 1.93 1.85 -0.81 -7.00 -0.84 3.06	0.0576 0.0686 0.4211 0.0000 0.4030
DEGREES OF OVERALL F ADJUSTED R R SQUARED RESID. MEAI UNWEIGHTED PREDICTOR VARIABLES	FREEDOM 33.26 33.26 SQUARED 0.731: 0.7546 N SQUARE 3.566 LEAST SQUARES  COEFFICIENT 3.1789 3.4522E-02 -1.8977E-01 -4.5733E-01 -2.2362E-03 2.8479E-02  JDED 72 FREEDOM 66 40.18 SQUARED 0.7340	STD ERROR	0.0000 ON OF TMFM  STUDENT'S T  1.93 1.85 -0.81 -7.00 -0.84 3.06  CASES 0	0.0576 0.0686 0.4211 0.0000 0.4030
DEGREES OF OVERALL F ADJUSTED R R SQUARED RESID. MEAI UNWEIGHTED PREDICTOR VARIABLES	FREEDOM 33.26 33.26 SQUARED 0.731. 0.7546 N SQUARE 3.566 LEAST SQUARES 3  COEFFICIENT 3.1789 3.4522E-02 -1.8977E-01 -4.5733E-01 -2.2362E-03 2.8479E-02  JDED 72 FREEDOM 66 40.18 SQUARED 0.7327	STD ERROR 1.6452 1.8645E-02 2.3443E-01 6.5288E-02 2.6567E-03 9.3031E-03 MISSING P VALUE	0.0000 ON OF TMFM  STUDENT'S T  1.93 1.85 -0.81 -7.00 -0.84 3.06  CASES 0	0.0576 0.0686 0.4211 0.0000 0.4030

PREDICTOR					
VARIABLES	COEFFICI	ENT	STD ERROR	STUDENT'S	T P
CONSTANT	4.2718		1.0080	4.24	0.0001
FFD	2.1663E		1.0666E-02	2.03	0.0462
FORMAT	-3.7985E		6.2788E-02	-6.05	0.0000
IIMODE	-4.5733E	E-01	6.5146E-02	-7.02	0.0000
13	2.8479E	-02	9.2829E-03	3.07	0.0031
CASES INCL	JDED	72	MISSING	CASES 0	
DEGREES OF	FREEDOM	67			
OVERALL F		50.26	P VALUE	0.0000	
ADJUSTED R	SQUARED 0	.7351			
R SQUARED		.7501			
RESID. MEAN	N SQUARE	3.515E	-01		
UNWEIGHTED	LEAST SQUA	RES LI	NEAR REGRESSI	ON OF TMFM	
PREDICTOR					
VARIABLES	COEFFICI	ENT	STD ERROR	STUDENT'S	T P
CONSTANT	4.3630		12.156	0.36	0.7208
FFD	1.9487E	C-02	2.8936E-01	0.07	0.9465
FORMAT	-3.7985E	E-01	6.3262E-02	-6.00	0.0000
IIMODE	-4.5733E		6.5637E-02	-6.97	0.0000
13	2.8479E		9.3529E-03	3.04	0.0033
FFD2	1.2908		1.7150E-03	0.01	0.9940
FFDZ	1.2906	05	1.71508-03	0.01	0.9940
CASES INCL		72	MISSING	CASES 0	
DEGREES OF		66			
OVERALL F		39.61	P VALUE	0.0000	
	SQUARED C				
R SQUARED	C	7501			
RESID. MEAN	N SQUARE	3.568E	-01		
UNWEIGHTED	LEAST SQUA	RES LI	NEAR REGRESSI	ON OF TMFM	
PREDICTOR					
<b>VARIABLES</b>	COEFFICE	ENT	STD ERROR	STUDENT'S	T P
CONSTANT	7.2986		1.7253	4.23	0.0001
FFD	2.1663E	C-02	1.0394E-02	2.08	0.0410
FORMAT	-3.7985E	C-01	6.1186E-02	-6.21	0.0000
IIMODE	-1.4139		4.5275E-01	-3.12	0.0027
I3	2.8479E	-02	9.0460E-03	3.15	0.0025
IIMODE2	6.9753E		3.2687E-02	2.13	0.0025
					0.0500
CASES INCL		72	MISSING	CASES 0	
DEGREES OF	FREEDOM	66			
OVERALL F		43.26	P VALUE	0.0000	
ADJUSTED R	SQUARED 0	.7485			
R SQUARED		.7662			
RESID. MEAN		3.338E-	-01		

PREDICTOR				•	
VARIABLES	COEFFICIENT	STD	ERROR	STUDENT'S T	P
CONSTANT	5.3298	4.98	73E-01	10.69	0.0000
PFD	2.1663E-02	5.22	13E-03	4.15	0.0001
FORMAT	-8.8108E-01	4.60	55E-02	-19.13	0.0000
IIMODE	-4.5733E-01	3.18	91E-02	-14.34	0.0000
I3	2.8479E-02	4.54	43E-03	6.27	0.0000
FORMAT2	3.7038E-02		44E-03	14.61	0.0000
CASES INCL	JDED	72	MISSING	CASES 0	
DEGREES OF	FREEDOM	66			
OVERALL F	210	. 5	P VALUE	0.0000	
ADJUSTED R	SQUARED 0.93	65			
R SQUARED	0.94	10			
RESID. MEAN		24E-02			
	_			011 OF 671/771	
OWMRIGHTED	LEAST SQUARES	LINEAR	REGRESSI	ON OF THEM	
PREDICTOR					
VARIABLES	COEFFICIENT	STD	ERROR	STUDENT'S I	r P
CONSTANT	8.3565		03E-01	11.19	0.0000
FFD	2.1663E-02		47E-03	4.83	0.0000
FORMAT	<b>-8.8</b> 108E-01	3.95	58E-02	-22.27	0.0000
IIMODE	-1.4139	1.95	35E-01	-7.24	0.0000
I3	2.8479E-02	3.90	32E-03	7.30	0.0000
IIMODE2	6.9753E-02	1.41	04E-02	4.95	0.0000
FORMAT2	3.7038E-02		68E-03	17.01	0.0000
CASES INCL	JDED '	72	MISSING	CASES 0	
			MISSING	CASES 0	
DEGREES OF	FREEDOM	65			
DEGREES OF OVERALL F	FREEDOM 241	65 .9	MISSING		
DEGREES OF OVERALL F ADJUSTED R	FREEDOM 241 SQUARED 0.95	65 .9 32			
DEGREES OF OVERALL F ADJUSTED R R SQUARED	FREEDOM 241 SQUARED 0.95 0.95	65 .9 32 71			
DEGREES OF OVERALL F ADJUSTED R R SQUARED RESID. MEAN	FREEDOM 241 SQUARED 0.95 0.95 N SQUARE 6.2	65 .9 32 71 15E-02	P VALUE	0.0000	
DEGREES OF OVERALL F ADJUSTED R R SQUARED RESID. MEAN	FREEDOM 241 SQUARED 0.95 0.95 N SQUARE 6.2	65 .9 32 71 15E-02	P VALUE	0.0000	
DEGREES OF OVERALL F ADJUSTED R R SQUARED RESID. MEAN UNWEIGHTED	FREEDOM 241 SQUARED 0.95 0.95	65 .9 32 71 15E-02	P VALUE	0.0000	
DEGREES OF OVERALL F ADJUSTED R R SQUARED RESID. MEAN UNWEIGHTED PREDICTOR	FREEDOM 241 SQUARED 0.95 0.95 N SQUARE 6.2	65 .9 32 71 15E-02	P VALUE	0.0000	
DEGREES OF OVERALL F ADJUSTED R R SQUARED RESID. MEAN UNWEIGHTED	FREEDOM 241 SQUARED 0.95 0.95 N SQUARE 6.2	65 .9 32 71 15E-02 LINEAR	P VALUE	0.0000 ON OF TMFM	·
DEGREES OF OVERALL F ADJUSTED R R SQUARED RESID. MEAN UNWEIGHTED PREDICTOR	FREEDOM  241 SQUARED 0.95 0.95 N SQUARE 6.2 LEAST SQUARES	65 .9 32 71 15E-02 LINEAR	P VALUE	0.0000	. P
DEGREES OF OVERALL F ADJUSTED R R SQUARED RESID. MEAN UNWEIGHTED PREDICTOR VARIABLES	FREEDOM  241 SQUARED 0.95 0.95 N SQUARE 6.2 LEAST SQUARES COEFFICIENT	65 .9 32 71 15E-02 LINEAR	P VALUE REGRESSI ERROR	0.0000 ON OF TMFM STUDENT'S T	
DEGREES OF OVERALL F ADJUSTED R R SQUARED RESID. MEAN UNWEIGHTED PREDICTOR VARIABLES	FREEDOM 241 SQUARED 0.95 0.95 N SQUARE 6.2 LEAST SQUARES COEFFICIENT 8.9680	65 .9 32 71 15E-02 LINEAR STD	P VALUE REGRESSI ERROR 21E-01	0.0000 ON OF TMFM STUDENT'S T	0.0000
DEGREES OF OVERALL F ADJUSTED R R SQUARED RESID. MEAN UNWEIGHTED PREDICTOR VARIABLES CONSTANT	FREEDOM  241 SQUARED 0.95 0.95 N SQUARE 6.2 LEAST SQUARES  COEFFICIENT 8.9680 2.1663E-02	65 .9 32 71 15E-02 LINEAR STD  5.85 3.46	P VALUE REGRESSI ERROR 21E-01 99E-03	0.0000 ON OF TMFM  STUDENT'S T  15.32 6.24	0.0000
DEGREES OF OVERALL F ADJUSTED R R SQUARED RESID. MEAN UNWEIGHTED PREDICTOR VARIABLES CONSTANT FFD FORMAT	FREEDOM 241 SQUARED 0.95 0.95 N SQUARE 6.2 LEAST SQUARES COEFFICIENT 8.9680 2.1663E-02 -1.5701	65 .9 32 71 15E-02 LINEAR STD  5.85 3.46 1.07	P VALUE REGRESSI ERROR 21E-01 99E-03 64E-01	0.0000 ON OF TMFM  STUDENT'S T  15.32 6.24 -14.59	0.0000 0.0000 0.0000
DEGREES OF OVERALL F ADJUSTED R R SQUARED RESID. MEAN UNWEIGHTED PREDICTOR VARIABLES CONSTANT FFD	FREEDOM 241 SQUARED 0.95 0.95 N SQUARE 6.2 LEAST SQUARES COEFFICIENT	65 .9 32 71 15E-02 LINEAR STD  5.85 3.46 1.07 1.51	P VALUE REGRESSI ERROR 21E-01 99E-03 64E-01 15E-01	0.0000 ON OF TMFM  STUDENT'S T  15.32 6.24 -14.59 -9.35	0.0000 0.0000 0.0000 0.0000
DEGREES OF OVERALL F ADJUSTED R R SQUARED RESID. MEAN UNWEIGHTED PREDICTOR VARIABLES 	FREEDOM 241 SQUARED 0.95 0.95 N SQUARE 6.2 LEAST SQUARES COEFFICIENT	65 .9 32 71 15E-02 LINEAR STD  5.85 3.46 1.07 1.51 3.02	P VALUE REGRESSI ERROR 21E-01 99E-03 64E-01 15E-01 00E-03	0.0000  ON OF TMFM  STUDENT'S T	0.0000 0.0000 0.0000 0.0000 0.0000
DEGREES OF OVERALL F ADJUSTED R R SQUARED RESID. MEAN UNWEIGHTED PREDICTOR VARIABLES 	FREEDOM 241 SQUARED 0.95 0.95 N SQUARE 6.2 LEAST SQUARES  COEFFICIENT	65 .9 32 71 15E-02 LINEAR STD  5.85 3.46 1.07 1.51 3.02 1.09	P VALUE REGRESSI ERROR 21E-01 99E-03 64E-01 15E-01 00E-03 12E-02	0.0000  ON OF TMFM  STUDENT'S T  15.32 6.24 -14.59 -9.35 9.43 6.39	0.0000 0.0000 0.0000 0.0000 0.0000 0.0000
DEGREES OF OVERALL F ADJUSTED R R SQUARED RESID. MEAN UNWEIGHTED PREDICTOR VARIABLES 	FREEDOM 241 SQUARED 0.95 0.95 N SQUARE 6.2 LEAST SQUARES  COEFFICIENT	65 .9 32 71 15E-02 LINEAR STD  5.85 3.46 1.07 1.51 3.02 1.09 2.29	P VALUE REGRESSI ERROR 21E-01 99E-03 64E-01 15E-01 00E-03 12E-02 66E-02	0.0000  ON OF TMFM  STUDENT'S T  15.32 6.24 -14.59 -9.35 9.43 6.39 8.27	0.0000 0.0000 0.0000 0.0000 0.0000 0.0000
DEGREES OF OVERALL F ADJUSTED R R SQUARED RESID. MEAN UNWEIGHTED PREDICTOR VARIABLES 	FREEDOM 241 SQUARED 0.95 0.95 N SQUARE 6.2 LEAST SQUARES  COEFFICIENT	65 .9 32 71 15E-02 LINEAR STD  5.85 3.46 1.07 1.51 3.02 1.09 2.29	P VALUE REGRESSI ERROR 21E-01 99E-03 64E-01 15E-01 00E-03 12E-02	0.0000  ON OF TMFM  STUDENT'S T  15.32 6.24 -14.59 -9.35 9.43 6.39	0.0000 0.0000 0.0000 0.0000 0.0000 0.0000
DEGREES OF OVERALL F ADJUSTED R R SQUARED RESID. MEAN UNWEIGHTED PREDICTOR VARIABLES CONSTANT FFD FORMAT IIMODE 13 IIMODE2 FORMAT2 FORMAT3	FREEDOM 241 SQUARED 0.95 0.95 N SQUARE 6.2 LEAST SQUARES  COEFFICIENT	65 .9 32 71 15E-02 LINEAR STD  5.85 3.46 1.07 1.51 3.02 1.09 2.29 1.24	P VALUE REGRESSI ERROR 21E-01 99E-03 64E-01 15E-01 00E-03 12E-02 66E-02	0.0000 ON OF TMFM  STUDENT'S T  15.32 6.24 -14.59 -9.35 9.43 6.39 8.27 -6.68	0.0000 0.0000 0.0000 0.0000 0.0000 0.0000
DEGREES OF OVERALL F ADJUSTED R R SQUARED RESID. MEAN UNWEIGHTED PREDICTOR VARIABLES	FREEDOM 241 SQUARED 0.95 0.95 N SQUARE 6.2 LEAST SQUARES  COEFFICIENT	65 .9 32 71 15E-02 LINEAR STD  5.85 3.46 1.07 1.51 3.02 1.09 2.29 1.24	P VALUE REGRESSI ERROR 21E-01 99E-03 64E-01 15E-01 00E-03 12E-02 66E-02	0.0000  ON OF TMFM  STUDENT'S T  15.32 6.24 -14.59 -9.35 9.43 6.39 8.27 -6.68	0.0000 0.0000 0.0000 0.0000 0.0000 0.0000
DEGREES OF OVERALL F ADJUSTED R R SQUARED RESID. MEAN UNWEIGHTED PREDICTOR VARIABLES	FREEDOM 241 SQUARED 0.95 0.95 N SQUARE 6.2 LEAST SQUARES  COEFFICIENT	65 .9 32 71 15E-02 LINEAR STD  5.85 3.46 1.07 1.51 3.02 1.09 2.29 1.24	P VALUE  REGRESSI  ERROR 21E-01 99E-03 64E-01 15E-01 00E-03 12E-02 66E-02 68E-03  MISSING	0.0000 ON OF TMFM  STUDENT'S T  15.32 6.24 -14.59 -9.35 9.43 6.39 8.27 -6.68	0.0000 0.0000 0.0000 0.0000 0.0000 0.0000
DEGREES OF OVERALL F ADJUSTED R R SQUARED RESID. MEAN UNWEIGHTED PREDICTOR VARIABLES	FREEDOM 241 SQUARED 0.95 0.95 N SQUARE 6.2 LEAST SQUARES  COEFFICIENT	65 .9 32 71 15E-02 LINEAR STD  5.85 3.46 1.07 1.51 3.02 1.09 2.29 1.24	P VALUE REGRESSI ERROR 21E-01 99E-03 64E-01 15E-01 00E-03 12E-02 66E-02	0.0000 ON OF TMFM  STUDENT'S T  15.32 6.24 -14.59 -9.35 9.43 6.39 8.27 -6.68	0.0000 0.0000 0.0000 0.0000 0.0000 0.0000
DEGREES OF OVERALL F ADJUSTED R R SQUARED RESID. MEAN UNWEIGHTED PREDICTOR VARIABLES	FREEDOM 241 SQUARED 0.95 0.95 N SQUARE 6.2 LEAST SQUARES  COEFFICIENT	65 .9 32 71 15E-02 LINEAR STD  5.85 3.46 1.07 1.51 3.09 2.29 1.24	P VALUE  REGRESSI  ERROR 21E-01 99E-03 64E-01 15E-01 00E-03 12E-02 66E-02 68E-03  MISSING	0.0000  ON OF TMFM  STUDENT'S T  15.32 6.24 -14.59 -9.35 9.43 6.39 8.27 -6.68  CASES 0	0.0000 0.0000 0.0000 0.0000 0.0000 0.0000
DEGREES OF OVERALL F ADJUSTED R R SQUARED RESID. MEAN UNWEIGHTED PREDICTOR VARIABLES	FREEDOM 241 SQUARED 0.95 0.95 N SQUARE 6.2 LEAST SQUARES  COEFFICIENT	65 .9 32 71 15E-02 LINEAR STD  5.85 3.46 1.07 1.51 3.02 2.29 1.24	P VALUE  REGRESSI  ERROR 21E-01 99E-03 64E-01 15E-01 00E-03 12E-02 66E-02 68E-03  MISSING	0.0000  ON OF TMFM  STUDENT'S T  15.32 6.24 -14.59 -9.35 9.43 6.39 8.27 -6.68  CASES 0	0.0000 0.0000 0.0000 0.0000 0.0000 0.0000
DEGREES OF OVERALL F ADJUSTED R R SQUARED RESID. MEAN UNWEIGHTED PREDICTOR VARIABLES	FREEDOM 241 SQUARED 0.95 0.95 N SQUARE 6.2 LEAST SQUARES  COEFFICIENT	65 .9 32 71 15E-02 LINEAR STD  5.85 3.46 1.07 1.51 3.09 2.29 1.24	P VALUE  REGRESSI  ERROR 21E-01 99E-03 64E-01 15E-01 00E-03 12E-02 66E-02 68E-03  MISSING	0.0000  ON OF TMFM  STUDENT'S T  15.32 6.24 -14.59 -9.35 9.43 6.39 8.27 -6.68  CASES 0	0.0000 0.0000 0.0000 0.0000 0.0000 0.0000

#### RANKITS VS RESID

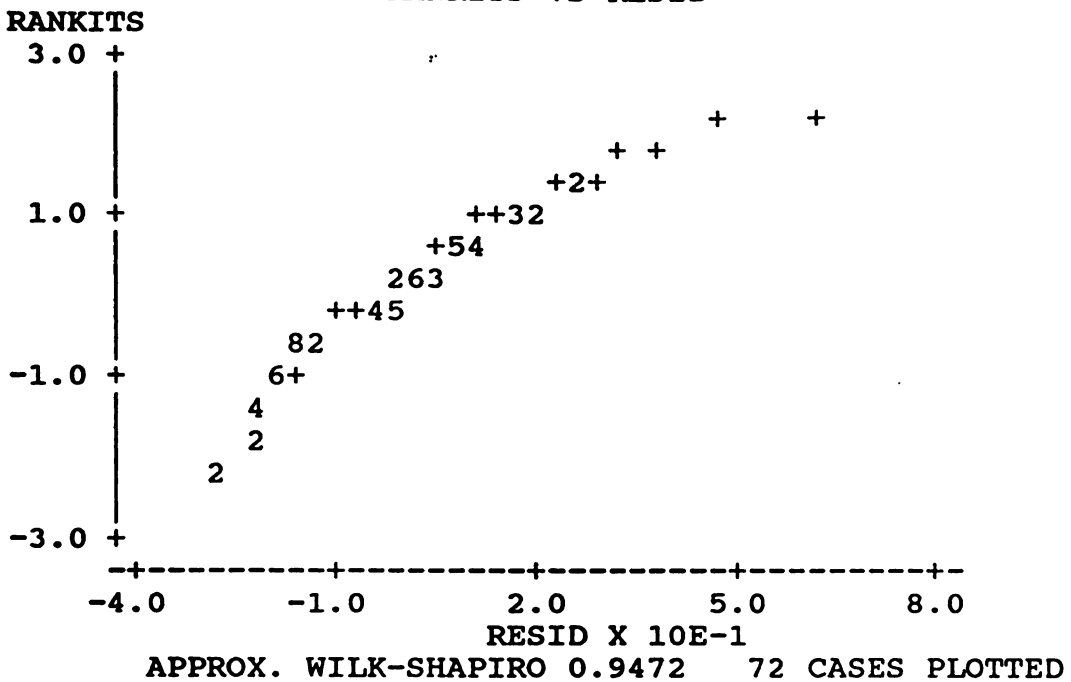


Table 8 A linear function, defined by linear regression analysis, was used to calculate fitted values for TMFm at each focal-film distance (FFD), image intensifier tube mode (II mode) and printer format.

*****		505) ( ) <b>5</b>				 		,	
FFD		FORMAT	TMFM	FITTED	RESID	 			
74.50	9.00	12.00	0.70	0.71	-0.01			<b> </b>	
79.50	9.00	12.00	0.73	0.82	-0.09	 	ļ	<b></b>	
84.50	9.00	12.00	0.77	0.93	-0.16		ļ	<u> </u>	
87.50	9.00	12.00	0.79	0.99	-0.20	 		ļ	
89.50	9.00	12.00	0.81	1.04	-0.23	 	<u> </u>		
94.50	9.00	12.00	0.86	1.14	-0.28	 	ļ		
74.50	6.00	12.00	1.01	0.79	0.22	 	ļ		
79.50	6.00	12.00	1.08	0.90	0.18	 			
84.50	6.00	12.00	1.12	1.00	0.12	 	ļ		
87.50 89.50	6.00	12.00	1.15	1.07	0.08	 <del> </del>	<del> </del>		
94.50	6.00	12.00 12.00	1.18	1.11	0.07	 	<b>}</b>	<u> </u>	
74.50	4.50	12.00	1.24	1.22	0.02			ļ	
79.50	4.50	12.00	1.50	1.41	0.10	 			
84.50	4.50	12.00	1.55	1.51					
87.50	4.50	12.00	1.61		0.04	 	<del> </del>		<u> </u>
89.50	4.50	12.00	1.66	1.58	0.03			<del>                                     </del>	
94.50	4.50	12.00	1.71		-0.02	 			
74.50	9.00	6.00	0.93	1.73 0.66	0.02		<del> </del>	<b></b>	
79.50	9.00	6.00	0.97	0.88	0.20	 	<del> </del>	<del></del>	
84.50	9.00	6.00	1.03	0.88	0.20				
87.50	9.00	6.00	1.05	0.95	0.10			<del></del>	
89.50	9.00	6.00	1.09	0.99	0.10				
94.50	9.00	6.00	1.14	1.10	0.04		<del> </del>		
74.50	6.00	6.00	1.33	1.25	0.08		<del></del>	<del></del>	
79.50	6.00	6.00	1.39	1.36	0.03	 		<b></b>	
84.50	6.00	6.00	1.50	1.47	0.03	 			
87.50	6.00	6.00	1.54	1.54	0.00	 	<del>                                     </del>		
89.50	6.00	6.00	1.59	1.58	0.01		<b></b>	<u> </u>	
94.50	6.00	6.00	1.65	1.69	-0.04			<u> </u>	
74.50	4.50	6.00	1.85	2.02	-0.17	 			
79.50	4.50	6.00	1.93	2.13	-0.20				
84.50	4.50	6.00	2.09	2.24	-0.15				
87.50	4.50 :	6.00	2.16	2.30	-0.14				
89.50	4.50	6.00	2.20	2.35	-0.15			<b>1</b>	
94.50	4.50	6.00	2.29	2.45	-0.16				
74.50	9.00	4.00	1.07	0.76	0.31				
79.50	9.00	4.00	1.13	0.87	0.26				
84.50	9.00	4.00	1.18	0.97	0.21			<u> </u>	
87.50	9.00	4.00	1.22	1.04	0.18				
89.50	9.00	4.00	1.25	1.08	0.17				
94.50	9.00	4.00	1.31	1.19	0.12				
74.50	6.00	4.00	1.54	1.52	0.02				
<i>7</i> 9.50	6.00	4.00	1.62	1.63	-0.01				
84.50	6.00	4.00	1.72	1.74	-0.02				
87.50	6.00	4.00	1.77	1.80	-0.03				
89.50	6.00	4.00	1.82	1.84	-0.02				
94.50	6.00	4.00	1.90	1.95	-0.05				
74.50	4.50	4.00	2.14	2.37	-0.23				
79.50	4.50	4.00	2.27	2.48	-0.21				
84.50	4.50	4.00	2.40	2.59	-0.19				
87.50	4.50	4.00	2.47	2.65	-0.18				

Table 8 continued

	111 (ODE	EODL (AT	773 (53.4	FIGURE	DECID					
FFD		FORMAT		FITTED	RESID					
89.50	4.50	4.00	2.53	2.70 2.80	-0.17					
94.50 74.50	4.50 9.00	4.00 1.00	2.64 2.15	2.37	-0.16 -0.22					
	9.00		2.13	2.48	-0.22					
79.50		1.00	2.39	2.48	-0.20					
84.50	9.00				-0.20					
87.50	9.00	1.00	2.47	2.66						
89.50	9.00	1.00	2.54	2.70	-0.16					
94.50	9.00	1.00	2.65	2.81	-0.16					
74.50	6.00	1.00	3.10 3.28	3.39	-0.29 -0.22					
79.50	6.00	1.00	3.47	3.61	-0.22					
84.50	6.00			3.67	-0.14					
87.50	6.00	1.00	3.61 3.69	3.72	-0.03					
89.50			3.88	3.83	0.05					
94.50	6.00	1.00			-0.02					
74.50	4.50	1.00	4.35	4.37	0.02					
79.50	4.50	1.00	4.57	4.48	0.09					
84.50	4.50 :	1.00	4.88	4.59						
87.50	4.50	1.00	5.04	4.65 4.70	0.39 0.47					
89.50	4.50	1.00	5.17		0.47					
94.50	4.50	1.00	5.41	4.80	0.61					
	ļ									
	<b></b>	<u> </u>								
	ļ									
		ļ								
		<b>!</b>		<b> </b>	· · ·					
	<u> </u>	<u> </u>	<del></del>	-						
				<b></b> -						
<b></b>				<u> </u>						
	<b></b>			<del></del>						
	<u> </u>		<del> </del>	<del>}</del>						
	<u> </u>			<del></del>						
	-		<u> </u>	<del> </del>						
	<b></b>		<del> </del>							
	<del> </del>	<del> </del>	<b> </b>							
<b></b>	<del> </del>	-	<del></del>	<del> </del>	<b>_</b>					
<u> </u>		<del> </del>		<del> </del>	<b></b>					
<b></b>		-	<del> </del>		<u> </u>					
<u> </u>	<del> </del>	<del> </del>	-	<del> </del>					<del></del>	
	ļ	<del> </del>	<del> </del>	<del> </del>					<del></del>	
<u> </u>	<u> </u>							<del></del>		<b> </b>
		<del> </del>	<del> </del>	<del> </del>	<del> </del>					
		<del>                                     </del>	<del> </del>			<b> </b>		<del> </del>	<del> </del>	ļ
<b></b>		<del> </del>						<b></b>	<b></b> -	<b> </b>
		<del> </del>		ļ	<del> </del>	<del></del>			<del> </del>	
ļ		<del> </del>	<del> </del>		<del>  </del>	<u> </u>	<b></b>	<b> </b>	<b></b>	
	<del> </del>	ļ			<del>                                     </del>			<del> </del>		<b> </b>
ļ	<b>ļ</b>	<del></del>	<del></del>	<del></del>		ļ			<u> </u>	
		<del> </del>		ļ	ļ	ļ	<del> </del>	<u> </u>	<u> </u>	
	ļ	<b></b>		<b> </b>	ļ	<b></b>	<u> </u>	<b></b>	<del> </del>	
	<u> </u>	<u></u>	L	L	L	L	<u> </u>	L	L	I

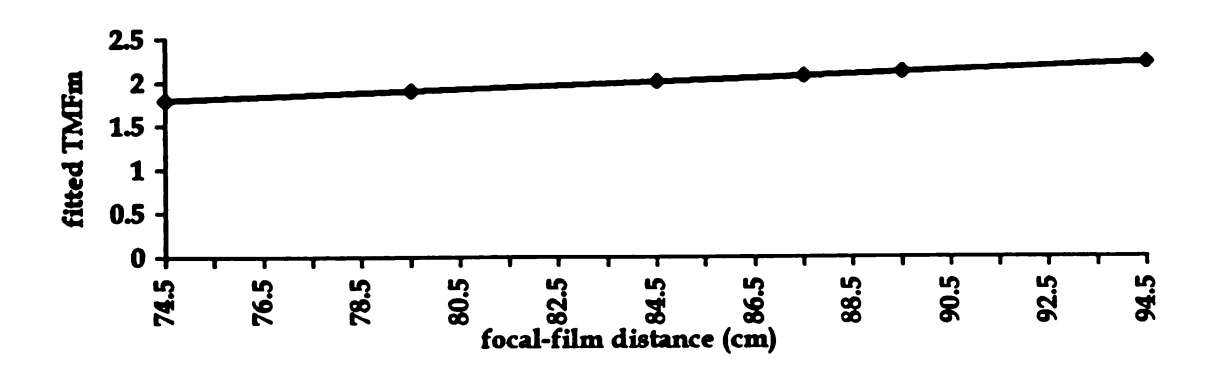


Figure 32 Fitted values for total magnification factors (TMFm), averaged over all II modes and formats, increased gradually with increasing FFD.

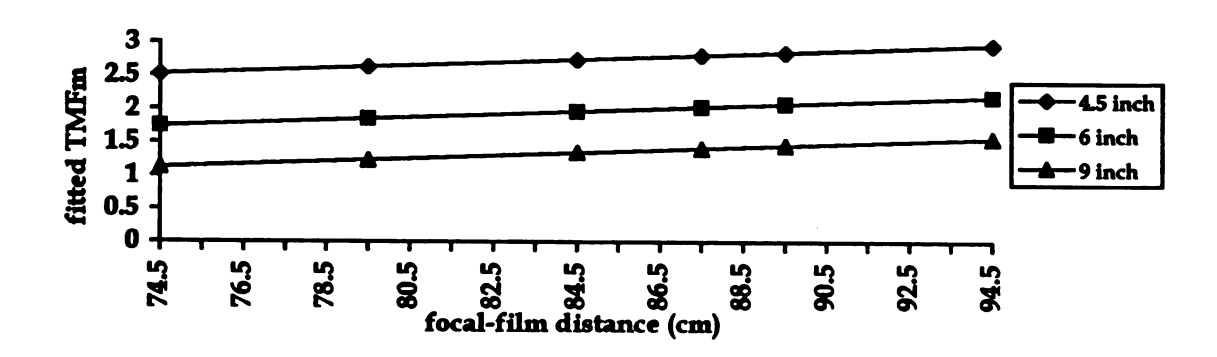


Figure 33 Fitted values for total magnification factors (TMFm), averaged over all formats were higher for smaller II modes, but as FFD increased, the trend of increasing magnification factors was the same for each II mode.

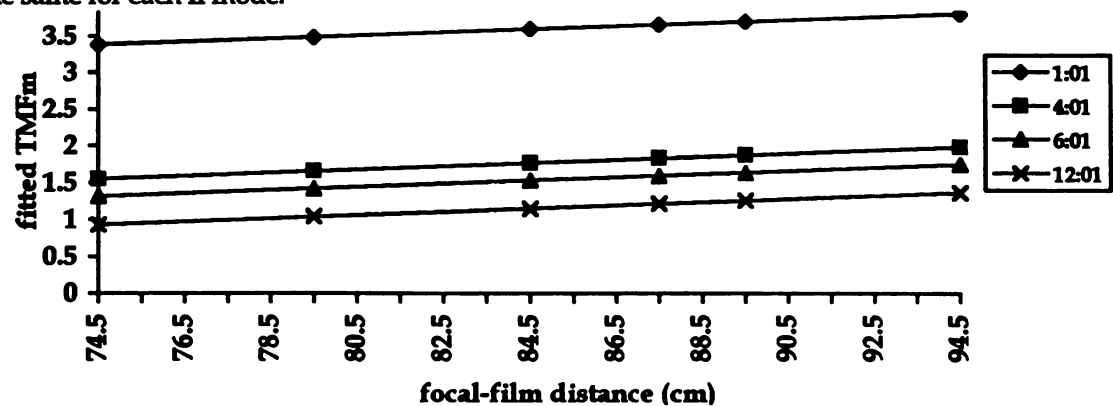


Figure 34 Fitted values for total magnification factors (TMFm), averaged over all II modes, were higher for formats with fewer images per sheet of film, but as FFD increased, the trend of increasing magnification factors was the same for each format.

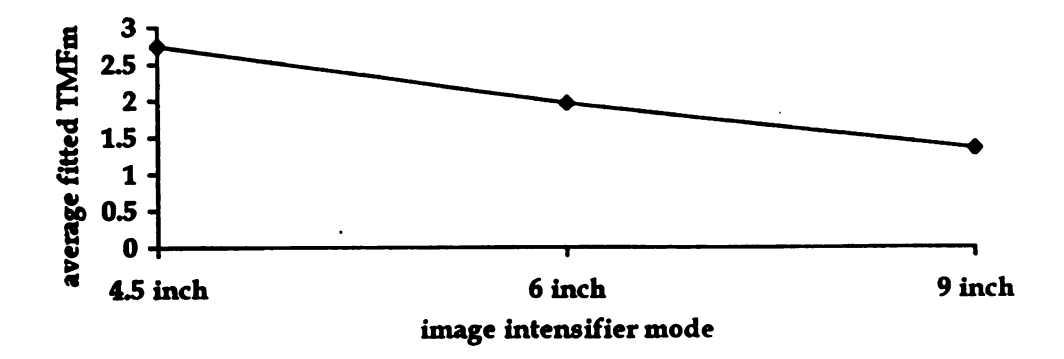


Figure 35 Fitted values for total magnification factors (TMFm), averaged over all FFD's and formats, decreased steadily with increasing II mode.

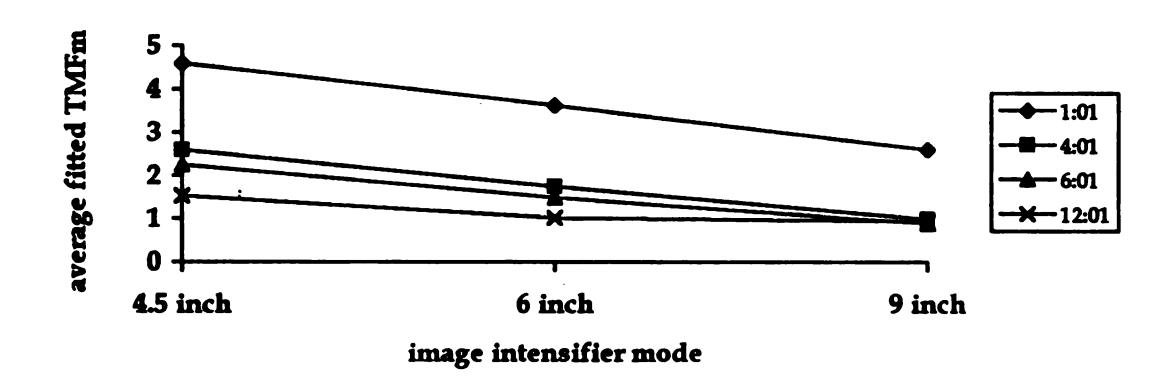


Figure 36 Fitted values for total magnification factors (TMFm), averaged over all FFD's, were higher for formats with fewer images per sheet of film. As II mode increased, fitted TMFm decreased at every format.

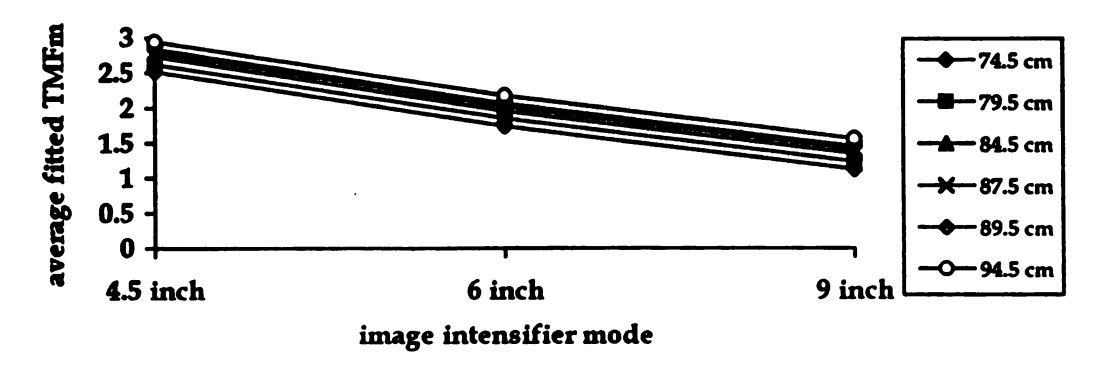


Figure 37 Fitted values for total magnification factors (TMFm), averaged over all formats, were higher for longer FFD's, but as II mode increased, the trend of decreasing magnification was the same for each FFD.

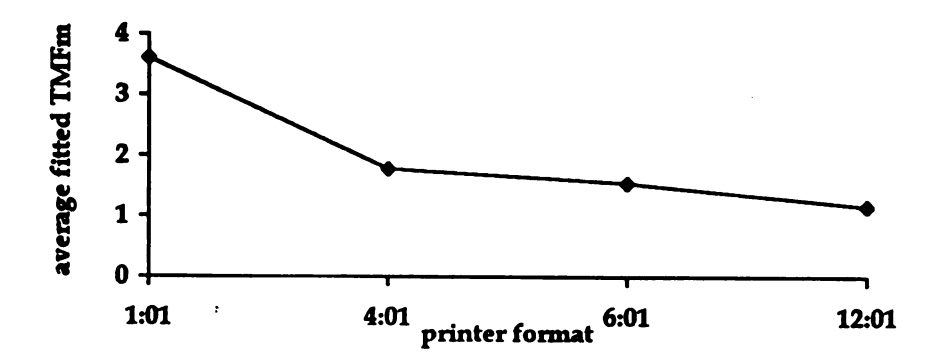


Figure 38 Fitted values for total magnification factors (TMFm), averaged over all FFD's and II modes, decreased as format increased.

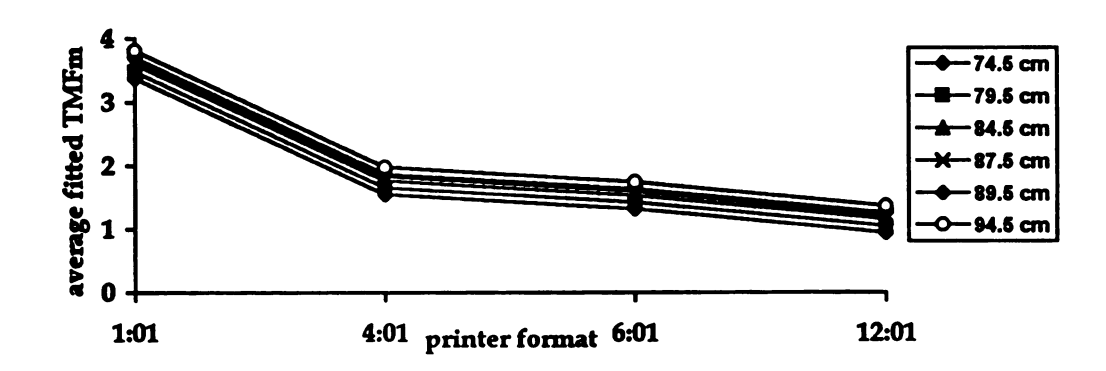


Figure 39 Fitted values for total magnification factors (TMFm), averaged over all II modes, were higher for longer FFD's, but as format increased, the trend of decreasing magnification factors was the same for each FFD.

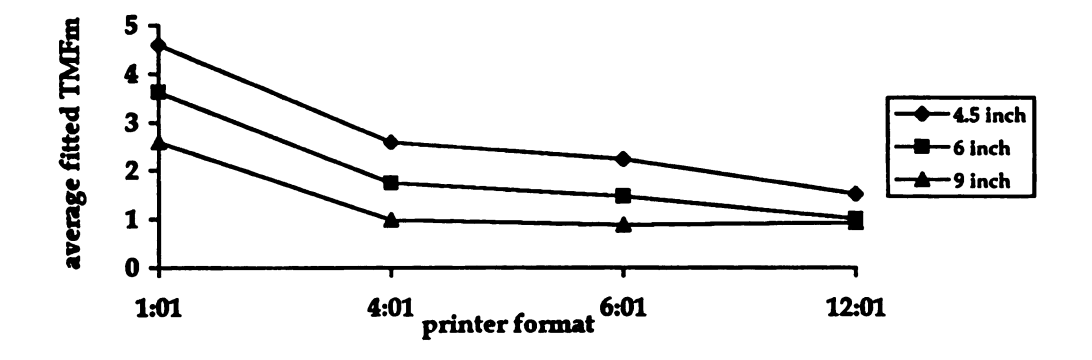


Figure 40 Fitted values for total magnification factors (TMFm), averaged over all FFD's, decreased as the number of images per sheet of film (format) increased.

#### **APPENDIX C**

#### **APPENDIX C**

Table 9 Magnification factors were calculated for individual components of the digital radiographic imaging system, at each focal-film distance, image intensifier mode and printer format.

FOCAL-FILM DISTANCE	MAGNIFICATION FACTOR
25 cm	Mg=1.50
30 cm	Mg=1.60
35 cm	Mg=1.70
38 cm	Mg=1.77
40 cm	Mg=1.80
45 cm	Mg=1.90
IMAGE INTENSIFIER MODE	
9 INCH	Me=0.10
6 INCH	Me=0.15
4.5 INCH	Me=0.20
PRINTER FORMAT	
1:1	Mp=4.1
4:1	Mp=5.5
6:1	Mp=6.4
12:1	Mp=12.8

## **Descriptive Statistics**

## Output of Statistix 3.1 Analytical Software

Table 10 There was some variation in the difference between measured and calculated total magnification factors (delta) between the radiographic technique variables.

VARIABLE	MEAN DELTA	SAMPLE SIZE	VARIANCE	STAND DEV
FFD				
74.5	0.1767	12	0.01444	0.120
79.5	0.1667	12	0.01272	0.113
84.5	0.1717	12	0.01654	.0129
87.5	0.1608	12	0.01604	0.127
89.5	0.1825	12	0.01873	0.137
94.5	0.1700	12	0.01818	0.135
TOTAL	0.1714	72		X=0.127
II MODE			<del>                                     </del>	
4.5	0.2771	24	0.02151	0.147
6	0.1167	24	0.003736	0.061
9	0.1204	24	0.003639	0.060
TOTAL	0.1714	72		X=0.089
FORMAT				
1	0.3200	18	0.02193	0.148
4	0.1333	18	0.00380	0.062
6	0.1267	18	0.003153	0.056
12	0.1056	18	0.002238	0.047
TOTAL	0.1714	72		X=0.078

# Statistical analysis of Delta (TMFm-TMFc)

# General Linear models proceure, multiple regression analysis

# Output of Statistix 3.1 Analytical Software

PREDICTOR VARIABLES	COEFFICIENT	STD ERROR	STUDENT'S T	P
CONSTANT	1.7772E-01	1.8932E-01	0.94 -0.03	0.3511
				0.9734
CASES INCLUDE	D 72	MISSING E-03 P VALUE	CASES 0	
DEGREES OF FR	REEDOM 70		0.0724	
OVERALL F	1.124	E-03 L ANTOE	0.9/34	
ADJUSTED R SC	UARED -0.0143			
RESID. MEAN S	0.0000 SQUARE 1.524	E-02		
DDPDT CTOD	-	LINEAR REGRESSI	STUDENT'S T	P
	2 6420R-01	4 6012B-02	7.78	
CUNSTANT	3.042UE-UI	4.00125-02	-4.29	0.0000
				0.0001
CASES INCLUDE	ED . 72	MISSING P VALUE	CASES 0	
DEGREES OF F	REEDOM 70	)		
OVERALL F	18.37	P VALUI	0.0001	
ADJUSTED R S	QUARED 0.1960	5		
R SQUARED	0.2079	)		
RESID. MEAN	0.2079 SQUARE 1.207	7E-02		
PREDICTOR		STD ERROR	STUDENT'S T	ъ
CONSTANT	2.6569E-01	2.1323E-02	12.46 -5.40	0.0000
FORMAT	-1.6401E-02	3.0384E-03	-5.40	0.0000
CASES INCLUDE	ED 72	MISSING P VALUE P VALUE P VALUE	CASES 0	
DEGREES OF FI	REEDOM 70	)		
OVERALL F	29.14	P VALUE	0.0000	
ADJUSTED R S	QUARED 0.2838	3	•	
D COTT DDD	0 0000	١.		
K SOOKED	0.2939	<b>)</b> .		

PREDICTOR VARIABLES		CIENT		STUDENT'S T	P
			1.7565E-01	2.11	0.0385
CONSTANT		2E-01 4E-05		-0.04	0.9703
FFD IIMODE		3E-02		-4.26	0.0001
	_		WTGGTN	CASES 0	
CASES INCLU DEGREES OF OVERALL F	DED	72 69	MISSING	CASES	
DEGREES OF	FREEDOM	9.054	P VALUE	B 0.0004	
OVERALL F ADJUSTED R	COULDED	0.1849	•		
R SQUARED	SQUALLED	0.2079			
RESID. MEAN	SQUARE	1.225	Z-02		
			INEAR REGRESS	ION OF DELTA	
VARIABLES	COEFFI	CIENT	STD ERROR	STUDENT'S T	P
CONSTANT		2E-01		1.69	0.0960
FFD		4E-05	1.8795E-03	-0.04	0.9685
FORMAT	-1.640	1E-02	3.0603E-03	-5.36	0.0000
CASES INCLUDEGREES OF	DED	72	MISSIN	G CASES 0	
OVERALL F	PREEDOM	69			
OAPKWIN L		14.30	F VALUE	E 0.0000	
ADJUSTED R R SQUARED	SQUAKED	0.2735			
RESID. MEAN	SOUARE				
UNWEIGHTED	-		INEAR REGRESS	ION OF DELTA	
PREDICTOR VARIABLES	COEFFI	OTRUM	STD ERROR	STUDENT'S T	P
AWINDIES		CIENT	SIU ERROR	5100681-5 1	
CONSTANT			4.0209E-02	11.40	0.0000
IIMODE		3 <b>E</b> -02			0.0000
FORMAT	-1.640	1 <b>E</b> -02	2.5707E-03	-6.38	0.0000
CASES INCL	JDED	72	MISSIN	G CASES 0	
	FREEDOM	69			
DEGREES OF					
		34.75		E 0.0000	
DEGREES OF OVERALL F ADJUSTED R		34.75		E 0.0000	
OVERALL F	SQUARED	34.75 0.4873 0.5018		E 0.0000	

PREDICTOR			•	
Variables	COEFFICIENT	STD ERROR	STUDENT'S T	P
CONSTANT	4.6483E-01	1.4111E-01	3.29	0.0016
FFD	-7.4434E-05	1.5903E-03	-0.05	0.9628
IIMODE	-2.9663E-02	5.5688E-03	-5.33	0.0000
FORMAT	-1.6401E-02	2.5894E-03	-6.33	0.0000
CASES INCLU	IDED 72	MISSING	CASES 0	
DEGREES OF	FREEDOM 68			
OVERALL F	22.83	P VALUE	0.0000	
ADJUSTED R	SQUARED 0.4798			
R SQUARED	0.5018			
RESID. MEAN	SQUARE 7.815	E-03		
UNWEIGHTED	LEAST SQUARES L	INEAR REGRESSION	ON OF DELTA	
PREDICTOR				
VARIABLES	COEFFICIENT	STD ERROR	STUDENT'S T	P
CONSTANT	3.8654E-01	E 22222 A1		
FFD	2.1311E-03	5.2278E-01	0.74	0.4623
IIMODE	-2.9385E-02	6.1028E-03	0.35	0.7281
FORMAT	-2.9385E-02 -2.2087E-02	7.1964E-02	-0.41	0.6844
I1	-2.208/E-02 -2.0088E-04	3.4428E-02	-0.64	0.5234
12		8.3909E-04	-0.24	0.8115
13	-1.5649B-04	3.9017E-04	-0.40	0.6897
13	2.9212E-03	1.3663E-03	2.14	0.0363
CASES INCLU		MISSING	CASES 0	
DEGREES OF	FREEDOM 65		4.000	
OVERALL F	12.51	P VALUE	0.0000	
ADJUSTED R	SQUARED 0.4932	1 111202	0.0000	
R SQUARED	0.5360			
RESID. MEAN	SQUARE 7.615	2-03		
UNWEIGHTED	LEAST SQUARES L	NEAR REGRESSIO	N OF DELTA	
PREDICTOR				
VARIABLES	COEFFICIENT	STD ERROR	STUDENT'S T	P
ANKINDLES	CORLLICIBUL	SID EKKOK	SIUDENI S I	F
	5 7044P-01	9.2441E-02	6.17	0.0000
CONSTANT	5.7044E-01			
IIMODE	-4.6460E-02	9.4598E-03	-4.91 -3.88	0.0000
FORMAT	-3.5388E-02	9.1175E-03	-3.88	0.0002
13	2.9212E-03	1.3480E-03	2.17	0.0338
FFD2	-3.8002E-07	9.1797E-06	-0.04	0.9671

72

7.412E-03

67 19.23

MISSING CASES

P VALUE

0

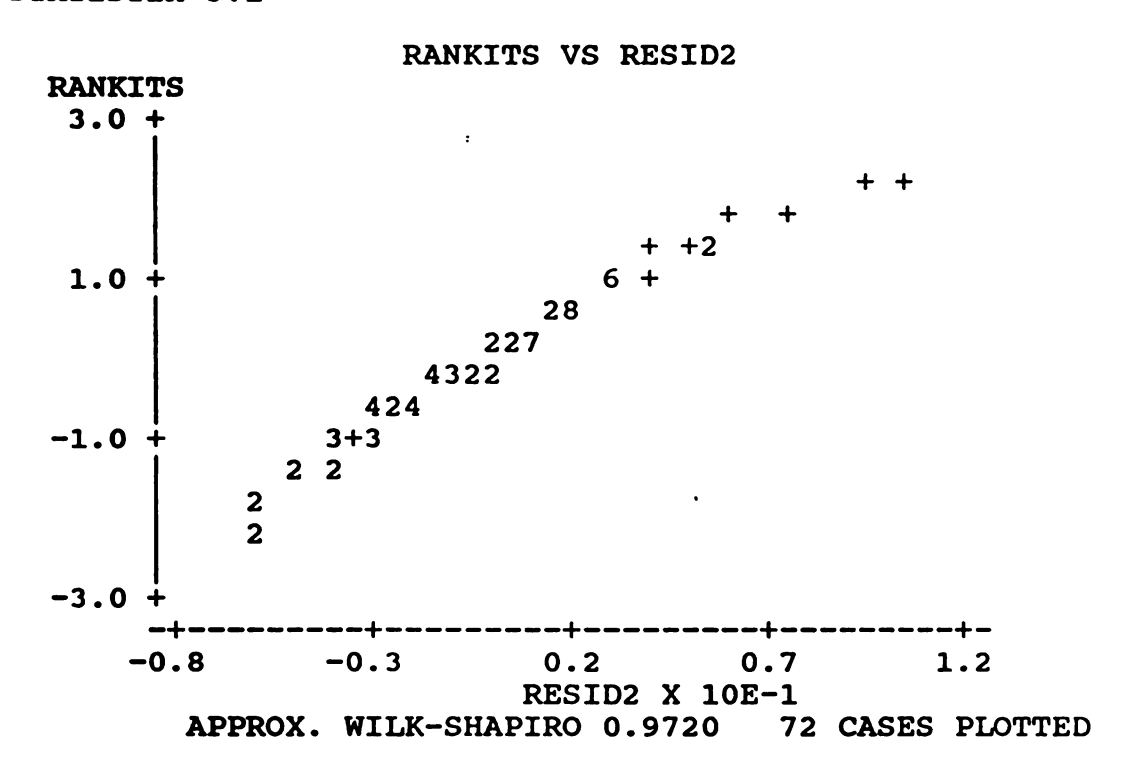
0.0000

CASES INCLUDED
DEGREES OF FREEDOM
OVERALL F

ADJUSTED R SQUARED 0.5066 R SQUARED 0.5344 RESID. MEAN SQUARE 7.4121

PREDICTOR				
VARIABLES	COEFFICIENT	STD ERROR	STUDENT'S T	P
CONSTANT		5 04600 00		
IIMODE	6.7826E-01 -4.6460E-02	5.2462E-02 7.3531E-03	12.93	0.0000
FORMAT	-8.7780E-02	1.0619E-02	-6.32 -8.27	0.0000
13	2.9212E-03	1.0478E-03	2.79	0.0000
FORMAT2	3.8715E-03	5.8435E-04	6.63	0.0000
010B0 THOTA				
CASES INCLU DEGREES OF			CASES 0	
OVERALL F	42.80			
ADJUSTED R			0.0000	
R SQUARED	0.7187			
RESID. MEAN				
		2 03		
	LEAST SQUARES L	INEAR REGRESSI	ON OF DELTA	
PREDICTOR VARIABLES	COEFFICIENT	STD ERROR	STUDENT'S T	P
CONSTANT	1.7216	1.0963E-01	15.70	0.0000
IIMODE	-3.7619E-01	3.3336E-02	-11.28	0.0000
FORMAT	-8.7780E-02	6.7504E-03	-13.00	0.0000
13	2.9212E-03	6.6607E-04	4.39	0.0000
FORMAT2	3.8715E-03	3.7147E-04	10.42	0.0000
IIMODE2	2.4043E-02	2.4068E-03	9.99	0.0000
CASES INCLU			CASES 0	
OVERALL F	104.7		0.0000	
ADJUSTED R			0.000	
R SQUARED	0.8880			
RESID. MEAN				
	LEAST SQUARES L		ON OF DELMA	
		INDIA REGRESSI	ON OF DEDIA	
PREDICTOR VARIABLES	COEFFICIENT	STD ERROR	STUDENT'S T	P
CONSTANT	1.8004	9.8532E-02	18.27	0.0000
IIMODE	-3.7619E-01	2.9465E-02	-12.77	0.0000
FORMAT 13	-1.7657E-01 2.9212E-03	2.0983E-02	-8.41	0.0000
FORMAT2	2.3579E-02	5.8872E-04 4.4769E-03	4.96	0.0000
IIMODE2	2.4043E-02	2.1273E-03	5.27 11.30	0.0000
PORMAT3	-1.0728E-03	2.4306E-04	-4.41	0.0000
	2101202 03	2.43002-04	-4.41	0.0000
CASES INCLU	IDED 72	MISSING	CASES 0	
DEGREES OF	FREEDOM 65			
OVERALL F	114.9	P VALUE	0.0000	
ADJUSTED R				
R SQUARED	0.9138			
RESID. MEAN	SQUARE 1.414	E-03		

#### STATISTIX 3.1



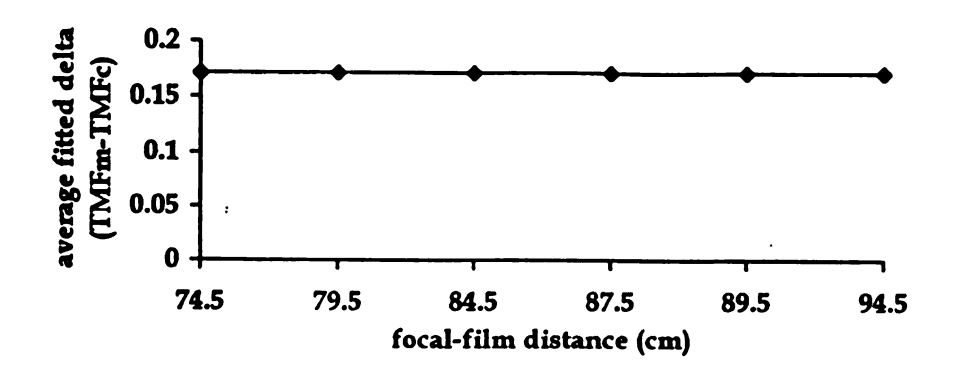


Figure 41 Fitted delta (difference between measured and calculated magnification factors), averaged over all II modes and formats, was the same at every FFD.

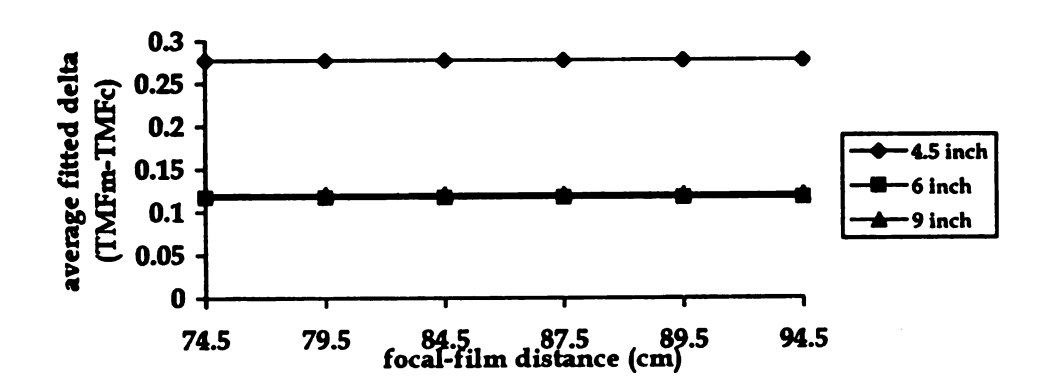


Figure 42 Fitted delta, averaged over all formats, was highest at the 4.5 inch II mode.

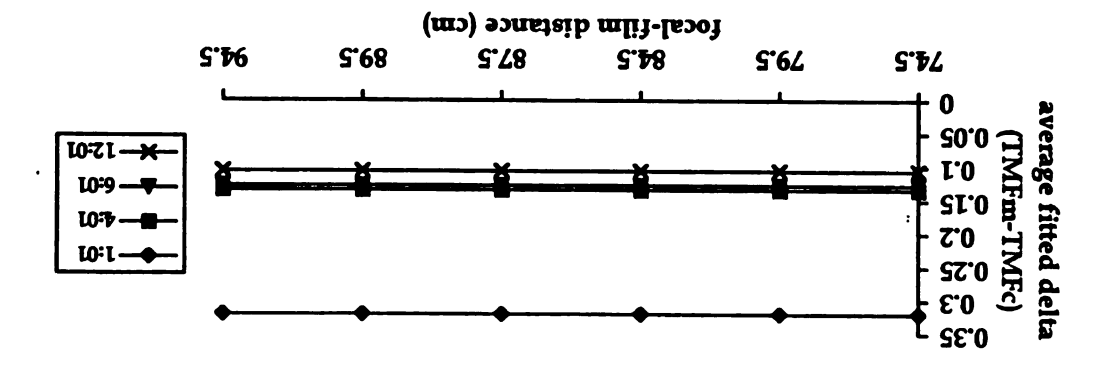


Figure 43 Fitted delta, averaged over all II modes, was highest at the 1:1 format.

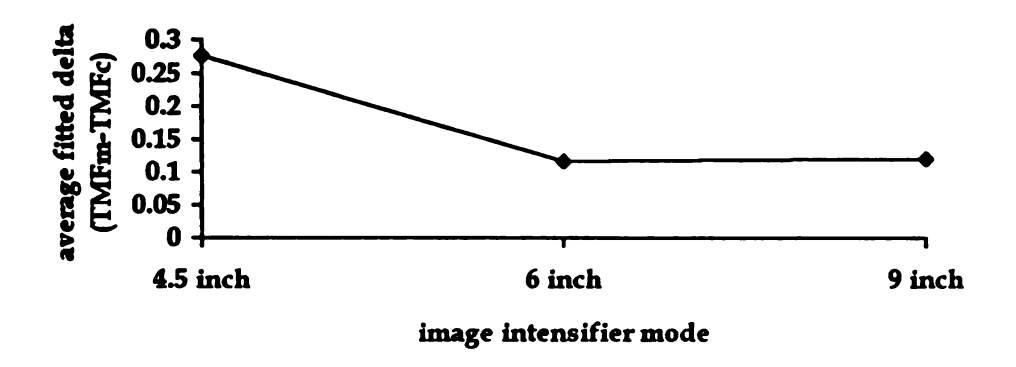


Figure 44 Fitted delta, averaged over all formats and FFD's, was highest at the 4.5 inch II mode.

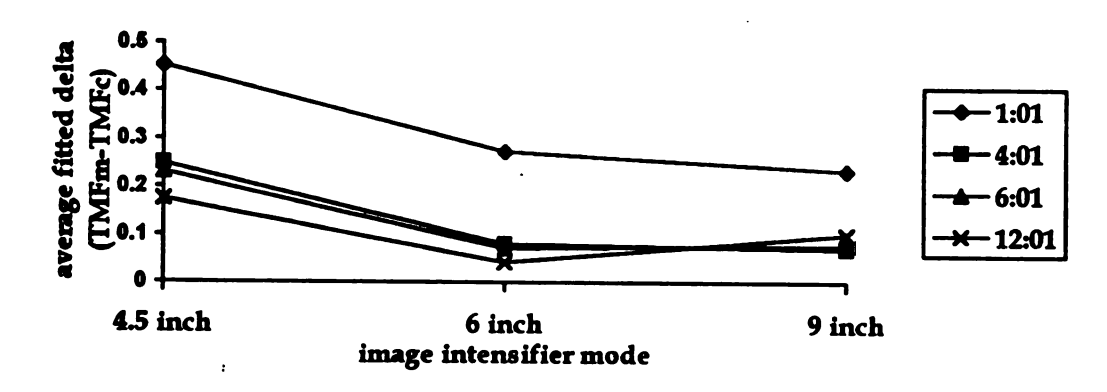


Figure 45 Fitted delta, averaged over all FFD's, was highest at the 1:1 format.

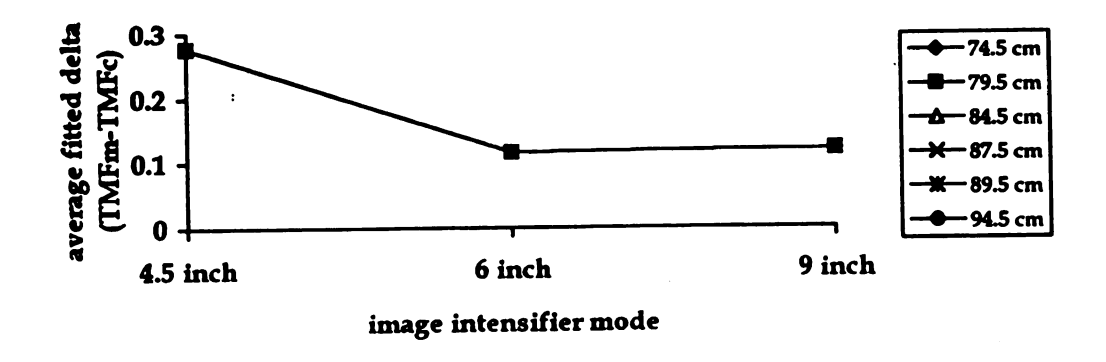


Figure 46 Fitted delta, averaged over all formats, was the same at every FFD.

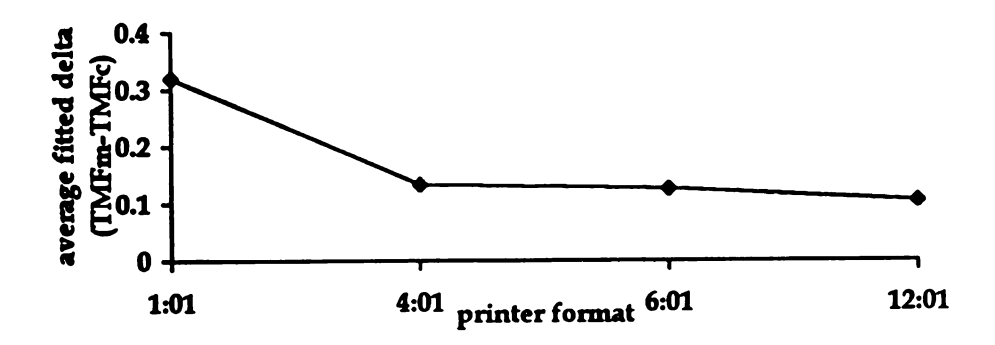


Figure 47 Fitted delta, averaged over all II modes and FFD's, was greatest at the 1:1 format.

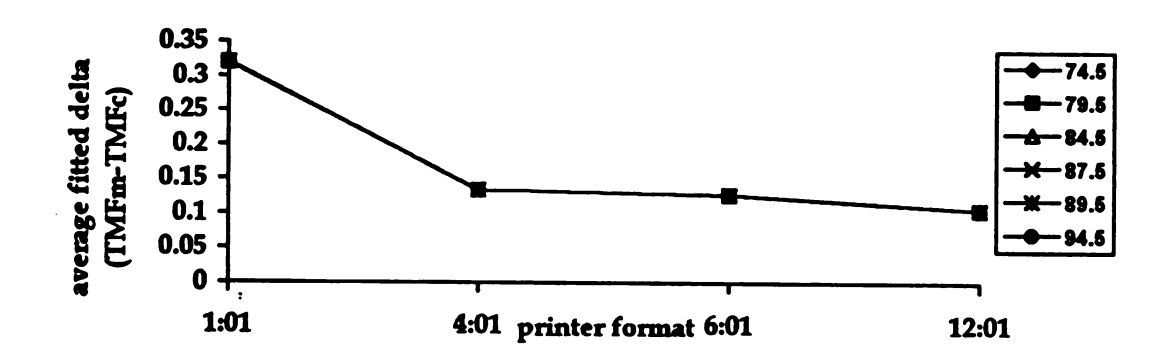


Figure 50 Fitted delta, averaged over all II modes, was the same at every FFD.

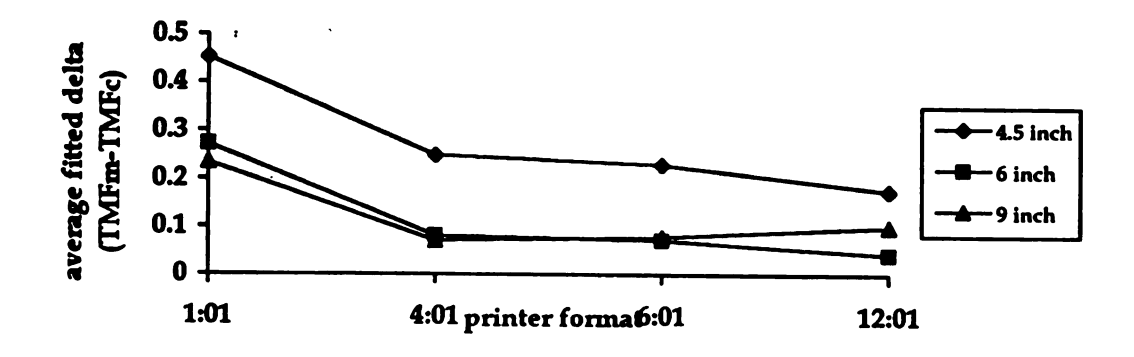


Figure 49 Fitted delta, averaged over all FFD's, was highest at the 4.5 inch II mode.

#### APPENDIX D

#### APPENDIX D

Table 11 Arterial vessels of six in-vitro equine feet were measured on digital angiograms (image size) in the palmarodorsal (PD) and lateromedial (LM) views. Measurements were corrected for magnification to determine the diameter of each vessel (vessel size).

	PALMAR DIGITAL A. PROXIMAL TO BULBAR A.			
HORSE	PD IMAGE SIZE (mm)	PD VESSEL SIZE (mm)	LM IMAGE SIZE (mm)	LM VESSEL SIZE (mm)
1	2.27	2.16	4.29*	3.23
2	2.85	2.71	2.03	2.18
3	2.60	2.48	2.09	2.25
4	3.02	2.88	2.14	2.30
5	1.41	1.34	2.15	2.20
6	2.22	2.11	2.85	3.06
X±SD		2.28±0.55		2.54±0.48
	PALMAR I	DIGITAL A. PROXIMAL TO	DORSAL PHALANGEAL A.	
HORSE	PD IMAGE SIZE (mm)	PD VESSEL SIZE (mm)	LM IMAGE SIZE (mm)	LM VESSEL SIZE (mm)
1	1.75	1.67	3.28*	2.47
2	1.74	1.66	1.73	1.86
3	2.01	1.91	1.82	1.96
4	2.63	2.50	2.06	2.22
5	1.27	1.21	2.10	2.26
6	2.05	1.95	1.90	2.04
X±SD		1.82±0.43		2.14±0.22
	PA	LMAR DIGITAL A. ENTER	ING SOLAR CANAL	
HORSE	PD IMAGE SIZE (mm)	PD VESSEL SIZE (mm)	LM IMAGE SIZE (mm)	LM VESSEL SIZE (mm)
1	1.80	1.71	2.73*	2.05
2	1.64	1.56	N/A	N/A
3	2.35	2.24	N/A	N/A
4	2.17	2.07	1.43	1.54
5	0.88	0.84	1.81	1.95
6	1.27	1.21	1.81	1.95
X±SD		1.61±0.53		1.87±0.23

<sup>\*</sup>In horse 1, the LM view was recorded in the 6 inch mode of the image intensifier tube. All other images were recorded in the 9 inch mode.

Table 11 continued

	BULBAR A.				
HORSE	PD IMAGE SIZE (mm)	PD VESSEL SIZE (mm)	LM IMAGE SIZE (mm)	LM VESSEL SIZE (mm)	
1	N/A	N/A	1.32*	0.99	
2	N/A	N/A	0.99	1.06	
3	N/A	N/A	2.38	2.55	
4	N/A	N/A	1.35	1.45	
5	N/A	N/A	1.06	1.14	
6	N/A	N/A	1.83	1.97	
X±SD		N/A		1.53±0.62	

	CORONARY A.				
HORSE	PD IMAGE SIZE (mm)	PD VESSEL SIZE (mm)	LM IMAGE SIZE (mm)	LM VESSEL SIZE (mm)	
1	N/A	N/A	1.12*	0.84	
2	0.84	0.80	0.68	0.73	
3	N/A	N/A	1.54	1.66	
4	N/A	N/A	0.83	0.89	
5	N/A	N/A	1.05	1.13	
6	N/A	N/A	1.21	1.30	
X±SD		0.80		1.09±0.35	

	DORSAL PHALANGEAL A.				
HORSE	PD IMAGE SIZE (mm)	PD VESSEL SIZE (mm)	LM IMAGE SIZE (mm)	LM VESSEL SIZE (mm)	
1	1.20	1.14	2.11*	1.59	
2	1.50	1.43	0.86	0.92	
3	1.28	1.22	1.72	1.85	
4	0.89	0.85	1.01	1.09	
5	1.03	0.98	0.85	0.91	
6	1.26	1.20	1.58	1.70	
X±SD		1.14±0.20		1.34±0.42	

Table 11 continued

	PALMAR PHALANGEAL A.				
HORSE	PD IMAGE SIZE (mm)	PD VESSEL SIZE (mm)	LM IMAGE SIZE (mm)	LM VESSEL SIZE (mm)	
1	0.95	0.90	1.53*	1.15	
2	0.85	0.81	0.78	0.84	
3	N/A	N/A	0.77	0.83	
4	0.60	0.57	0.65	0.70	
5	0.65	0.62	1.11	1.19	
6	0.80	0.76	1.01	1.09	
X±SD		0.73±0.14		0.97±0.20	

	DISTAL DORSAL PHALANGEAL A.				
HORSE	PD IMAGE SIZE (mm)	PD VESSEL SIZE (mm)	LM IMAGE SIZE (mm)	LM VESSEL SIZE (mm)	
1	1.34	1.28	3.96°	2.98	
2	1.05	1.00	1.09	1.17	
3	0.72	0.69	0.97	1.04	
4	1.51	1.44	1.35	1.45	
5	1.43	1.36	1.76	1.89	
6	0.91	0.87	1.58	1.70	
X±SD		1.11±0.30		1.71±0.70	

	DISTAL PALMAR PHALANGEAL A.				
HORSE	PD IMAGE SIZE (mm)	PD VESSEL SIZE (mm)	LM IMAGE SIZE (mm)	LM VESSEL SIZE (mm)	
1	1.16	1.10	4.04°	3.04	
2	0.83	0.79	0.85	0.91	
3	0.77	0.73	0.96	1.03	
4	0.80	0.76	0.89	0.96	
5	1.27	1.21	1.09	1.17	
6	1.27	1.21	1.09	1.17	
X±SD		0.97±0.23		1.38±0.82	

Table 11 continued

	DORSAL BRANCH OF DISTAL DORSAL PHALANGEAL A.				
HORSE	PD IMAGE SIZE (mm)	PD VESSEL SIZE (mm)	LM IMAGE SIZE (mm)	LM VESSEL SIZE (mm)	
1	1.14	1.09	2.63*	1.98	
2	0.65	0.62	0.89	0.96	
3	0.96	0.91	1.05	1.13	
4	0.87	0.83	0.75	0.81	
5	0.76	0.72	0.73	0.78	
6	1.03	0.98	1.47	1.58	
X±SD		0.8 <del>6±</del> 0.17		1.21±0.48	

	PALMAR BRANCH OF DISTAL DORSAL PHALANGAL A.				
HORSE	PD IMAGE SIZE (mm)	PD VESSEL SIZE (mm)	LM IMAGE SIZE (mm)	LM VESSEL SIZE (mm)	
1	0.57	0.54	1.89*	1.42	
2	0.62	0.59	0.51	0.55	
3	0.91	0.87	0.95	1.02	
4	0.91	0.87	0.68	0.73	
5	0.93	0.89	0.92	0.99	
6	0.76	0.72	0.66	0.71	
X±SD		0. <del>75±</del> 0.15		0.90±0.31	

	TERMINAL ARCH (AT SAGITTAL MIDLINE)				
HORSE	PD IMAGE SIZE (mm)	PD VESSEL SIZE (mm)	LM IMAGE SIZE (mm)	LM VESSEL SIZE (mm)	
1	1.37	1.30	3.25*	2.44	
2	1.64	1.56	1.13	1.21	
3	1.49	1.42	N/A	N/A	
4	1.88	1.79	1.40	1.51	
5	1.16	1.10	2.06	2.22	
6	1.42	1.35	1.49	1.60	
X±SD		1.42±0.24		1.80±0.51	

Table 11 continued

	DORSAL BRANCH OF TERMINAL ARCH				
HORSE	PD IMAGE SIZE (mm)	PD VESSEL SIZE (mm)	LM IMAGE SIZE (mm)	LM VESSEL SIZE (mm)	
1	0.65	0.62	1.86*	1.40	
2	1.00	0.95	0.36	0.39	
3	0.91	0.87	0.74	0.80	
4	0.53	0.50	0.58	0.62	
5	0.76	0.72	0.94	1.01	
6	0.64	0.61	0.92	0.99	
X±SD		0.71±0.17		0.87±0.35	

SOLAR BRANCH OF TERMINAL ARCH						
HORSE	PD IMAGE SIZE (mm)	PD VESSEL SIZE (mm)	LM IMAGE SIZE (mm)	LM VESSEL SIZE (mm)		
1	0.97	0.92	1.54°	1.16		
2	0.86	0.82	0.40	0.43		
3	0.90	0.86	0.77	0.83		
4	1.30	1.24	0.60	0.65		
5	0.78	0.74	0.78	0.84		
6	0.57	0.54	1.23	1.32		
X±SD		0.85±0.23		0.87±0.33		

SOLAR MARGIN A.						
HORSE	PD IMAGE SIZE (mm)	PD VESSEL SIZE (mm)	LM IMAGE SIZE (mm)	LM VESSEL SIZE (mm)		
1	0.71	0.68	0.90°	0.68		
2	0.73	0.70	0.68	0.73		
3	1.10	1.05	N/A	N/A		
4	0.81	0.77	0.66	0.71		
5	0.75	0.71	0.63	0.68		
6	0.95	0.90	0.84	0.90		
X±SD		0.80±0.15		0.74±0.09		

# Paired T-test for comparative analysis of vessel diameters in palmarodorsal and lateromedial view angiograms

STATISTIX 3.1 ID: vessel size

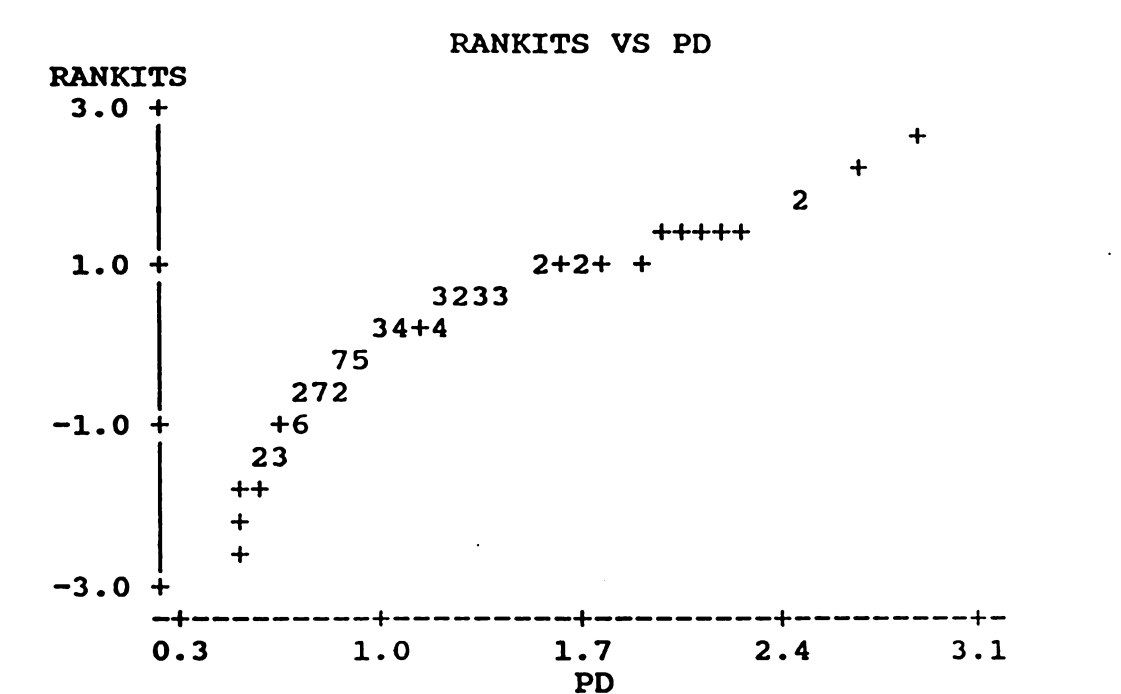
PAIRED T TEST FOR PD - LM

MEAN -2.643E-01 STD ERROR 5.972E-02

T -4.43 DF 73 P 0.0000

CASES INCLUDED 74 MISSING CASES 16

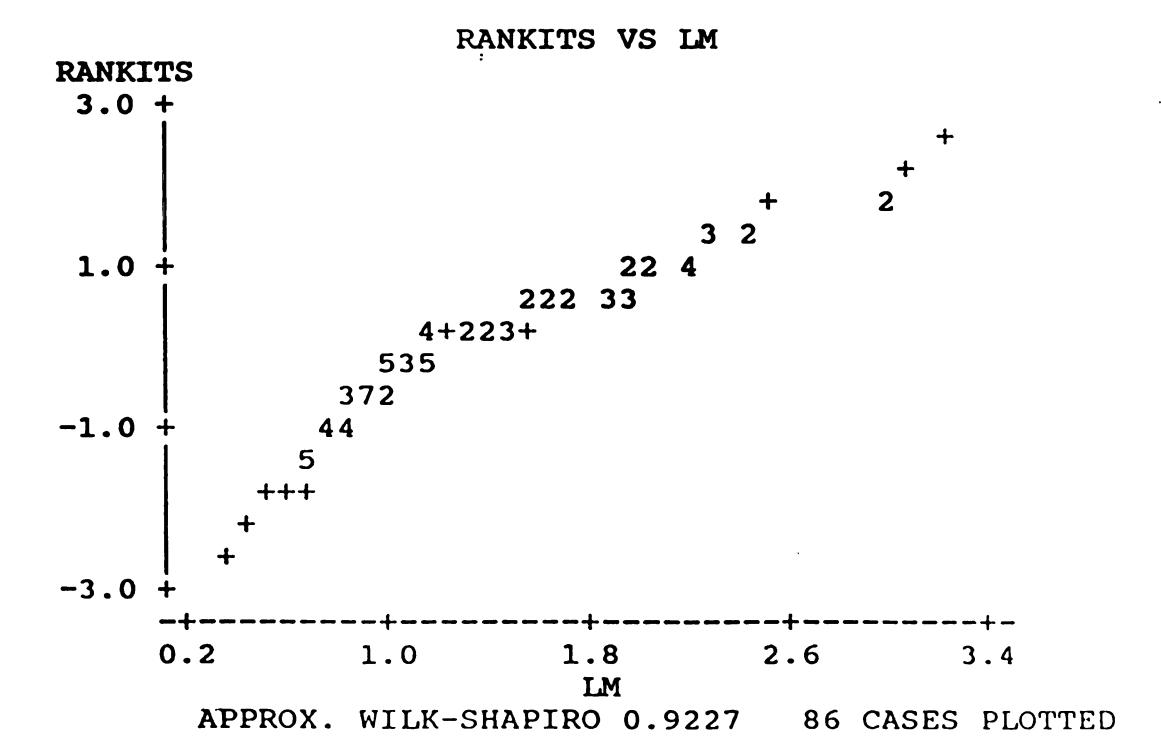
STATISTIX 3.1 ID: vessel size



APPROX. WILK-SHAPIRO 0.8700 78 CASES PLOTTED

STATISTIX 3.1

ID: vessel size



#### LIST OF REFERENCES

#### LIST OF REFERENCES

- 1. Curry TS, Dowdy JE, Murry RC. Christensen's physics of diagnostic radiology, 4th ed. Philadelphia: Lea & Febiger, 1990.
- 2. General Electric medical systems Advantx® specifications manual. Direction 46-019357, revision 3, 1992.
- 3. Kruger RA, Reiderer SJ. Basic concepts of digital subtraction angiography. Boston: G. K. Hall Medical Publishers, 1984;27.
- 4. 3M Service manual, M959 Laser Imager XL, 3M Medical Imaging Systems Division, 1991.
- 5. Webster's new collegiate dictionary. Sprinfield: G. & C. Merriam Company, 1974.
- 6. Greenspan RH. Magnification angiography. In: Abrams angiography-vascular & interventional radiology, 3rd ed. Abrams, ed. Boston: Little, Brown and Company, 1983;205-216.
- 7. Johnsrude IS, Jackson DC. A practical approach to angiography. Boston: Little, Brown and Company, 1979.
- 8. Meridith WJ, Massey JD. Ch.18 Geometric factors which influence the radiographic image. In: Fundamental physics of radiology, 3rd ed. Chicago: John Wright & Sons LTD Publication, 1977;211-232.

- 9. Eastman Kodak Co., The fundamentals of radiography, 12th ed. Rochester: Eastman Kodak Co., 1980;23-25.
- 10. Tortorici MR. Fundamentals of angiography. St. Louis: The C.V. Mosby Company, 1982;3-35.
- 11. Sugimoto K, Sakurai N, Kaneko M, Shirasawa H, Shibata K, Miyata M, Noguchi T, Uematsu K, Shimoda K, Sakata J. Application of renal microangiography to normal and diseased kidneys of cattle and mice. Am J Vet Res 1991;52(1)157-163.
  - 12. General Electric service engineers; personal communications, 1994.
- 13. Sprawls P. Intensified radiography. In: The physical principles of diagnostic radiology. Baltimore: University Park Press, 1977;237-270.
- 14. Abrams HL. The opaque media: physiologic effects and systemic reactions. In: Abrams angiography-vascular & inter-ventional radiology, 3rd ed. Abrams, ed. Boston: Little, Brown and Company, 1983;15-39.
- 15. White RI. Fundamentals of vascular radiology. Philadelphia: Lei & Febiger, 1976;27-42.
- 16. Katzberg RW, Morris TW, Schulman G, Faillace RT, Boylan LM, Foley MJ, Spataro RF, Fischer HW. Reactions to intravascular contrast media, part I: severe and fatal cardiovascular reactions in a canine dehydration model. Rad 1983;147:327-330.
- 17. Katzberg RW, Morris TW, Schulman G, Caldicott WJ, Boylan LM, Foley MJ, Spataro RF, Fischer HW. Reactions to intravascular contrast media, part II: acute renal response in euvolemic and dehydrated dogs. Rad 1983;147:331-334.
- 18. Almen T. Development of nonionic contrast media. Invest Rad 1985;20(Supp):S2-S9.

- 19. Strain WH, Rogoff SM. The radiopaque media: nomenclature and chemical formulas. In: Angiography, 2nd ed. Abrams, ed. Boston: Little, Brown and Company, 1971.
- 20. Dennis R, Herrtage ME. Low osmolar contrast media, a review. Vet Rad 1989;30(1):2-12.
- 21. Dawson P. Chemotoxicity of contrast media and clinical adverse effects: a review. Invest Rad 1985;Supp;S84-S91.
- 22. Bettmann MA, Bourdillon PD, Barry WH, Brush KA, Levin DC. Contrast agents for cardiac angiography: effects of a nonionic agent vs. a standard ionic agent. Rad1984;153:583-587.

- 23. Steinberg EP, Moore RD, Powe NR, Gopalan R, Davidoff AJ, Litt M, Graziano S, Brinker JA. Safety and cost effectiveness of high-osmolality as compared with low-osmolality contrast material in patients undergoing cardiac angiography. NEJM 1992;326(7):425-430.
- 24. Spears JR, Sandor T, Als AV, Malagold M, Markis JE, Grossman W, Serur JR, Paulin S. Computerized image analysis for quantitative measurement of vessel diameter from cineangiograms. Circulation 1983;68(2):453-461.
- 25. Linford RL, O'Brien TR, Wheat JD, Meagher DM. Radiographic assessment of epiglottic length and pharyngeal and laryngeal diameters in the thoroughbred. AJVR 1983;44(9):1660-1666.
- 26. Myer CW. Radiography review: the vascular and bronchial patterns of pulmonary disease. Vet Rad 1980;21(4):156-160.
- 27. van den Broek AHM, Darke PGG. Cardiac measurements on thoracic radiographs of cats. J Small Anim Prac 1987;28:125-135.
- 28. Suter PF, Lord PF. Thoracic radiography. Wettswil, Swizterland: Peter F. Suter, 1984.

- 29. Morton WG, Hammer EW. The xray, or, photography of the invisible and its value in surgery. New York: American Technical Book Co., 1986.
- 30. Wise M. Non-selective angiocardiography in the normal dog and cat. Vet Rad 1982;23(4):144-151.
- 31. Carlsten J. Imaging of the equine heart: an angiographic and echocardiographic investigation. Uppsala, Merkantil-Tryckeriet AB, 1986.
- 32. Stickle RL, Anderson LK. Diagnosis of common congenital heart anomalies in the dog using survey and nonselective contrast radiography. Vet Rad 1987;28(1):6-12.
- 33. Singh AP, Singh GR, Sharma DN, Nigam JM, Bhargava AK. Arteriographic anatomy of the abdominal aorta in the goat, dog, pig, and rabbit. Vet Rad 1982;23(6):279-281.
- 34. Singh AP, Singh GR, Bhargava AK. Angiographic evaluation of bovine intestinal healing following inverting, everting, and end-on anastomosis. Vet Rad 1983;24(1):35-40.
- 35. Singh AP, Nigam JM. Vascular response to fracture healing in the bovine, an angiographic study. Vet Rad 1983;24(4):174-180.
- 36. Rendano VT, Georgi JR, White KK, Sack WO, King JM, Bianchi DG, Theodorides VJ. Equine verminous arteritis. an arteriographic evaluation of the larvicidal activity of albendazole. Eq Vet J. 1979;11(4):223-231.
- 37. Rantanen NW, Ewing RL. Principles of ultrasound application in animals. Vet Rad 1981;22(5):196-203.
- 38. Wallace KD, Selcer BA, Tyler DE, Brown J. Transrectal ultrasonography of the cranial mesenteric artery of the horse. Am J Vet Res 1989;50(10):1699-1703.

- 39. Wallace KD, Selcer BA, Becht JL. Technique for trans-rectal ultrasonography of the cranial mesenteric artery of the horse. Am J Vet Res 1989;50(10):1695-1698.
- 40. Edwards GB, Allen WE. Aorto-iliac thrombosis in two horses: clinical course of the disease and use of real-time ultrasonography to confirm diagnosis. Eq Vet J 1988;20(5):384-386,391.
- 41. Reef VB, Roby KA, Richardson DW, Vaala WE, Johnston JK. Use of ultrasonography for the detection of aortic-iliac thrombosis in horses. JAVMA 1987;190(3):286-288.
- 42. Hedrick WR, Hykes DL. Doppler physics and instrumentation, a review. JDMS 1988;4:109-120.
- 43. Scoutt LM, Zawin ML, Taylor KJ. Doppler US, part II. clinical applications. Rad 1990;174:309-319.
- 44. Welch RD, Dean PW, Miller MW. Pulsed spectral doppler evaluation of a peripheral arteriovenous fistula in a horse. JAVMA 1992;200(9):1360-1361.
- 45. Adair HS, Goble DO, Shires GM, Sanders WL. Evaluation of laser doppler flowmetry for measuring coronary band and laminar microcirculatory blood flow in clinically normal horses. Am J Vet Res 1994;55(4):445-449.
- 46. Thomson CE, Kornegay JN, Burn RA, Drayer BP, Hadley DM, Levesque DC, Gainsburg LA, Lane SB, Sharp NJ, Wheeler SJ. Magnetic resonance imaging-a general overview of principles and examples in veterinary neurodiagnosis. Vet Rad & US 1993;34(1):2-17.
- 47. Edelman RR. MRI angiography: approaches and strategies. MRI decisions 1989:13-13-23.
- 48. Koblik PD, Hornof WJ, Rhode EA, Kelly AB. Left ventricular ejection fraction in the normal horse determined by first-pass nuclear angiocardiography. Vet Rad 1985;26(2):53-62.

- 49. Koblik PD, Hornof WJ. Diagnostic radiology and nuclear cardiology: their use in assessment of equine cardiovascular disease. In: VCNA, Eq Prac, J Bonagura (guest ed.) Philadelphia: W.B. Saunders Company, 1985; 289-309.
- 50. Daniel GB, Wantschek L, Bright R, Silva-Krott I. Diagnosis of aortic thromboembolism in two dogs with radionuclide angiography. Vet Rad 1990;31(4):182-185.
- 51. Gogoi SN, Nigam JM, Singh AP. Angiographic evaluation of bovine foot abnormalities. Vet Rad 1982;23(4):171-174.
- 52. Burns J, Cornell C. Angiography of the caprine digit. Vet Rad 1981;22(4):174-176.
- 53. Coffman JR, Johnson JH, Guffy MM, Finocchio EJ. Hoof circulation in equine laminitis. JAVMA 1970;156(1):76-83.
- 54. Ackerman N, Garner HE, Coffman JR, Clement JW. Angiographic appearance of the normal equine foot and alterations in chronic laminitis. JAVMA 1975;166(1):58-62.
- 55. Scott EA, Thrall DE, Sandler GA. Angiography of equine metacarpus and phalanges: alterations with medial palmar artery and medial palmar digital artery ligation. Am J Vet Res 1976;37(8):869-873.
- 56. Scott EA, Sandler GA, Shires MH. Angiography as a diagnostic technique in the equine. J Eq Med Surg 1978;2(6):270-278.
- 57. Lindbom A. Arterial spasm caused by puncture and catheterization. Acta radiol 1957;449-459.
- 58. van Kraayenburg FJ, Fairall N, Littlejohn A. The effects of vertical force on blood flow in the palmar digital arteries of the horse. Proc 1st Int Conf, Equine Exercise Physiology, Oxford, 1982; 144-154.

- 59. Elmes PJ, Eyre P. Vascular reactivity of the bovine foot to neurohormones, antigens, and chemical mediators of anaphylaxis. Am J Vet Res 1977;38(1):107-112.
- 60. Harkema JR, Robinson NE, Scott JB. Cardiovascular, acid-base, electrolyte, and plasma volume changes in ponies developing alimentary laminitis. Am J Vet Res 1978;39(5):741-744.
- 61. Schummer A, Wilkens H, Vollmerhaus B, Habermehl KH. The circulatory system, the skin, and the cutaneous organs of the domestic mammals. New York:Springer Verlag, 1981;552-597.
- 62. Colles CM, Garner HE, Coffman JR. The blood supply of the horse's foot. Proc 25th Ann Mtg, Am Assoc Eq Prac, Miami, FL, 1980; 385-389.
- 63. Mishra PC, Leach DH. Extrinsic and intrinsic veins of the equine hoof wall. J Anat 1983;136(3):543-560.
- 64. Stashak TS. Adams' lameness in horses. 4th ed. Philadelphia: Lea & Febiger, 1987;14.
- 65. Pepine CJ. Diagnostic and therapeutic cardiac catheterization. 2nd edition. Philadelphia: Williams and Wilkins, 1994; 171.

AICHIGAN STATE UNIV. LIBRARIES
31293014051845